Investigating Biotic and Abiotic Transformation Processes of Selected Pesticides Using Electrochemistry Coupled to Mass Spectrometry

Dissertation

zur Erlangung des akademischen Grades
doctor rerum naturalium
(Dr. rer. nat.)
im Fach Chemie: Spezialisierung: Angewandte Analytik und Umweltchemie

eingereicht an der
Mathematisch-Naturwissenschaftlichen Fakultät der Humboldt-Universität zu Berlin

Von
M.Sc. Chemie, Tessema Fenta Mekonnen

Präsidentin der Humboldt-Universität zu Berlin
Prof. Dr.-Ing. Dr. Sabine Kunst

Dekan der Mathematisch-Naturwissenschaftlichen Fakultät
Prof. Dr. Elmar Kulke

Gutachter:

1. Prof. Dr. rer. nat. Ulrich Panne
   Bundesanstalt für Materialforschung und -prüfung; Humboldt-Universität zu Berlin
2. Prof. i. R. Dr. Michael W. Linscheid
   Humboldt-Universität zu Berlin, School of Analytical Sciences Adlershof (SALSA)
3. Dr. rer. nat. habil. Rudolf J. Schneider
   Bundesanstalt für Materialforschung und -prüfung

Tag der mündlichen Prüfung: 15 März 2019

Erklärung/Declaration

Hiermit erkläre ich, die Dissertation selbstständig und nur unter Verwendung der angegebenen Hilfen und Hilfsmittel angefertigt zu haben. Ich habe mich nicht anderwärts um einen Doktorgrad in dem Promotionsfach beworben und besitze keinen entsprechenden Doktorgrad. Die Promotionsordnung der Mathematisch-Naturwissenschaftlichen Fakultät, veröffentlicht im Amtlichen Mitteilungsblatt der Humboldt-Universität zu Berlin Nr. 42 am 11. Juli 2018, habe ich zur Kenntnis genommen.

I declare that I have completed the thesis independently using only the aids and tools specified. I have not applied for a doctor's degree in the doctoral subject elsewhere and do not hold a corresponding doctor's degree. I have taken due note of the Faculty of Mathematics and Natural Sciences PhD Regulations, published in the Official Gazette of Humboldt-Universität zu Berlin no. 126 on July 18 2014.

I. Publication in Peer-reviewed Journals

[1]. **Mekonnen, T.F.**, Panne, U., Koch., M. Electrochemistry coupled online to liquid chromatography-mass spectrometry for fast simulation of biotransformation reactions of the insecticide chlorpyrifos, *Anal Bioanal Chem*, 2017, 409: 3359-3368. doi 10.1007/s00216-017-0277-y.

[2]. **Mekonnen, T.F.**, Panne, U., Koch., M. Prediction of biotransformation products of the fungicide fluopyram by electrochemistry coupled online to liquid chromatography-mass spectrometry and comparison with *in vitro* microsomal assays, *Anal Bioanal Chem*, 2018, 410: 2607 – 2617. doi 10.1007/s00216-018-0933-x.

[3]. **Mekonnen, T.F.**, Byrne, L., Panne, U., Koch, M. Investigation of chlorpyrifos and its transformation products in fruits and spices by combining electrochemistry and liquid chromatography coupled to tandem mass spectrometry, *Food Anal. Methods*, 2018, 11: 2657-2665. doi 10.1007/s12161-018-1245-7.

[4]. **Mekonnen, T.F.**, Panne, U., Koch., M. New photodegradation products of the fungicide fluopyram: Structural elucidation and mechanism identification, *Molecules*, 2018, 23(11), 2940 – 2952. doi:10.3390/molecules23112940.

[5]. **Mekonnen, T.F.**, Panne, U., Koch., M. Glucosylation and glutathione conjugation of chlorpyrifos and fluopyram metabolites using electrochemistry/mass spectrometry, *Molecules*, 2019, 24(5), 898 – 910.

[6]. Kotthoff, L., Keller, J., Lörchner, D, **Mekonnen**, **T.F**., Koch, M. Transformation products of organic residues and contaminants – Overview of recently used simulation methods, *Molecules*, 2019, 24(4), 753 – 775.

II. Communication/Conferences

Oral Presentations

[1]. **Mekonnen, T.F.**, Byrne, L., Panne, U., Koch, M. Transformation products of pesticides: simulation and detection, *XIX European Analytical Chemistry Conference (EuroAnalysis2017), 28.08 – 01.09.2017, Stockholm, Sweden*.

[2]. **Mekonnen, T.F**., Byrne, L., Panne, U., Koch, M. Electrochemistry coupled online to mass spectrometry for prediction of metabolic transformation processes of pesticides, *13th Annual LC-MS/MS workshop on environmental and food safety, 11 – 12.06.2017, Buffalo, USA*.

[3]. **Mekonnen, T.F.**, Panne, U., Koch, M. Metabolic transformation products of chlorpyrifos, fluopyram and glyphosate by EC/ESI-MS: simulation to in-vitro assay metabolites, *European Conference on Pesticides and Related Organic Micropollutants in the Environment & Symposium on Chemistry and Fate of Modern Pesticides (9th EU pesticides), 04 – 07.10.2016, Santiago de Compostela, Spain.*

Poster Presentations

[1]. **Mekonnen, T.F.**, Panne, U., Koch, M. Electrochemistry coupled online to mass spectrometry for biotransformation and metabolite elucidation of pesticides, *European Mass Spectrometry Conference (EMSC2018), 11 – 15.03.2018, Saarbrücken, Germany*.

[2]. **Mekonnen, T.F**., Byrne, L., Panne, U., Koch, M. Investigation of chlorpyrifos and its transformation products in food samples, *8th International symposium on Recent Advances in Food Analysis (RAFA2017), 07 – 10.11.2017, Prague, Czech Republic.*

[3]. **Mekonnen, T.F.**, Panne, U., Koch. Simulation of metabolic transformation products of pesticides by EC/LC/MS, *International conference series on Environmental and Food Monitoring (ISEAC39), 18 – 22.07.2016, Hamburg, Germany.*

[4]. **Mekonnen, T.F.**, Panne, U., Koch. Investigating metabolic transformation processes of pesticides, *44. Deutschen Lebensmittelchemikertag, 14 – 16.09.2015, Karlsruhe, Germany.*

Acknowledgments

It is difficult to realize this work without a great support of many people. First and for most, I would like to thank my supervisor Prof. Dr. Ulrich Panne (President of BAM, and SALSA HU) for giving me an opportunity to realize my scientific dreams. My great thanks also go to my second supervisor Dr. habil. Rudolf J. Schneider (BAM Division 1.8) for your wonderful and constructive ideas and continuous follow ups to my interim reports. Furthermore, my special thanks to Dr. Matthias Koch (BAM Division 1.7) who allow me to work on this topic and gave me the chance to see the complexity of pesticides transformation processes. Many thanks for the scientific freedom you gave me and continuous guidance for this three and half wonderful years. It is my true privilege to work with you Matthias, especially for your understanding between work and family responsibilities, patience, and the confidences on my work. I am always delighted for the great discussions.

I am profoundly thanking the Deutsche Forschungsgemeinschaft (DFG) and Bundesanstalt für Materialforschung und -prüfung (BAM) for funding my research work through structured postgraduate program at School of Analytical Sciences Adlershof (SALSA), Humboldt University in Berlin (HU). Thank you, all SALSA team, for endless help and administrative support. It is my true honor to be part of SALSA, not only wonderful scientific discussions but also continuous couching and skill-based trainings.

My lab mates and BAM Division 1.7 staffs, thank you all for always being there whenever I need your help. Thank you for being nice to me and understanding me as a foreign scholar. Especially, I would like to thank Dr. Robert Köppen for introducing me LC- MS/MS systems and Dr. Jan Lisec for UPLC-TripleTOF-HRMS and teaching me how I annotate metabolites. My BAM colleagues, Lisa and Maike, thank you for your support and patient to translate my endless German letters as well as for the scientific discussions.

Thank you, Liam Byrne (Erasmus student from Ireland) for an incredible six months work with me, especially in the real sample investigation part, and proof reading of the manuscripts. Many thanks, Gaby Bosc-Bierne (BAM Division of Protein Analysis) for the Orbitrap access, and Boris Neumann (Proteome Factory AG, Berlin, Germany) for the FT-ICR HRMS measurements.

I would like to thank all the members of the doctoral committee, Michael W. Linscheid (Prof. i. R. Dr.), Ulrich Panne (Prof. Dr.), and Rudolf Schneider (Dr. habil.) for spending your time to review my thesis, Christoph Arenz (Prof. Dr.) for being a chairman of the doctoral disputation, and Franziska Emmerling (PD. Dr.) for being the member of the doctoral committee.

My brother, Kelem Gashu (from Israel), thank you for encouraging me, sharing ideas, or chatting about day-to-day life. At last but not list, my wife, Selam and my daughter, Edom, I very thankful for your kind support, love, and understand whenever I am not with you in the early evenings or weekends. Thank you Selam, for taking care of most household responsibilities and our little once during this work. My daughters, Edom and Yabi, thank you for being a joy in my life. My parents, Mennen Getnet and Fenta Mekonnen, you are my rock model, thank you for being always with me and praying for me.

Table of Contents

ABSTRACT

One of the crucial steps of developing a new agrochemical product is predicting its fate following biotic or abiotic stress, so as to determine potential consequences to a living organism's health and ecology as a whole. In this regard, pesticides undergo transformation processes in response to biotic and abiotic stress. Therefore, it is important to investigate pesticides' transformation products (TPs) and the formation processes they undergo. Various conventional in vivo and in vitro enzymatic methods are applied for such investigations. However, time, cost, and matrix complexity often hinder the success of these methods. Since short-lived intermediates react fast, using conventional approaches may be insufficient to gain comprehensive understanding of their mechanisms. Hence, developing alternative faster and more efficient methods is crucial. Meanwhile, investigation of TP residues in real food and environmental samples represents an analytical challenge due to the complexity of matrices and a lack of standards. Herein, we propose an alternative non-enzymatic method, using electrochemistry (EC) coupled online to liquid chromatography-mass spectrometry (EC/LC/MS) for simulation, production and mechanism elucidation of metabolites of chlorpyrifos (insecticide) and fluopyram (fungicide).

The experimental design involved an EC-flow-through cell equipped with a boron-doped diamond electrode. The intended compounds are oxidized by EC, separated by LC-column and detected using online ESI-MS. As a reference method, the compounds were incubated in liver microsomal assays (human and rat) and compared with EC products using LC-MS and LC-MS/MS. Further, phase II conjugative metabolites produced by glucosylation and glutathione conjugation were studied by trapping EC oxidative products before entering the ESI-MS. Abiotic TPs were modelled by irradiating aqueous solutions of chlorpyrifos and fluopyram using ultraviolet (UV) light at 200-280 nm. Structural elucidation and mechanism identification of each product (from EC, liver microsomes and UV-C) were achieved by retention time, isotopic configuration, fragmentation (EC/LC/MS, LC/MS/MS and MS/MS) and accurate mass and molecular formula measurements via high-resolution MS (FT-ICR, Orbitrap and/or TripleTOF-HRMS). Finally, TPs of chlorpyrifos and fluopyram were detected in real foodstuff samples by synthesizing authentic standards of TPs using the EC cell.

Five main phase I metabolites of chlorpyrifos – namely oxon, desethyl chlorpyrifos, trichloropyridinol, diethylthiophosphate and diethylphosphate – were confirmed using the above method and simulated into liver microsome incubates. Furthermore, three products (monodechlorinated chlorpyrifos, desethyl oxon and monoethylphosphate) were observed as TPs of oxidative stress using EC/MS. Four glutathione and three glucoside phase II conjugates of chlorpyrifos TPs were also elucidated. Hence, chlorpyrifos undergoes phase I metabolism mainly via P-oxidation and O-dealkylation and phase II conjugation through one of the halogen sites (lost HCl). On the other hand, fluopyram is intensively metabolised via hydroxylation, N-dealkylation, cyclisation and dehalogenation under oxidative stress (Phase I). In both liver microsomes and EC/MS, further N-dealkylation of hydroxyl TPs, hydroxylation of lactam and oxidation of hydroxyl TPs to hydroxylimide metabolites were investigated. It was found that single electron abstraction from amine free electrons is the basic oxidation step initiating the formation of imine and olefin. The olefin and imine are easily hydroxylated (via epoxide intermediate) or N-dealkylated. Additionally, oxidation via dissociation electron transfer initiates fluopyram metabolism through dehalogenation and lactam formation. Glutathione and glucoside phase II conjugates of monohydroxyl fluopyram, formed by losing water molecule, was also studied in this work. Photodegradation identified seven new TPs of fluopyram through three main roots (cyclisation, hydroxylation and rearrangement). Lastly, TPs of chlorpyrifos were investigated in fruits and spice samples; four of these were found in different samples alongside the parent chlorpyrifos.

In summary, a fast, reliable, cost-effective and matrix-free simulation of oxidative metabolism (phase I and II) of fluopyram and chlorpyrifos was achieved here by EC/(LC)/MS. EC/MS could, therefore, be scaled up to synthesis TP reference standards for real sample investigation. Additionally, new TPs and their mechanisms were identified for both investigated compounds.

ZUSAMMENFASSUNG

In der Entwicklung neuer Agrochemikalien ist es essentiell das weitere Schicksal im Bezug zum Abbau durch abiotische und biotische Einflüsse vorherzusagen, um potentielle Konsequenzen für die Gesundheit von lebenden Organismen und die Umwelt bestimmen zu können. Pestizide gehören zu den Agrochemikalien und durch abiotischen und biotischen Stress werden Transformationsprodukte (TPs) gebildet. Daher ist es von Bedeutung, die TPs von Pestiziden und deren Entstehungsprozess zu untersuchen. Bekannte und häufig genutzte Methoden mit dieser Zielstellung sind enzymatische Tests. Allerdings sind diese zeit- und kostenintensiv und bei komplexen Matrices schlecht anwendbar. Kurzlebige Intermediate reagieren schnell weiter, wodurch sie mit konventionellen Methoden kaum messbar sind. Die Entwicklung schneller und effizienter Alternativmethoden ist daher von großer Bedeutung. Unterdessen stellt die Untersuchung von TPs Rückständen in Lebensmittel- und Umweltproben durch die Komplexität der Matrices und das Fehlen von Standardsubstanzen eine große Herausforderung der Analytik dar. In dieser Arbeit wird eine alternative nicht-enzymatische Methode vorgestellt, die auf der online-Kopplung zwischen Elektrochemie (EC) mit Hochleistungsflüssigkeitschromatographie und Massenspektrometrie (EC/LC/MS) basiert. Mit dieser Methode werden die Pestizide Chlorpyrifos (Insektizid) und Fluopyram (Fungizid) untersucht, dabei werden die TPs simuliert und produziert, sowie der Mechanismus der Bildung aufgeklärt.

Der verwendete experimentelle Aufbau bestand aus einer EC-Durchflusszelle, die eine bordotierte Diamant-Elektrode enthielt. Die untersuchten Substanzen wurden in der EC oxidiert, durch die LC aufgetrennt und mittels ESI-MS detektiert. Lebermikrosomen-Assays (Humane und Rattenmikrosomen) wurden durchgeführt, um einen Vergleich der EC-generierten TPs zu erhalten. Neben den Oxidationsreaktionen wurden auch Phase-II-Metabolite, die durch Glucosylierung und Glutathion-Konjugation entstanden, mit der EC untersucht, dazu wurde nach der EC-Durchflusszelle ein Konjugationsreagenz hinzugegeben und die Konjugatprodukte wurden anschließend mittels ESI-MS detektiert. Die Bildung von abiotischen TPs wurde durch UV-Bestrahlung (200 – 280 nm) von wässrigen Lösungen von Chlorpyrifos und Fluopyram simuliert. Zur Strukturaufklärung und Identifizierung der Entstehungsmechanismen wurden die Retentionszeiten, die Isotopenkonfiguration, die Fragmentierung (EC/LC/MS, LC/MS/MS und MS/MS) und die hochauflösende MS genutzt, aus den hochauflösenden Daten (mit Hilfe von FT-ICR, Orbitrap und/oder Triple-TOF-HRMS) wurde die genaue Masse und die Summenformel ermittelt. Schließlich wurden Lebensmittel auf die TPs von Chlorpyrifos und Fluopyram getestet, indem authentische Standards der TPs durch die Verwendung der EC hergestellt wurden.

Fünf Hauptmetabolite der Phase I – Oxon, Desethylchlopyrifos, Trichloropyridinol, Diethylthiophosphat und Diethylphosphat – konnten mit Hilfe der hier vorgeschlagenen Methode und mit den Lebermikrosomen-Tests identifiziert werden. Darüber hinaus wurden mit der EC drei Produkte – Monodechloriertes Chlorpyrifos, Desethyloxon und Monoethylphosphat – als durch oxidativen Stress verursachte TPs gefunden. Des Weiteren konnten vier Glutathion- und drei Glucosid-konjugierte Phase-II-Metabolite mit der gezeigten Methode nachgewiesen werden. Folglich kann darauf geschlossen werden, dass Chlorpyrifos im Phase-I Metabolismus hauptsächlich P-oxidiert und O-dealkyliert wird und im Phase II Metabolismus Verknüpfungen an einer der Halogengruppen unter Verlust von HCl ausbildet. Fluopyram hingegen wird bei oxidativem Stress häufig hydroxyliert, N-dealkyliert, cyclisiert und dehalogeniert (Phase-I). Mit beiden Methoden, Lebermikrosomen-Assays und EC/MS, wurden weitere N-dealkylierungen der hydroxylierten TPs, die Hydroxylierung des Lactams und die Oxidation von hydroxylierten TPs zu Hydroxylimiden untersucht. Es wurde bereits nachgewiesen, dass das Entfernen einzelner Elektronen aus dem freien Elektronenpaar eines Amins ein grundlegender Schritt in der Bildung von Iminen und Olefinen ist. Diese können leicht hydroxyliert (über ein Epoxidintermediat) oder N-dealkyliert werden. Darüber hinaus löst die Oxidation durch Elektronentransfer-Dissoziation die Metabolisierung des Fluopyrams durch Dehalogenisierung und Lactambildung aus. Ebenso wurde die Umsetzung von Monohydroxy-Fluopyram zu den Glutathion- und Glucosid-Konjugaten unter Verlust eines Wassermoleküls innerhalb dieser Arbeit betrachtet. Sieben neue TPs von Fluopyram wurden bei der Untersuchung des Photoabbaus auf drei verschiedenen Wegen (Cyclisierung, Hydroxylierung und Umlagerung) gebildet. Abschließend wurden Obst- und Gewürzproben auf die TPs von Chlorpyrifos getestet. Neben Chlorpyrifos konnten vier dieser TPs nachgewiesen werden.

Zusammenfassend konnte die Kopplung von EC/(LC)/MS als schnelle, zuverlässige, kostengünstige und matrix-unabhängige Methode genutzt werden, um den oxidativen Phase-I und II Metabolismus von Fluopyram und Chlorpyrifos zu simulieren. EC/MS könnte weiterhin zur Synthese von TP Referenzstandards und zur Messung von Realproben genutzt werden. Neue TPs und deren Bildungsmechanismen konnten im Rahmen dieser Dissertation für beide untersuchten Substanzen identifiziert werden.

List of Figures

List of Appendix Figures

List of Tables

Abbreviations

ACN	Acetonitrile
APVMA	Australian Pesticides and Veterinary Medicine Authority
BDD	Boron doped diamond
CAD	Collision gas
CE	Counter electrode
CES	Collision energy spread
CPF	Chlorpyrifos
CPF-oxon	Chlorpyrifos oxon
cps	Counts per second
CUR	Curtain gas
CV	Coefficient of variance
CXP	Cell exit potential
CY	Cytochrome
DC	Direct current
Dec-CPF	Dechlorinated chlorpyrifos
Des-CPF	Desethyl chlorpyrifos
Des-Oxon	Desethyl chlorpyrifos oxon
DEP	Diethylphosphate
DETP	Diethylthiophosphate
DNA	Deoxyribonucleic acid
DP	Declustering potential
EC	Electrochemistry
EC/LC/MS	Electrochemistry/Liquid chromatography/Mass spectrometry
EC/MS	Electrochemistry/mass spectrometry
EIC	Extracted ion chromatogram
EFSA	European Food Safety Authority
EPI	Enhanced product ion
EPA	Environmental Protection Agency
EU	European Union
FAO	Food and Drug Administration Organization
FLP	Fluopyram
FT-ICR	Fourier Transform-Ion Cyclotron Resonance
n-Glc	n-nonyl-β-D-glucoside
Glc	D-glucose
GSH	D-Glutathione (reduced)
GSSG	L-Glutathione (oxidized)
GST	Glutathione-S-transferase
HFA	Formic acid
HLM	Human liver microsome
HPLC	High performance liquid chromatography
HRMS	High resolution mass spectrometry
IS	Ion-spray
LC	Liquid chromatography
LIT	Linear ion trap
LM/s	Liver microsome/s

LOD	Limit of detection
LOQ	Limit of quantification
ME	Matrix effect
MeOH	Methanol
MRL/s	Maximum residue level/s
MRM	Multiple reaction monitoring
MS	Mass spectrometry
MS/MS	Tandem mass spectrometry
NH_4FA	Ammonium formate
NMR	Nuclear magnetic resonance spectrometry
p.a.	pro analysis
PA	Peak area
PAN	Pesticides Action Network
PANNA	Pesticides Action Network North America
PI	Product ion scan
PP/s	Photodegradation product/s
QTRAP	Quadrupole Triple
R^2	Square of correlation coefficient
RASFF	Rapid Alert System for Food and Feed
RLM	Rat liver microsome
rpm	rotation per minute
RSD	Relative standard deviation
RSD_R	Inter-day repeatability
RSD_r	Intra-day repeatability
RT	Room temperature
SIM	Single ion monitoring
TCP	Trichloropyridinol
TIC	Total ion chromatogram
TOF	Time of flight
TP/s	Transformation product/s
TPP	Triphenylphosphate
t_R	Retention time
UV	Ultra-Violate
US	United states
WE	Working electrode
λ	Wavelength

1. INTRODUCTION

Synthetic compounds are often found inside living organisms (i.e. xenobiotics – foreign compounds inside living organisms) or in the environment. After reaching biota or the environment, these compounds are usually exposed to multiple stressors, which lead to the formation of other by-products – termed transformation products (TPs). A diverse and large number of agrochemicals and pharmaceuticals are used daily throughout the world; they are the most common synthetic compounds that undergo several transformation processes in both living organisms and environmental compartments [1-2]. Despite their advantages, these compounds often pose a threat to the health of organisms and environmental ecosystems. Exposure to them can occur directly (e.g. through inhalation, topical absorption or oral administration) or indirectly through food webs (i.e. plant- and animal-based food products and water). There are many factors causing transformation of agrochemical residues or pharmaceutical pollutants. For instance, biotransformation (metabolism in living organisms), microbial activities, environmental factors (e.g. thermal and hydrolysis), photodegradation, human activities (e.g. industrial, cooking) and natural activities all drive the transformation of organic compounds [3-6]. The TPs of pharmaceuticals marketed for patients are rarely toxic as they are primarily intended for therapeutic efficacy – i.e. for treatment of disease. However, both parent compounds and the TPs of most agrochemicals, especially pesticides, are shown to adversely affect the health of living organisms.

Sometimes, TPs are more toxic, acute or chronic contaminants than their parent compound. For example, aflatoxin B_1 metabolism produces epoxide, which binds to guanine residues in DNA and exherts a carcinogenic effect [7]. Before the intended application of any compound, it is mandatory practice to predict the biological fate of newly produced compounds so as to identify any health risks. Reduction of polyhalogenated compounds could produce halocarbene, which is detrimental to cellular enzyme function. Most TPs are more polar and mobile than the parent compounds; thus, they easily interact with different biomolecules, such as proteins or nucleic acids [2]. On the other hand, their consumption through plant- and animal-based foods is virtually inevitable. Hence, regulating the production and thorough investigation of TPs of pesticides and their formation mechanisms is a must.

In general, the transformation processes of organic compounds can be classified into two groups: biotic and abiotic. Biotic transformation (also called biotransformation) processes are reactions produced by xenobiotics inside a living organism; this can occur in humans, animals, plants and microbes. In contrast, abiotic transformation processes are chemical and take place outside living organisms in environmental compartments or industrial processes. Unlike biotransformation, abiotic transformation of a compound occurs as a result of multiple stressors; it is hard to identify a specific cause of certain TPs being produced in the environment. Biotic TPs can also go through further environmental degradation after excretion [8]. Meanwhile, there is no clear demarcation between degradation products and abiotic TPs, as well as biotransformation and metabolism, with many authors using them interchangeably. According to Parkinson, the term 'metabolism' is often used to describe the total fate of a xenobiotic, which includes absorption, distribution, biotransformation and elimination [9]. Hence, biotransformation is a part of metabolism. In the context of this thesis, TPs are referred to as any products produced as a result of modification of the parent compound either by biological or by abiotic reaction pathways. Similarly, abiotic-TPs are referred to as any products formed through transformation processes outside of living organisms; these may not be necessarily be degradation products but also conjugation, dimerisation, isomerisation or sulfonation reaction products. In line with this, TPs produced from biotransformation processes could be used interchangeably with the term 'metabolites'.

1.1. Transformation Processes of Xenobiotics

1.1.1. Biotransformation

Any foreign compound undergoes chemical modifications after entering a living organism, whereby immune cells convert xenobiotics to more hydrophilic compounds. This is mainly to increase solubility and excretion of the xenobiotics in order to reduce toxicity [9]. The modification process usually involves breakdown of the parent compound or insertion of more polar functional groups. Most metabolism processes take place in the liver and, to a lesser extent, in renal, gastric and other tissues. Based on the physicochemical nature of the parent compounds, the metabolites formed can be more active, inactive, and/or toxic than the starting compounds. The biotransformation processes are usually enzymatic in nature and yield reactive intermediates, which are more implicated in toxicity more than the final

metabolites. Their toxic effect is largely mediated by inhibition of a specific (often enzymatic) cellular function. For instance, *N*-acetyl-*p*-benzoquinone imine produced during *N*-oxidation metabolism of acetaminophen (4-hydroxyacetanilide or paracetamol) shows more hepatotoxicity than the parent compound itself. It can easily react with glutathione (GSH) or protein thiol groups, leading to disruption of cellular calcium regulation and cellular proteins [10]**.** Furthermore, tienilic acid metabolism by cytochrome (CY) in the human liver leads to a formation of 5-hydroxytienilic acid through an electrophilic intermediate, which is capable of alkylating specific CY-enzymes leading to its deactivation. The binding of the metabolite to CYP triggers an immune response, generating antibodies against the protein [2, 11].

There are two principal biotransformation processes in metabolism: phase I and phase II. Phase I metabolism occurs either by introducing polar functional groups to the parent compound or unmasking a polar group from the parent compound. Reactions such as oxidation, reduction and hydrolysis occur during phase I metabolism. This represents a functionalisation step to introduce polar functional groups to a molecule. Groups like –OH, –SH, epoxide, $–NH_2$, or –COOH are introduced to the molecule by a series of enzymatic reactions. In contrast, non-polar groups are cleaved (e.g. dealkylation, dearylation, dehalogenation) from heteroatoms (like –O, –S, –N) to unmask hydrophilic functional groups from the parent compound. The majority of phase I metabolites are generated by redox catalysis of CY enzymes. CYP450 plays a particularly important role in detoxification of xenobiotics and endogenous bioactive compounds, such as amino acids, cholesterol, saturated/unsaturated fatty acids and melatonin [12]. CYP comprises a large family of heme-containing protein isoforms, with 57 putatively functional CYPs encoded by the human genome alone. Over 500 forms of CYP450 have been found in different life forms (plants, bacteria, animals). Among these CYPs, the ones belonging to the CYP1, 2, and 3 families are responsible for the metabolism of 70-80% of xenobiotics used today [13]. The reactive site of all CYP450 enzymes contains an iron protoporphyrin IX (Fig. 1a), which enables oxygen binding and inserting. The main steps of CYP450 catalysis are shown in Fig. 1b. The substrate first binds to the enzyme P450 ferric complex (❶ in Fig. 1b). A single electron from nicotinamide adenine dinucleotide phosphate bound enzyme (NADPH-P450 reductase) then reduces Fe^{3+} to Fe^{2+} (❷ in Fig. 1b) and this leads to binding of molecular O_2 to the ferrous-P450 (❸). This Fe^{2+}-O_2 complex is unstable and can generate ferric iron (Fe^{3+}) and the superoxide

anion, $O_2^{\bullet-}$ (❹). Next, a second electron from NADPH-P450 reductase and a proton are introduced, which leads to the generation of H_2O molecule by O-O bond cleavage (❻ in Fig. 1b). The substrate radical ion (R•) finally gets hydroxylated (❽). In artificial systems, like porphyrin or other electrochemical techniques, oxygen surrogates (like hydrogen peroxide, periodate, perchlorate, cumene hydroperoxide and iodosylbenzene) may be used to convert the ferric iron to high-valent iron-oxygen complexes [14]. All enzymes in the CYP450 family catalyse the incorporation of one oxygen atom of dioxygen into the substrate (monooxygenases), while the other oxygen atom is reduced by two electrons (from NADPH) to yield water (1.1).

$$\text{Substrate} + O_2 + 2e^- + 2H^+ \xrightarrow{\text{CYP450}} \text{Substrate(O)} + H_2O \qquad (1.1)$$

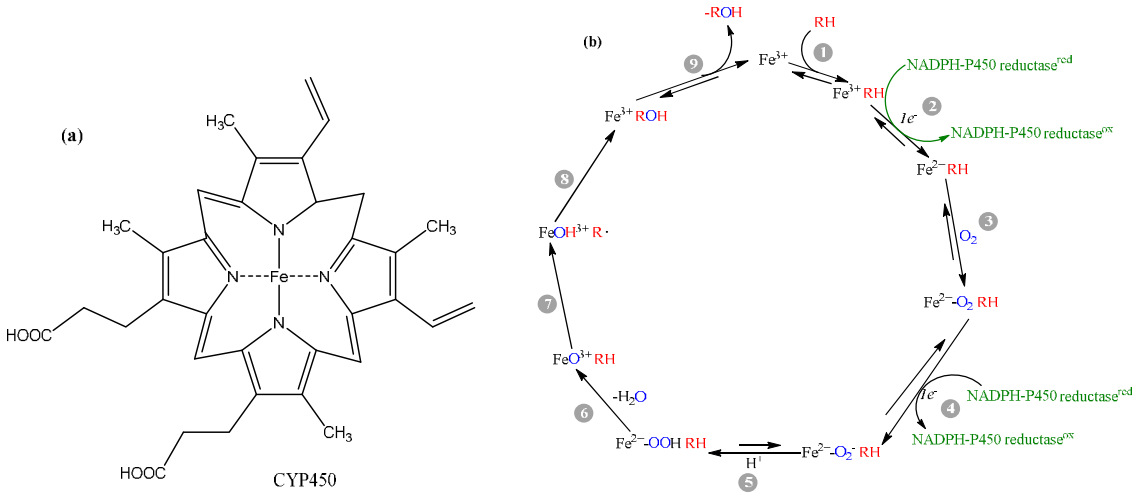

Fig. 1 Simplified representation of CYP450 (a) and general scheme of CYP450 catalytic activities (b) Fe = iron atom at the P450 heme, RH = substrate, ROH = product, ox and red indicate reduced and oxidized states of the reductase involved in the electron transfers (modified from Munro et al. *[15])*

CYP450 catalyses a broad range of biotransformation reactions, including –C–H oxidation (C-hydroxylation), heteroatom oxygenation (e.g. N–oxide and sulfoxide formation), heteroatom cleavage (e.g. N–, O–, S–dealkylation), and epoxidation. Oxidation of carbonyl functional groups is also a common detoxification mechanism of many drugs, alcohol and phenol, catalysed (via hydrogen abstraction) by CYP450 (Fig. 2). FeO^{3+} (Fig. 1b) is an electron-deficient complex that abstracts an electron from the substrate, which leads to a variety of biotransformation reactions, as shown in Fig. 2a–e.

C-oxidation:- This reaction occurs through H–abstraction and O–rebound mechanisms via formation of the carbon radical (Fig. 2a). This mechanism often occurs as part of detoxification or activation of polyaromatic hydrocarbons and compounds without heteroatoms.

Heteroatom oxygenation:- many N– and S–oxides are less toxic than their parent molecules, although N–oxygenation of aryl and heterocyclic amines is a vital step in bioactivation [16]. Heteroatom oxygenation reactions generally occur via two successive single electron transfer pathways, in which the first electron transfers from the heteroatom to the $[FeO]^{3+}$ complex and the second electron transfers to the binding 'O' (Fig. 2b). Heteroatom oxidation depends on the oxidation potential of the heteroatom, acidity of the adjacent hydrogens and, to some extent, steric effect.

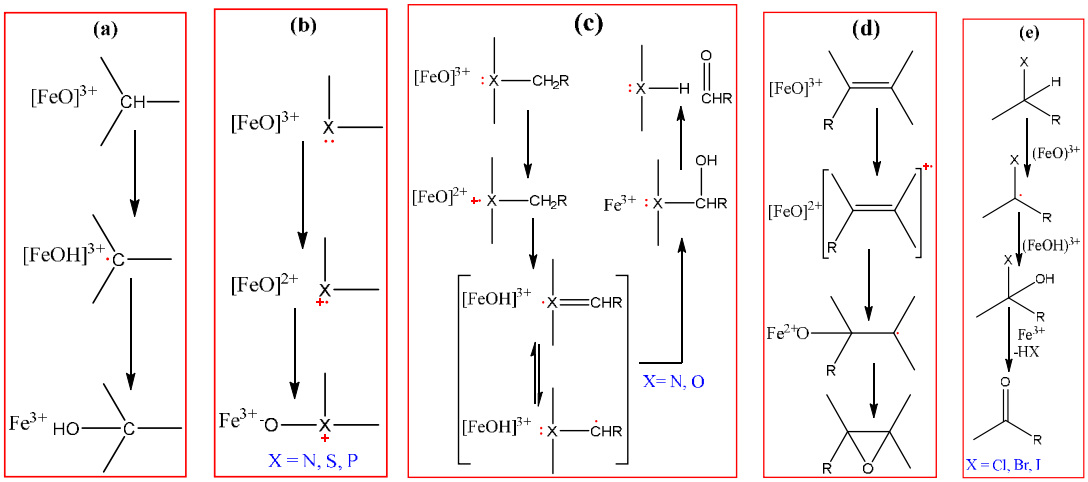

Fig. 2 Reaction mechanisms of C–hydroxylation (a), heteroatom oxygenation (b), heteroatom cleavage (c), epoxidation (d) and oxidative dehalogenation (e) catalysed by the ferric-CYP450 heme complex

Heteroatom cleavage:- This mechanism serves to unmask polar functional groups from the parent compounds. Reactions such as O–, N–, and S–dealkylation or dearylation underlie an array of xenobiotic metabolic processes. Often, heteroatom cleavage occurs via two successive single electron abstraction steps, ultimately leading to hydroxylation of α-carbon (Fig. 2c). This product, however, is cleaved at X–C and results in α-carbon oxidation (alcohol to ketone or aldehyde) and reduction of the heteroatom (addition of 'H').

Epoxidation:- Epoxidation is of particular interest in toxicology as the products can be unstable and react with nucleophilic groups in macromolecules (e.g. proteins and DNA). To prevent this, CYP450 enzymes further introduce hydroxyl to the epoxides (arene oxides, oxeranes) and produce diols (Fig. 2d).

Oxidative dehalogenation:- This process is often observed in the bioactivation mechanisms of xenobiotics. When the carbon bearing the halogen also contains a hydrogen, hydroxylation may occur on the same carbon. The hydroxylation product is unstable and converted to an aldehyde or ketone by losing HX (Fig. 2e). Some C–halogen bonds are strong enough and could not break easily (e.g. –C–F), which then leads to the formation of acyl-halides that can react with macromolecules (e.g. as observed during toxicity of chloroform and halothane).

Hence, in general, all phase I metabolism reactions are initiated by a single electron transfer (SET) or hydrogen atom transfer (HAT) between the ferric-CYP450 heme complex and the substrate. Two electron transfer reactions, such as O-dealkylation, also pass through two successive SET or HAT/oxygen rebound mechanisms. In the first step, CYP450 removes a hydrogen atom from the α-carbon and generates neutral carbon radical. Hydroxyl recombination occurs in the second step to form a hemiacetal intermediate, which then dissociates non-enzymatically into an alcohol and a carbonyl compound [17]**.** Rearrangement and isomerisation reactions are also frequently observed metabolic mechanisms. Although both the products and the starting materials assume the same oxidation state, CYP450 is still required for the rearrangement and isomerisation reactions. For example, rearrangement of prostaglandin to thromboxane and hydroxyheptatrienoic acid, as well as isomerisation of *trans*-tamoxifen to its *cis*-enantiomer, are catalysed by CYP450 enzymes [16]**.**

In the case of SET mechanisms, a relatively free electron is transferred from the substrate to the high valent $(FeO)^{3+}$ complex, which is followed by HAT from the α-carbon to the $(FeO)^{3+}$; this yields Fe–OH and attaches a neutral radical to the substrate. Finally, as –OH is attached to the α-carbon of the substrate, presence of an electron donor heteroatom in the substrate is necessary for a SET mechanism to occur (Fig. 3a). In contrast, in the case of HAT, a hydrogen atom is transferred directly from the substrate to the high valent $(FeO)^{3+}$ without formation of a radical cation on the heteroatom (Fig. 3b). Thus, it is not compulsory for the heteroatom to bear free electrons in the structure of the molecule for HAT mechanisms to occur. The last two steps are identical to SET. Fig. 3a, b show SET and HAT mechanisms of α-carbon hydroxylation of amine functional groups.

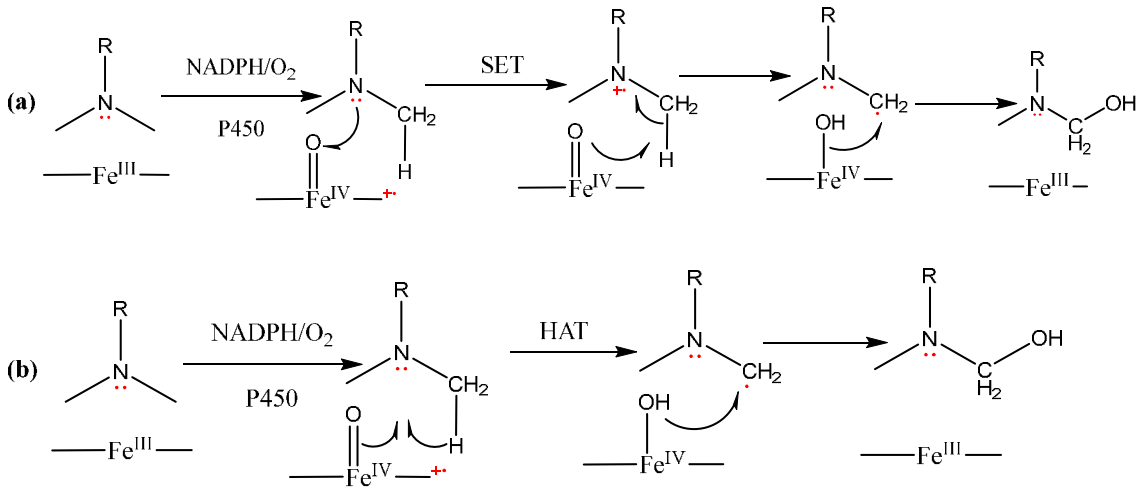

Fig. 3 Proposed N-dealkylation biotransformation by SET (a) and HAT (b) mechanisms

Phase II of metabolism involves the attachment of phase I metabolites to endogenous biomolecules. Polar and abundant *in vivo* molecules become conjugated to susceptible functional groups of phase I metabolites in the presence of catalysing enzymes (Fig. 4). Phase II reaction includes glucuronidation, sulfation, glutathione-S-conjugation, methylation, amination and acetylation. In general, xenobiotics and their metabolites that contain HO–, HOOC–, N–, N-oxide, electrophilic C-atom, NH_2– and SH– are susceptible to phase II conjugative metabolism [6, 18].

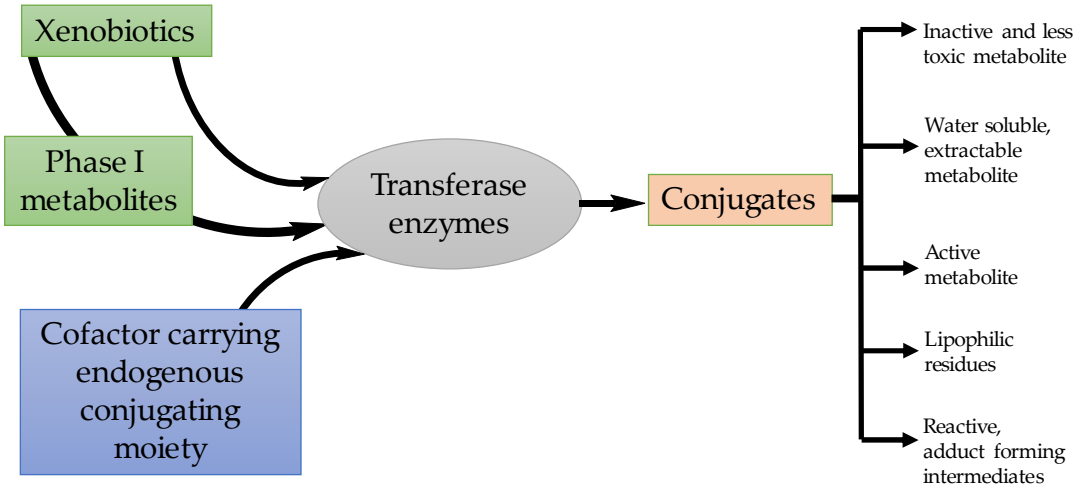

Fig. 4 Schematic diagram of phase II metabolism principles (modified from Testa and Krämer [6])

Unlike phase I metabolism, phase II attaches bulky ionic molecules to active metabolites, thereby producing a more polar molecule that cannot diffuse across membranes. To a greater extent, conjugation produces readily excretable and non-toxic metabolites – thus referred to as detoxification – although some exceptions occur for each class of conjugation reactions [19].

In rare cases, phase II conjugation reactions result in bioactivation of molecules rather than detoxification (Fig. 4). For instance, GSH conjugation of vicinal dihalogenated compounds produces monosubstituted derivatives, which may in turn cyclize into a highly electrophilic episulfonium ion [20]. Additionally, Monks *et al*. [21] have demonstrated four mechanisms of GSH reactions that lead to bioactivation: (1) formation of directly toxic GSH conjugates e.g. with vicinal dihaloalkanes; (2) cysteine conjugate β-lyase-dependent bioactivation; (3) formation of GSH conjugates of hydroquinone and isothiocyanates; and (4) release of toxic agents from thiocyanates and *N*-methyl-*N'*-nitro-*N*-nitroguanidine.

Often, transferase enzymes like glutathione S-transferase (GST), acetyltransferase, or glucuronosyltransferase (UGT) activate the nucleophilic or electrophilic positions of a co-factor in the conjugation reaction. Meanwhile, glucuronidation and glutathione-S-conjugation are the major phase II pathways of xenobiotic transformation in mammals [18]. Glucuronidation tends to involve conjugation of electron-reach nucleophilic heteroatoms, such as O–, N–, and S– sites (Fig. 5a). Conversely, GSH conjugation features an enormous array of substrates, namely electrophilic xenobiotics or biotransformation products. GSH is found in high concentration in most living cells and participate in a variety of vital intracellular pathways; an important protein, it contains a tripeptide sequence of γ-glutamic acid (Glu)-cysteine (Cys)-glycine (Gly) (Fig. 5b).

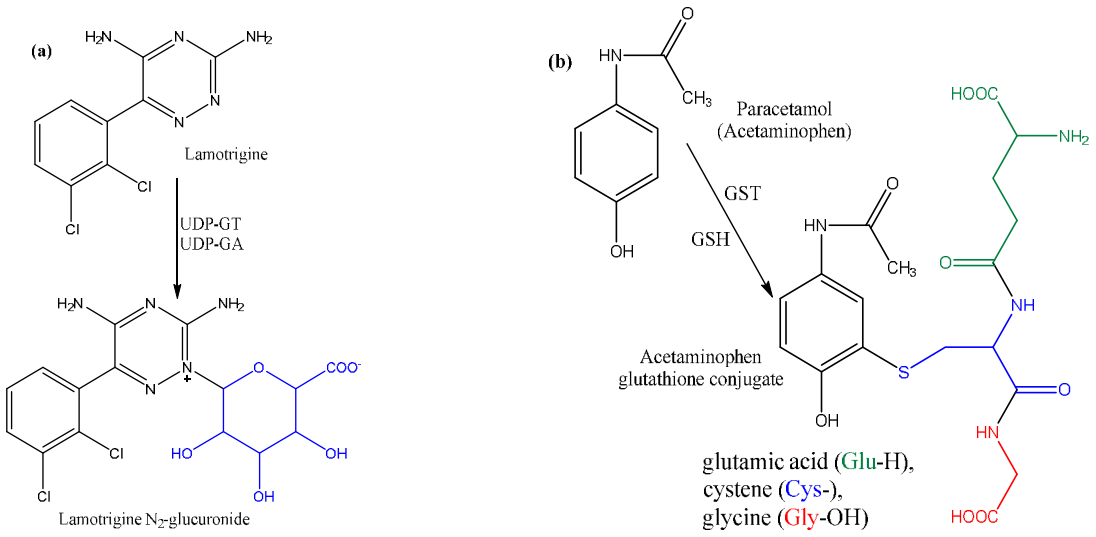

Fig. 5 Conjugative phase II metabolism by glucuronidation (a) and glutathione S-conjugation (b)
UDP-GA – uridine 5'-diphospho-glucuronic acid; UDP-GT – uridine 5'-diphospho-glucuronosyltransferase

The thiol functional group of –Cys– is electron-rich and radially conjugated with electrophilic molecules. Furthermore, GSH functions as a scavenger of harmful electrophilic compounds produced during the metabolism process. In this context, most reactive oxygen species (ROS) are generated during mitochondrial oxidative metabolism, as well as a cellular response to xenobiotics. Sequential reduction of molecular oxygen through the addition of electrons leads to the formation of a number of ROS, including: hydrogen peroxide (H_2O_2), superoxide ($\bullet O_2^-$), peroxide ($\bullet O_2^{-2}$), hydroxyl radical ($\bullet OH$), hydroxyl anion (HO^-), hypochlorous acid (HOCl), peroxynitrite ($ONOO^-$) and nitric oxide ($NO\bullet$) [22]. Hence, these reactive species are tightly regulated by a variety of proteins. Glutathione peroxidase enzymes catalyse the detoxification of these ROS by conjugation with GSH. Reaction with ROS molecules oxidises GSH; however, the reduced form is regenerated in a redox process by an NADPH-dependent reductase enzyme. Apart from the above endogenous reactions, numerous exogenous stressors, such as tobacco smoking, pollutants, organic solvents, drugs and pesticides lead to production of harmful ROS. In this context, $\bullet OH$ is shown to be the most reactive species [23].

1.1.2. Abiotic Transformation

Xenobiotics and their by-products enter environmental compartments either through direct contact (e.g. agrochemicals and personal care products) or indirectly through excretion (e.g. pharmaceuticals) [8]. Once they enter the environment, these compounds undergo different physicochemical processes that transforms them into their TPs. Natural and man-made processes, such as photodegradation, thermal degradation, hydrolysis, industrial processes (e.g. waste treatment plants, disinfection treatments) and atmospheric changes convert the parent compounds to their TPs. Furthermore, day-to-day activities, such as cooking, can lead to degradation of organic molecules. As an example, some widely used water treatment technologies, known as 'advanced oxidation processes', that are based on ozone, UV, electrochemistry, plasma or sonolysis, are shown to cause degradation of organic pollutants into their TPs [24].

There are currently intensive scientific efforts aimed to develop more effective treatment methods and catalysts. These include Fenton reagents (Fe^{2+}/H_2O_2), photo-assisted Fenton ($UV/Fe^{2+}/H_2O_2$), UV/Fe^{3+}-oxalate/H_2O_2, photocatalysis, O_3/H_2O_2, Mn^{2+}/oxalic acid/O_3, UV/H_2O_2, O_3/UV, chlorination, among others, and have been used for the treatment of organic traces

found in water and other wastes [25-37]. These methods are based on a common objective, which is to complete mineralisation of contaminants into CO_2, water, inorganics or harmless TPs [36]. Meanwhile, it is worth mentioning two obstacles in such abiotic transformation processes: their efficiency and the effect of the treatment mechanisms. Regarding the former, degradation kinetics of the parent compounds, as well as the cost and time, are taken into account. The effect of treatment, on the other hand, represents a growing concern these days: *what type of TPs could be produced? How are TPs characterised in their stability, persistence, physicochemical properties, toxicity and side reactions?* These are pertinent questions for a variety of man-made abiotic transformation processes [24, 38]. Although many effective treatment methods are available, they are not realistic or straight-forward for all compounds either because they cannot be completely degraded or form more toxic TPs than the parent compound. For example, disinfectant by-products (DBPs) pose an interesting issue that should be addressed from a health perspective. Wang *et al*. identified many halogenated DBPs that are linked to cancer during treatment of chlorophenols [39]. Furthermore, acrylamide and its metabolite glycidamide are carcinogenic and genotoxic compounds formed during high-temperature (+120 ^{0}C) cooking. They are formed by the Maillard reaction from naturally available sugars and amino acids in different foodstuffs [40]. Therefore, in any man-made abiotic transformation process, it is critical to consider the efficiency of degradation of the parent compound and identify the TPs associated with health risks [24]. For instance, the formation of chloroform during triclosan chlorination [41], genotoxic *N*-nitrosodimethylamine during ozonation of a fungicide tolyfluanide [42] and estrogenic compounds during quinoline UV-photolysis [4] involve production of TPs that are more toxic than their parent compounds.

1.2. Pesticide Residues and their TPs

The first use of synthetic pesticides is dated back to 1940. In that era, pesticides such as DDT were directly sprayed on humans to kill lice (Fig. 6a, b). Moreover, until recently, some developing countries permitted spraying of DDT over cattle and the environment to kill ticks and mosquitos [43].

Fig. 6 Soldier in an Italian home spraying a mixture of DDT and kerosene to control malaria, 1945, © National Museum of Health and Medicine, USA (a) and a nurse spraying DDT onto a child's hair to kill lice © Stavanger Museum, Norway (b)

Nowadays, meeting the world's food requirement is unthinkable without the application of these agrochemicals. In 2012, global pesticides usage accounted for £6 billion per annum ($56 billion in total) [44]. Agrochemicals are a large variety of different compound classes (pesticides and plant growth regulators) with diverse properties and applications. Among them, pesticides are widely used in the agricultural sector to kill, reduce or repel pests (e.g. insects, weeds, rodents and fungi) that threaten public health and the economy. In 2014, global pesticide usage comprised approx. 47.5% herbicides, 29.2% insecticides, 17.5% fungicides and 5.5% other chemicals (nematicides, rodenticides, acaricides and molluscicides). In the EU, pesticide usages comprises approx. 44% fungicides, 33% herbicides, 5% insecticides and 18% other chemicals; a total of 400,000 tons per annum [45].

Despite their benefits for agricultural productivity, pesticides pose a threat to food quality and safety. Although they are widely regulated by governmental and non-governmental authorities, pesticides continue to be a major concern regarding food safety. As pesticides come into direct contact with terrestrial animals and plants, their consumption is virtually unavoidable. According to the Rapid Alert System for Food and Feed (RASFF) of the EU 2016 annual report, pesticide residues are ranked third in terms of risk to food safety [46]**.** This year alone, 236 cases of pesticide contamination have been reported by different EU member states [47-48]**.** In accordance with this, the European Food Safety Authority (EFSA) 2016 report revealed that 96% of samples analysed this year were within legal limits, with 51% free from

quantifiable pesticide residues [49]. Currently, the EU regulates the legal maximum residue level (MRL) of pesticides under directives No.1107/2009, 396/2005. The Codex Alimentarius Committee on Pesticides (CCPR) is also responsible for establishing MRLs for pesticide residues in foodstuffs that are imported into EU through international trade [50]. There is, therefore, no doubt that the EU employs successful methods of ensuring food safety and security. However, the opposite is true for most developing countries; there, most people drink untreated water and used pesticide containers for household purpose. Needless to say, pest management is rarely practiced or not at all. Although widely regulated in developed countries, contaminated foodstuffs from these developing countries find their way into the EU.

Pesticide residues are shown to bioaccumulate in living organisms over a long period of time after exposure. For instance, triadimefon fungicide bioaccumulates in four isomeric forms [51]. Persistent organic pollutants (POPs) are mostly of low water solubility, lipophilic, can spread across long distances, concentrate in marine animals, persist in the environment and accumulate in the food-chain. To mention a few, aldrin, dieldrin, chlordane, DDT, heptachlor and endrin are POPs that are banned in EU by the Stockholm convention from 2004 due to their persistency and bioaccumulation in the environment. However, some of these POPs are still in use in developing countries [52] and can change their form based on seasonal variation. For example, Mackintosh *et al*. identified 45 DDT-related bioaccumulated compounds from dolphin serum using GCxGC-TOF/MS. In their report, they showed that 80% of the TPs are currently not monitored, 33% are produced by degradation and 77% are yielded by isomerisation [53]. Thus, pesticides can degrade, bioaccumulate, undergo metabolism or change into different isoforms.

Like other pharmaceuticals, pesticides undergo various biotic and abiotic transformation processes. Multiple stressors in biota or environmental compartments result in the transformation of the parent residue into a new product that may be more toxic than the parent compound [24, 54]. For example, Westlund *et al*. found TPs produced from pesticides during ozonation of water are disruptive to endocrine function [55]. The following sections will focus on the current status and analytical challenges of studying TPs of pesticides in real samples. In addition to the parent residue, TPs of pesticides could contaminate animal- and plant-based foods. Bioaccumulation of pesticides and their TPs in aquatic animals is highly

common [56-58]. After the parent compound or its TPs enter a living organism, they become metabolised and disrupt cellular function. Furthermore, reaction of TPs with native biomolecules can result in acute or chronic toxicity. For this reason, gaining more comprehensive knowledge of the types of TPs of pesticides and their mechanisms of formation is of utmost importance.

Several regulatory bodies currently control the MRLs of pesticides globally. However, these regulations do not concern the MRLs of pesticide TPs included in food and environmental risk assessments. Hence, little is known about TPs and their mechanisms, regardless of their frequent occurrence in food products [59], water bodies [60] and animals [61-62]. Besides this, most studies on pesticide residues in different matrices focus on the parent compound and few investigate the TPs [1]. One of the many reasons for this is the lack of experimental reference standards for TPs [60, 63]. For instance, Bauer and co-workers detected many TPs of azoxystrobin, difenoconazole and thiacloprid in vegetables [59]. However, they were able to confirm only three TPs of thiacloprid (thiacloprid-amide, thiacloprid-O-analogue and 4-hydroxythiacloprid) due to the lack of commercially available standards. Zhang *et al*. investigated *N*-dealkylation, nucleophilic substitution of chlorine and many glucuronidation metabolites of forchlorfenuron (a total of 17 TPs) in kiwifruit using untargeted time-of-flight-MS approach [58]. From similar studies it has been shown that the complexity of matrices, instability (immediate degradation or conjugation) and varied concentrations of TPs in a specific matrix pose challenges to their investigation in real samples [64].

Two methods are usually employed to investigate TPs; targeted and untargeted. The targeted approach involves detecting known TPs using commercially available authentic standards or analytical techniques to assess their structures. Although this approach is more accurate, it is limited to known TPs and cannot identify novel compounds. More precisely, the method requires quantification of the parent pesticides/TPs and knowledge of the respective MRLs in a certain commodity in order to predict the health risk for consumers. The untargeted approach, on the other hand, is useful for identifying unknown TPs. After the sample is prepared, the novel TPs are identified using analytical techniques such as liquid chromatography (LC) coupled with different mass spectrometry (MS). In the review by Pico and Barcelo on current challenges and analytical techniques for TP investigation in environmental and food samples, LC-MS is chosen as most TPs are hydrophilic and polar [65].

Modern MS techniques, such as high resolution, high mass accuracy and mass fragmentation, enable the identification of TPs without the need for authentic standards. However, confirmation of results by NMR or authentic standards is still desirable in this case [1].

The focus of this thesis is to investigate biotic and abiotic transformation processes of two model pesticides;: chlorpyrifos (Fig. 7a) and fluopyram (Fig. 8). These pesticides belong to different groups and were selected based on their usage and associated health risk in the EU.

1.2.1. Chlorpyrifos

O, O-diethyl-O(3,5,6-trichloropyridin-2-yl)-phosphorothioate, or chlorpyrifos (CPF), is an organophosphate (OP) insecticide currently approved for use in the EU (until the next reviewing period in January 2019). Since its discovery in 1965 by the Dow Chemical Company, it has been used under different trade names such as Brodan, Dursban, Dowco and Lorsban – accounting for £8 million in production costs per annum. CPF is also one of the five most frequently detected pesticides in the EU food system, with 208 alerts raised by RASFF related to CPF residue occurrence in different food commodities this year alone [48]. A 2017 report showed that CPF was found in 20% of investigated fruit samples in UK schools, despite no authorisation for its use in the country. Similarly, in 2016 CPF was found in 8 out of 10 tested water basins in Spain. Many European countries, such as Germany, Denmark, Finland, Ireland and Sweden have started to ban CPF [66]. The US-Environmental Protection Agency (EPA) is currently reviewing a ban on CPF usage. Although different actions have been taken by authorities, CPF alone is included in 224 formulated products available in different countries [67]. The EU guide limits CPF content to a range of 0.01 – 3.0 mg/kg in fruits and 0.1 – 5.0 mg/kg in spices; however, the approved content range for TPs is not specified [68]. Because of this frequent detection of CPF, the EU commission body has changed the MRLs of CPF and CPF-methyl (CPFM) in several food items as of May 2018 [69].

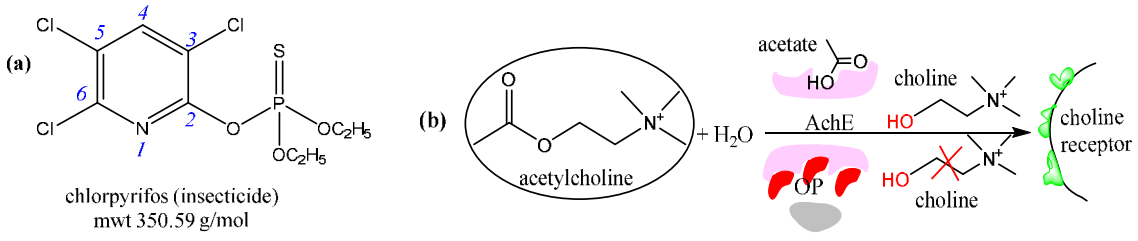

Fig. 7 Molecular structure of chlorpyrifos (CPF) (a) and schematic diagram of AchE inhibition by OPs

Like other OPs, the primary mechanism of insecticidal action of CPF is inhibition of the enzyme acetylcholinesterase (AchE), which regulates action of the neurotransmitter acetylcholine (Ach) in the central nervous system. AchE degrades Ach to produce choline and acetate, a reaction important for regulating the activity of cholinergic synapses underlying numerous vital brain functions (Fig. 7b). AchE is inactivated by formation of a covalent bond between the active site of the enzyme and the OP pesticide, which results in pyrolysis and can disrupt neural processes (Fig. 7b). CPF inhibits virtually all plasma AchE and more than 30% of red blood cell cholinesterase before the brain becomes clinically affected, leading to overt symptoms of neurotoxicity. CPF can also impede neurodevelopmental processes in children, who are more vulnerable to its toxicity [66, 70].

Regarding the biotic and abiotic transformation processes of CPF, the pesticide is transformed into its active oxon metabolites, inactive trichloropyridinol (TCP) and dialkylphosphate (DAPs) metabolites in response to both biotic [71-75] and abiotic stressors [33, 76-78]. Among these, diethylphosphate (DEP) and diethylthiophosphate (DETP) are known biomarkers used for forensic investigation of OP exposure or environmental contamination. Its metabolism in *in vitro* (e.g. in microsomes, hepatocytes or cell culture) and *in vivo* (in laboratory animals) has been extensively studied [72-75, 79-80]. Additionally, its abiotic transformation processes have been investigated mostly using photocatalytic [81-85] and, to a lesser extent, by electrochemical methods [86]. The same is true regarding the presence of the parent CPF residue in food and environmental compartments. The type of CPF TPs found vary greatly, depending on the applied method. For example, Supreeth and Raju have detected further hydrolysis of DETP and DEP TPs to thiophosphate and monoethylphosphate in bacteria and fungi [71]. Furthermore, CPF and its active TP, oxon, is metabolised during phase II via conjugation with glucoside, glutathione, and sulfonation [72]. However, very few studies have assessed the TP content in food. Hence, CPF was chosen here as a model insecticide, the biotransformation mechanisms of which were investigated by electrochemistry-mass spectrometry (EC/MS).

1.2.2. Fluopyram

The second model compound used in this work is a fungicide, *N*-[2-[3-chloro-5-(trifluoromethyl)-2-pyridinyl]ethyl]-2-(trifluoromethyl)benzamide – also called fluopyram

(FLP) (Fig. 8). It is a relatively new fungicide developed by Bayer Crops GmbH (Germany), which entered the market in 2013 under the trade name Luna Privilege. FLP is a broad-spectrum fungicide used to fight fungal species during cultivation and post-harvest/storage of fruits and vegetables. The EU approved its use since February 2014 and this decision will be re-evaluated in January 2024. The EU-permitted MRL range is 0.01 – 20.00 mg/kg in fruits and vegetables. FLP exists as two technical products approved in the US, 264-1077: fluopyram technical and 432-1538: fluopyram 500 SC [67].

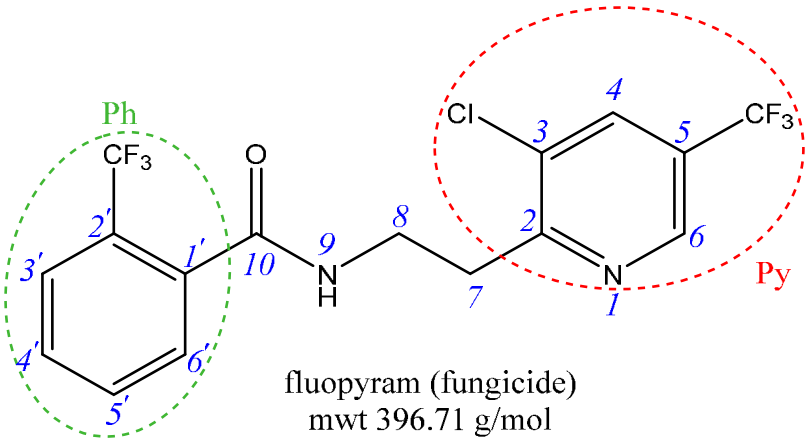

Fig. 8 Molecular structure of the fungicide fluopyram (FLP)

It is a succinate dehydrogenase inhibitor (SDHI) that blocks the active site of the enzyme. SDH is mainly found in bacterial cells and in the inner mitochondrial membrane of eukaryotes; the enzyme catalyses the oxidation of succinate to fumarate (Fig. 9a) as part of the citric acid cycle and the is the only enzyme also involved in the electron transport chain in the mitochondrial membrane (Fig. 9b). In the first step of catalysis, two electrons are produced by oxidation of succinate, which is then used to reduce ubiquinone to ubiquinol (Fig. 9c) – an important step for pore growth and elongation of many fungal species.

Many SDHI fungicides, including FLP, block the active sites of SDH to prevent the oxidation of succinate to fumarate. Although these fungicides are structurally diverse, they have one common essential feature – the amide bond. The other parts of the molecule are the head (or core), attached to the carbonyl of the amide (trifluoromethylphenyl-; Ph- in Fig. 8), the hydrophobic rest (chloro-(fluoromethyl)pyridine-; Py- in Fig. 8) and the linker, which attaches the amine to the hydrophobic tail (ethyl in this case). Notably, unlike the amide bond, these parts can vary between different fungicides.

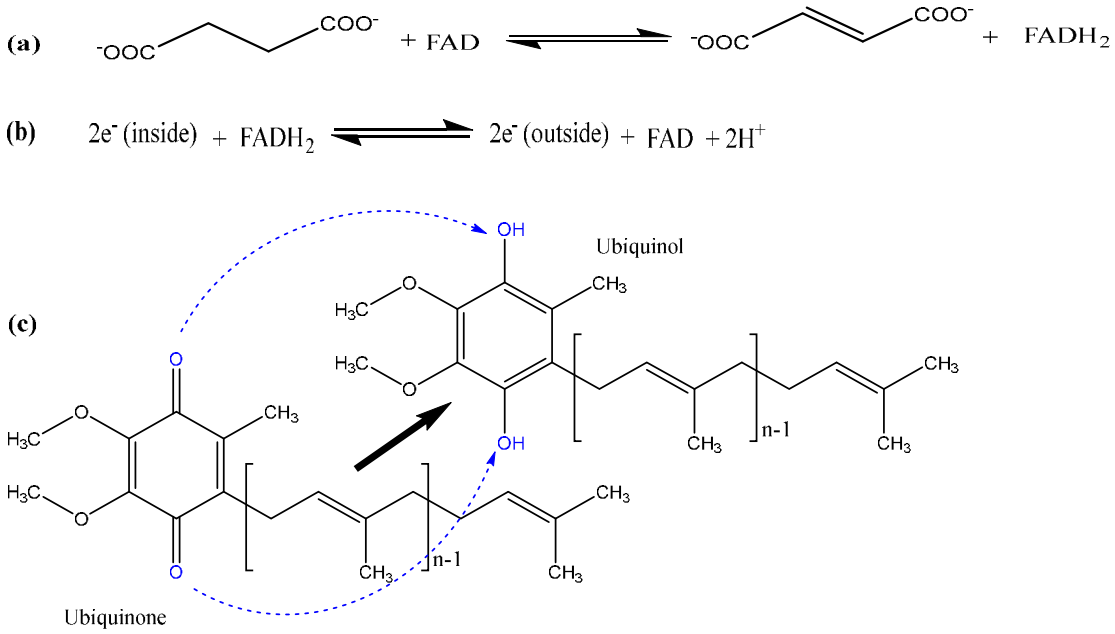

Fig. 9 Mechanism of SDH-mediated oxidation of succinate to fumarate: oxidation (a), electron transport (b), and ubiquinone to ubiquinol reduction (c) steps

The head of the molecule is important in enabling stable interaction with the SDH active site, which serves as a pocket for the ubiquinone. By doing so, the fungicide blocks access of the enzyme to the substrate and prevents further cyclising of succinate oxidation [87].

The transformation mechanisms of FLP and its TPs have not been thoroughly investigated, as it is a new fungicide. However, its toxic potential has been highlighted in preliminary reports of the EFSA and Australian Pesticides and Veterinary Medicines Authority (APVMA) [88-89]. FLP is metabolised through hydroxylation, *N*-dealkylation and conjugation with glucosides. Wei *et al*. also demonstrated *N*-dealkylation of FLP in vegetables and detected trifluoromethylbenzamide and (3-chloro-5-trifluoromethylpyridin)-yl acetic acid metabolites [90]. Regarding abiotic transformation, Dong and Hu showed that for FLP, lactam, Cl– substitution by H–, and HO– are the main photodegradation products (PPs) upon photocatalytic exposure [91]. However, to the best of the authors' knowledge, no other investigations of FLP metabolism and its environmental fate exist in literature. The fate and transformation mechanisms of FLP by liver microsomes, oxidative stress or direct photolysis remain to be elucidated, as well as its occurrence in different environmental and food compartments. Thus, one of the goals of this project was to use EC/MS as a method for thorough investigation of FLP biotransformation mechanisms and UV-photodegradation for identification of abiotic TPs.

1.3. Analytical Methods for Generation of TPs

In addition to the analytical instruments currently used for identification and quantitation of TPs, development of other experimental approaches for effectively generating TPs (both in variety and abundance) is important so as to enable investigation of the fate of organic molecules in both biotic and abiotic systems. Abiotic and biotic transformation processes have been successfully simulated in the laboratory for centuries. The latter mainly involves enzymatic approaches in laboratory animals or *ex vivo* [92] and, more recently, non-biological (in-silico and organ-on-chips) approaches (**Fig. 10**) [93-96]. Since biological samples are complex matrices and require time-consuming preparation steps, numerous groups have aimed to develop analytical methods that can overcome these limitations.

On the other hand, the array of factors underlying abiotic transformation processes would be hard to recapitulate experimentally; this would require precise simulation of each condition. For instance, UV irradiation cannot sufficiently represent ozonation or Fenton oxidation reactions occurring in a real environment. The next section of this thesis will, therefore, discuss application of enzymatic and non-enzymatic approaches for investigating the above. In particular, EC/MS will be discussed as a non-enzymatic simulation method that has both pros and cons compared to biological methods.

1.3.1. Enzymatic Methods/*In Vivo* and *In Vitro*/

The immune system of mammals is sensitive to foreign compounds and is able to convert them into non-harmful products as part of their elimination from the body. This is largely mediated by CY and GST enzymes. *In vivo* (laboratory animals) and *in vitro* (microsomal assays) experiments have been used to study such reactions. For instance, biofluids, such as urine and blood, from animals can be exposed to target compounds *in vivo* and subjected to MS or LC-MS to identify the metabolites produced. Tests can also be carried out in laboratory animals, such as horses, dogs, pigs, mice, rabbits and chicken [97]. However, use of animals is expensive and training animals or preparing biological samples can be time-consuming. There are also ethical considerations to animal use, which poses a further challenge to using *in vivo* approaches for investigations into biotransformation processes.

In vitro methods use whole organs, cells or other bioassays obtained from a living organism [98]. In general, foreign compounds are mostly metabolised in the liver by CYP450. *In vitro*

human assays, including supersomes, microsomes, S9-fraction, cell lines, transgenic cell lines, primary hepatocytes and organotypic liver slices can be used to evaluate generated metabolites [92]. These days, liver microsomes from human, rat, horse or fish are even commercially available. However, standards for such metabolomic analyses are currently unavailable. Hence, a non-target screening approach, along with statistical analyses (e.g. multivariate), is normally used to identify or predict metabolites formed in assays. Since both the above *in vivo* and *in vitro* methods involve enzymatically catalysed reactions, the selectivity and specificity of the reactions or of the produced metabolites, will vary greatly compared to non-enzymatic experiments. Unlike *in vivo* work, *in vitro* methods enable sufficient incubation conditions for abundant metabolite production and screening. However, the financial costs of biological samples, complex biological matrices and experimental consumables, as well as the ethical considerations surrounding the use of animal (or especially human) samples, can limit the above experiments [99]. Moreover, most phase I metabolites are formed through a series of catalytic reactions involving short-lived intermediates that become immediately conjugated to phase II; this can be difficult to model experimentally. On the other hand, bacterial CYP450 are non-expensive to use, do not pose ethical issues and allow for large-scale *in vitro* incubations [100].

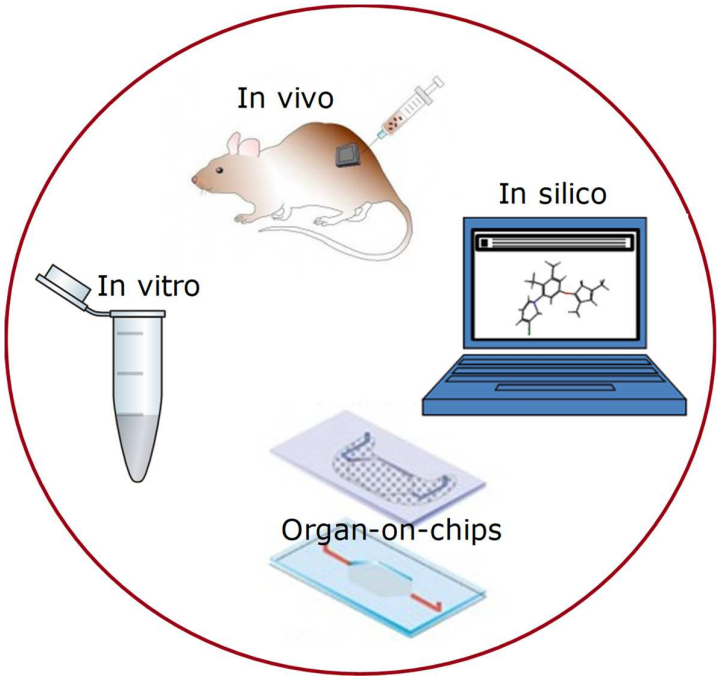

Fig. 10 Schematic of experimental metabolic methods; *in vivo*, *in vitro*, in silico, and organ-on-chips approaches

Numerous studies have been conducted over decades to attempt to solve the above problems. The development of in-silico technology is one of such efforts, which can predict and simulate

the fate of an organic molecule in both biological and abiotic systems using artificial intelligence [93, 101]. Additionally, microfluidic systems, or 'organ-on-chips'/'chips-on-organ', are major scientific developments that represent an alternative method for predicting biotransformation processes [96]. Obviously, such methods cannot fully recapitulate naturally occurring transformation processes; nevertheless, they are preferred based on their superiority to the aforementioned conventional animal models in terms of experimental time, cost, ethics and matrix burden. In line with this, EC/MS has received considerable attention in the last two decades – in particular as an alternative technique for prediction of redox metabolic processes. Redox reactions are the most part of all cellular metabolic mechanisms; these can be easily reacreated in a simple electrochemical cell by keeping the applied potential near to the Gibbs free energy of the bonds. Nowadays, MS is the superior and most widely used technique for identification, characterisation and quantification of TPs from biotic and abiotic processes. Therefore, the EC/MS techniques could achieve efficient investigation of redox metabolisms in a matrix-free environment.

The main aim of this work is to establish online EC/MS or EC/LC/MS as an alternative method to investigating biotransformation processes, as well as UV-photolysis for identification of abiotic transformation products. The principles and strategies behind these two approaches will be reviewed in detail in the following section.

1.3.2. Non-enzymatic Methods: Photodegradation and EC/MS

Besides conventional *in vivo* and *in vitro* experiments, simulation of both biotic and abiotic transformation processes using non-biological models is common. These methods do not use biological or environmental samples, but mimic naturally occurring processes by applying synthetic stress. For instance, exposing parent compounds to UV light, heat or advanced oxidation has been widely used to simulate natural abiotic processes [34, 36, 102].

Up until now, several photolysis-based methods have been developed to simulate PPs. For instance, hydroxylation and -OH oxidation PPs of carbofuran were reported by Tomašević *et al*. after irradiation by UV/ZnO [103]. Furthermore, degradation of herbicide sethoxydim by UV in aqueous media [104], bentazon by UV-A/H_2O_2 [105], TCP by UV-A/TiO_2 [76], FLP by UV-A/fluvic acid, TiO_2, Fe^{3+} or NO_3^- [91], and CPF by UV/H_2O_2 [81] are other examples of using photocatalytic methods to generate TPs. Based on the radiation source (visible, UV-A, UV-B

or UV-C) and chemical composition, the type and mechanism of TPs from a single compound may vary greatly. Another commonly used method is chemical oxidation. This includes strong oxidizing agents, like permanganate (MnO_4^-), O_3, H_2O_2, O_3/H_2O_2, chlorination, Fe^{2+}/H_2O_2 (Fenton reactions) and Mn^{2+}/oxalic acid/O_3 [36, 106]. Often, both photolysis and chemical methods are collectively considered as advanced oxidation processes (AOPs). However, their principles and reaction mechanisms vary. The Fenton reaction is depicted below (1.2):

$$Fe^{2+} + H_2O_2 \rightarrow Fe^{3+} + HO^- + \bullet OH \qquad (1.2)$$

whereby important hydroxyl radicals are produced for nucleophilic attack on many pollutants. The regeneration of Fe^{2+} from Fe^{3+} is mediated by chemical reduction with ascorbic acid or an electrochemical reaction. Subsequent modifications, such as Fenton-like (1.3) or photo-assisted Fenton (1.4), were later developed.

$$Fe^{3+} + H_2O_2 \rightarrow FeOOH^{2+} + H^+ \qquad (1.3)$$

$$FeOOH^{2+} \rightarrow HO_2 \bullet + Fe^{2+}$$

$$Fe(OH)^{2+} + hv \rightarrow Fe^{2+} + HO \bullet \qquad (1.4)$$

Several studies have aimed to modify or create a newer, more effective methods for treating pollutants. Gamma radiolysis is another, more efficient advanced oxidation mechanism used to complete mineralisation of organic pollutants; it is based on the generation of radicals (HO• and H•), highly reactive electrons (e_{aq}^-), ions (e.g. HO^-) and neutral molecules (e.g. H_2, O_2, or H_2O_2) by exposing water to high energy gamma radiation (1.5 to 1.8).

$$O_2 + e^- \rightarrow \bullet O_2^- \qquad (1.5)$$

$$2H^+ + \bullet O_2^- + \bullet O_2^- \rightarrow H_2O_2 + O_2 \qquad (1.6)$$

$$H_2O_2 + e^- \rightarrow HO^- + \bullet OH \qquad (1.7)$$

$$2H^+ + 2e^- + H_2O_2 \rightarrow 2H_2O \qquad (1.8)$$

These chemical entities are radiolytic products that subsequently modify and degrade the pollutant molecules [36].

Often, photocatalytic methods use a metal oxide (e.g. ZnO, TiO_2) as a catalyst and oxygen as an oxidizing agent. Under UV, the metal oxide produces an electron, which can reduce some metals, along with dissolved O_2, and produce superoxide radicals ($O_2\bullet^-$). During this process, H_2O molecules are converted to HO•. This approach is of value to oxidation processes due to the high concentration of radicals formed from water [36]. These methods generally involve

degradation kinetics, remediation of a contaminated environment, disinfection (to kill microbials), waste treatment and/or identification of TPs. Importantly, all methods are designed to produce ROS for degradation of pollutants. However, application of photocatalytic and chemical methods for mimicking biotransformation processes in the lab is limited for three main reasons. First, they are strong oxidizing agents which complete mineralisation of some organic molecules; thus, it is difficult to control the reactions required for the production of metabolites. Second, many ROS are produced and can induce unintended reactions. This leads to the production of TPs that are not realistic in biotransformation processes (e.g. multiple hydroxylations and subsequent degradation of metabolites). For example, photocatalytic reactions prefer modification of halogenated positions, which does not occur in CYP450-catalysed metabolism. Finally, advanced oxidation methods are not equipped with automated detection techniques as of yet (which would be required for separation and characterisation of the TPs).

Electrochemically-based redox methods have been widely used to mimic both biotic and abiotic transformation process for many years. Hussain *et al*. studied the mechanism and kinetics of sulfamethoxazole degradation by photo-assisted electrochemistry [107]. Many electrochemical redox treatments of pollutants follow either direct or indirect methods. In direct redox processes, the electron exchange is between the target organic compound and the surface of the working electrode, while in indirect processes targeted compounds are oxidized/reduced by electrochemically-generated redox reagents (intermediates). Hence, the indirect method is mostly useful for preventing wear of electrodes with time. Two types of reactions could occur during electrochemical oxidation of organic contaminants: oxidation of the target compound ($R \rightarrow RO + e^-$) and complete mineralisation ($R \rightarrow CO_2 + H_2O + e^-$). Compared to photocatalytic or chemical processes, electrochemical methods are cheaper and green for the environment as they utilise electrical energy instead of chemicals [35, 108].

As mentioned, redox processes are vital to the function of living organisms and these can be experimentally recreated using electrochemistry. In support of this, Evan showed single-electron and two-electron transfer mechanisms in EC and their correlation with the molecular structure of compounds [109]. Although using EC to understand the physiological phenomenon in a living organism goes back by many decades, difficulties in characterising the products and controlling the reaction variables have limited its bioapplication. Recently,

the development of EC/(LC)/MS has garnered considerable attention as they enable online production and characterisation of products. The background, principles and current applications of EC/(LC)/MS will be discussed in the next sections.

(a) Background and application of EC/MS

The idea of EC online coupling to MS is not a novel one. In early 1970, Bruckenstein *et al*. used a porous working electrode (WE) for the detection of volatile products of electrochemical reactions with electron ionization (EI)-MS [110]. In 1986, redox reactions of *N*, *N*-dimethylaniline by Hambitzer and Heitbaum [111] and acetaminophen by Getek *et al*. were studied by coupling EC to thermospray-MS. In addition, the notion of using EC for generation of reactive species to identify bioconjugates of xenobiotics (Phase II metabolites) is dated back to 1989. The same group (Getek *et al*.) investigated GSH and Cys-conjugates of acetaminophen by coupling a coulometric cell with thermospray-MS [112]. In the same year, Volk *et al*. studied electrochemical oxidation of uric acid by EC/thermospray-MS/MS. The same group later scaled up their setup to include an HPLC-column, prior to MS. This was seen as a major milestone by producing, separating and detecting the oxidative products online [113]. In late 1990-2000, the use of EC coupling to ESI-MS significantly increased [114-117]. In 1996, Lu and co-workers developed three-electrode EC cell coupling to ESI-MS and investigated intermediates and products of anodic oxidation of diphenyl sulfide and 9,10-diphenylanthracene, as well as reduction of nitrobenzene [117]. In the same year, Regino and Brajter-Toth developed a thin-layer flow-through EC cell that can avoid the high backpressure of EC/LC/MS configuration [116]. Another interesting study by Jurva *et al*. compared the metabolic oxidation of numerous drugs by CYP450 using EC/ESI-MS [118]. In this work, the authors found that EC/MS can mimic the oxidative metabolites formed by SET mechanisms (e.g. N–dealkylation, S–oxidation, P–oxidation, alcohol oxidation and dehydrogenation). CYP450 processes take place via HAT (e.g. O–dealkylation and aromatic hydroxylation) and, therefore, require a higher potential for stimulation by EC/MS. In 2001, and in subsequent years, Karst and co-workers conducted several such studies aimed to mimic drug oxidative metabolism, as well as to miniaturise and automate EC/MS methods [119-125].

Nowadays, EC/(LC)/MS (MS, MS/MS, HRMS) are heavily involved in predicting of oxidative metabolites. In addition to recapitulating metabolism, EC/MS has many other life science applications, such as peptide and protein modification [126-127] and disulfide bond cleavage

[128]. However, these applications are restricted to drug metabolism. Very few studies of oxidative metabolism of non-pharmaceutical compounds have been conducted, including: PAHs [122, 129], mycotoxins [119, 130], and pesticides [131]. Extending the use of this technique for simulation of pollutant fate is, therefore, an exciting idea.

Electrochemistry is also used by researchers to synthesis of numerous vital compounds, as demonstrated by Mohle *et al*. [132]. In this regard, EC has been used in industrial processes to synthesis organic products. For instance, synthesis of benzaldehyde from dimethoxylation of 4-tert-butyltoluene and reduction of acrylonitrile to adiponitrile for polyamide production (e.g. nylon-6,6 production) are such industrial-scale processes. Instead of using reagents, applying electricity to chemical production is green (as no waste is generated) and economically valuable. Furthermore, EC uses environmentally friendly reagents like water as a source of hydrogen or hydroxyl groups, molecular oxygen for oxidation, and CO_2 for carboxylation processes [132]. Thus, EC/MS can be used to synthesise valuable TP standards that are commercially scarce.

Another interesting application of EC/MS is studying bioconjugates of reactive species produced during metabolism. As metabolism produces many short-lived intermediates that can immediately conjugate with biomolecules, such as Glc and GSH (*sec 1.1.1*), conventional *in vivo* and *in vitro* methods are unsuitable. Using EC/MS allows for these reactive species to be detected very rapidly and in clean matrices. Furthermore, these reactive species can be trapped by the biomolecules and conjugates (phase II metabolites) detected by online MS. Since the first report of acetaminophen intermediates conjugating with GSH and Cys by Getek *et al*. in 1989 [112], several other groups have used EC/MS to mimic phase II metabolism. In 2009, Lohman and Karst showed GSH conjugates of toremifene by EC/MS [133]. In 2013, Bussy *et al*. developed the solution phase NMR method to characterise EC-generated unstable intermediates [134]. Büter, Vogel, and Karst have also reported several drug intermediates generated by EC that form adducts with biomolecules [135]. Using EC/MS to mimic conjugative phase II metabolism has two advantages: time efficiency and online characterisation of the products. However, unlike its successful application for recapitulating phase I, it is not as well adapted to conjugative phase II reactions.

(b) In-situ electrochemical phenomena of ESI

A 1992 study by van Brekel and co-workers discussed the electrochemical phenomena in ESI sources of MS [114]. This principle incited wider discussion between six prominent scientists in the field, who have yet to reach an agreement [136]. As reported by Girault *et al*. [137], application of a high voltage during ESI causes the emitter to act as a WE, whereby redox reactions occur radially and can be electrochemical or photo-electrochemical in nature. This concept inspired the idea of using the ESI source for in-situ investigation of biological processes – particularly redox metabolism. For instance, in ESI-MS of peptides, electrochemical tagging of cysteines by in-situ oxidation of hydroquinone into benzoquinone has been widely discussed [138-139]. In-situ monitoring of the electrode-electrolyte interface is in great demand for better understanding of real-time redox processes. Lu, Hua and Long reviewed the possible methods of in-situ analysis of the ESI interface and the different designs for EC cells, which could be configured together in the ESI-chamber [140]. Furthermore, Wang *et al*. developed a method called 'in-situ liquid secondary ion mass spectrometry' (SIMS) using a vacuum-compatible microfluidic EC device [141]. Obviously, understanding the inherent electrochemical processes is very important to the study of oxidative reactive species; however, the challenge lies in controlling the potential. Thus, ex-situ EC cells (separated from ESI) controlled by their own potentiostat are currently available.

(c) Principles and coupling to MS

Depending on the activation energy of chemical bonds, organic compounds are oxidized/reduced upon application of potential energy (Fig. 11a, b). Current (I) is generated by the movement of ions and electrons through the solution and the electrode, respectively. Hence, the overall current passed through the system depends on the rate of the reaction (Red → Ox, electron exchanging between the electrode surface and compounds) and mass transport (related to flow rate). Moreover, I is increased in correlation to the surface area of the working electrode (the bigger the surface area, the more products).

$$I = nFAK[Red] \qquad (1.9)$$

Where, I-current, n-number of electron transferred, F-Faraday's constant, A-surface area of the electrode, K-rate constant, [Red]-concentration of the reactant.

Furthermore, mobile phase composition and pH, the organic modifier and the scan rate play important roles in the type of oxidative products and interferences formed. Although EC/MS-

based metabolite identification is generally clean, interfering artefact products, such as dimers, trimers and proton-bound adducts are very common [142].

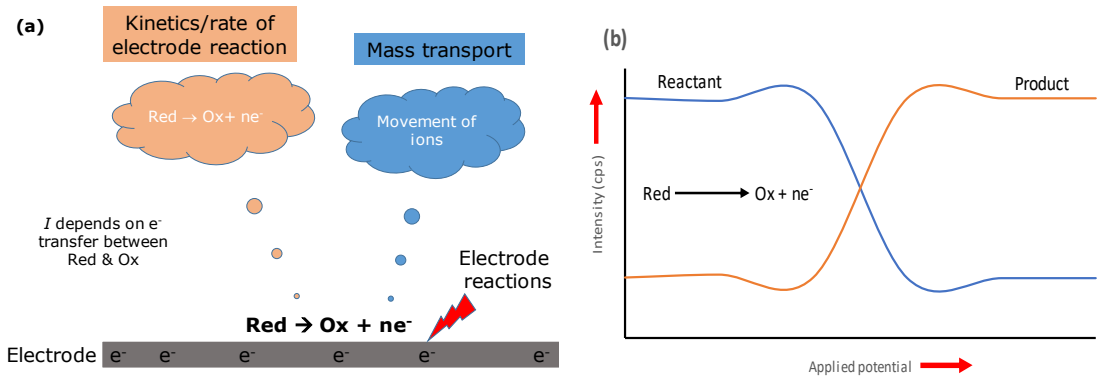

Fig. 11 Schematic diagram of reaction on electrode surface (a) and reactant and product intensity vs applied potential (b)

MS is the most widely applied technique for characterisation and identification of organic molecules in biological and environmental matrices. In particular, MS has profound applications in the field of '-omics' [143]. Hence, coupling of EC to MS creates an opportunity for furthering our understanding of natural processes. Typically, a compound with an appropriate organic modifier and electrolyte solution (e.g. a salt or an acid) is infused into an electrochemical cell consisting of the WE coupled to online MS or LC-MS (Fig. 12a). The oxidative products and other by-products are transferred online to the ESI source of the MS for characterisation. In general, two types of electrochemical modifications can be applied to the compound of interest: direct (between the electrode surface and the molecule of interest) or indirect (between EC-generated intermediates; e.g. HO•, H^+ and organic molecules).

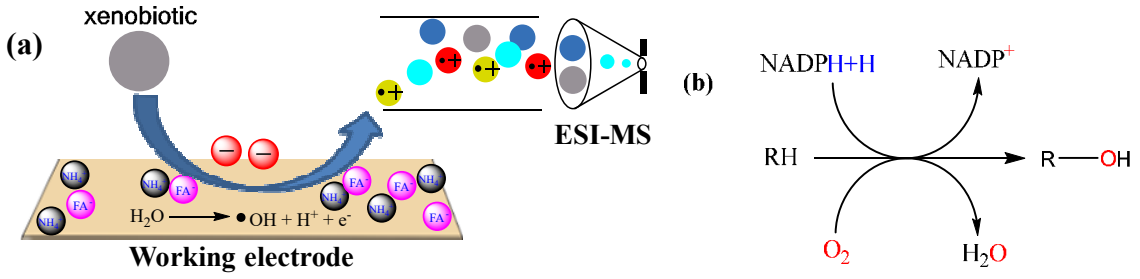

Fig. 12 Schematic diagram of online EC/MS reaction (a) and CYP450 based oxidative metabolism (b)

Anodic oxidation of water from loss of one electron leads to the formation of adsorbed hydroxyl radicals (•OH_{ads}) at the WE surface (1.10).

$$H_2O \rightarrow \bullet OH_{ads} + H^+ + e^- \qquad (1.10)$$

(or) higher oxide formation by active WE (1.11).

$$\bullet OH_{ads} \rightarrow O_{ads} + H^+ + e^- \qquad (1.11)$$

This higher oxide mediates oxidation of organic compounds as (1.12):

$$O_{ads} + R \rightarrow RO \qquad (1.12)$$

The higher oxide can also decompose as $2O_{ads} \rightarrow O_2$. On non-active electrodes, such as boron-doped diamond (BDD), the interaction between the working electrode surface and the HO• radical or another ROS is much lower. Therefore, the oxidation of organic compounds by a BDD electrode can be directly mediated by ROS. This provides an even better advantage, in that the active radicals can react with molecules that are not prone to electron transfer reactions – such as unsubstituted poly aromatic hydrocarbons [144]. Hence, hydroxylation reactions like those catalysed by CYP450 (Fig. 12b) can occur on the WE surface. Its main disadvantage, however, is that complete mineralisation (formation of CO_2 and H_2O) of some organic compounds could occure depend on the applied potential and experimental conditions (1.13).

$$\bullet OH_{ads} + R \rightarrow mH_2O + nCO_2 + H^+ + e^- \qquad (1.13)$$

There may also be a competitive reaction like $\bullet OH_{ads} \rightarrow 1/2O_2 + H^+ + e^-$. It is, therefore, crucial to carefully optimise the applied potential and type of organic modifiers applied, as the production of CO_2, O_2, and/or H_2 gases (from electrolysis of water and mineralisation of organic molecules) results in highly unstable current flow.

In addition to online MS coupling, EC/LC/MS configuration is now becoming a realistic concept. This enables the generation, separation and detection of oxidative products online, which provides additional structural information (retention time of adducts and isotopes). Typically, external valve is used to separate the flowrate of the EC reaction step from the LC separation, which requires a very low flow rate (10-50 µL/min for a longer time of analyte-WE surface interaction). Recent development of HPLC systems, such as nano-HPLC, allows direct coupling without external valve [129, 145].

Different types of flow-through cells that can handle 175 nL to 80 mL samples can be found commercially. Likewise, there are different types of commercially available WEs, including BDD, porous glassy carbon (GC), platinum (Pt) and gold (Au). Usually, a three-electrode cell,

a reference (usually Pd/H_2 or Ag/AgCl) and an auxiliary or counter electrode (from inert metals like Pt, Ti) are used [146].

To reiterate, EC/MS experiments are performed without ethical issues, relatively inexpensively, using clean matrixes and in a short time compared to conventional enzymatic approaches in bioassays. However, as it is non-enzymatic, the EC/MS method is less specific and non-stereoselective than the *in vitro* and *in vivo* approaches. Obviously, not all EC/MS products will be metabolites and these could not be mimicked in a single EC/MS experiment. The online electrochemical generation of pesticide metabolites, which are a focus of this thesis, is one field that could merit from further research in the near future. In addition to oxidative metabolism prediction, EC/MS could be used to enhance detection of many compounds that are difficult to ionise in ESI-MS by oxidising or adding electrochemically active tags. Furthermore, EC equipment is inexpensive and easy to use. We expect the application of EC/LC/MS to further broaden, especially towards determining the fate of xenobiotics by oxidative stress and production of TP standards.

1.4. Research Demands

In view of the shortcomings mentioned earlier, the following three categories of research demands are a current concern in the field of transformation processes of pesticides and EC/MS application.

Biotransformation

- The need for a fast, clean, cheap and reliable method for prediction of metabolites
- Replacing ethical concern of *in vivo* and *in vitro* methods by non-enzymatic approaches
- The need for methods which are able to detect short-lived reactive species

Pesticides and their TPs

- Identifying the TPs in both biotic and abiotic processes
- Investigating and continuous monitoring of TPs of pesticides in foodstuffs and the environment
- Lack of authentic TP standards
- Unavailability of MRLs for TPs

EC/(LC)/MS techniques

- The need for miniaturisation and automation
- Methods to quantify TPs
- Extending its application to routine food and environmental research
- Extending its application to the synthesis of organic compounds

1.5. Objectives and Scope of the Thesis

The overall objective of this thesis was to establish EC/MS as a powerful method to study biotransformation processes. The specific aims of this dissertation are consisting of the following three different phases:

i. The first objective was to mimic biotic transformation processes using a purely instrumental approach: EC/(LC)/MS. This includes identification of TPs and their formation mechanisms. As a subcategory to this objective, the project also sought to establish the formation mechanism of each of the oxidative metabolites. Thus, the aims for this specific objective were to: (1) elucidate oxidative transformation products (phase I and phase II) of CPF and FLP using online EC/(LC)/MS; (2) simulate the oxidative transformation products of CYP450 metabolites in liver microsomes (HLM and RLM), and (3) predict the mechanism/metabolism pathways of identified metabolites.
ii. The second phase of this thesis was to identify abiotic transformation processes of the targeted pesticides (CPF and FLP) using direct photolysis as a model system. The aim was to elucidate PPs of the targeted pesticides and identify the degradation mechanisms after exposure to UV-light.
iii. The last objective of this thesis was to extend the application of EC/MS for investigation of TP residues in real samples. The project aims to synthesis TP standards using EC, which could be used for authentication of TPs in real environmental and biological samples.

2. MATERIALS AND METHODS

2.1. Reagents and Chemicals

Analytical standard of CPF (99.7% purity), HPLC grade methanol (MeOH, 99.85%) and acetonitrile (ACN, 99.90%), as well as extraction and clean-up kits were purchased from Th. Geyer (Berlin, Germany). Analytical standard FLP (99.9% purity) and reagent-grade GSH were purchased from Sigma-Aldrich (Steinheim, Germany). Nicotinamide adenine dinucleotide phosphate (NADPH) and ammonium formate (NH_4FA) were obtained from Fluka Chemie Merck (Buchs, Switzerland). Other chemicals, including formic acid (HFA) and $MgCl_2.6H_2O$ from J.T. Baker (Arnhem, The Netherlands), n-nonyl-β-D-glucoside (n-Glc) from Anatrace (Maumee, USA), and anhydrous $MgSO_4$, K_2HPO_4/KH_2PO_4, KCl, and NaCl from Merck (Darmstadt, Germany) were purchased in their p.a. grade. Ultrapure water was produced by a Seralpur PRO 90 CN system (Ransbach-Baumbach, Germany).

Rat liver microsomes (RLM) from Sprague Dawley male rats and human liver microsomes (HLM) from a female gender pool were obtained from Thermo Fischer Scientific GmbH (Schwerte, Germany), both containing 20 mg/L protein. An equine liver glutathione-S-transferase enzyme (GST, 74.7% protein) was purchased from Sigma-Aldrich (Steinheim, Germany).

2.2. Equipment and Apparatus

For sample processing and preparation, a microtron®MB550 blender (Luzern, Switzerland), minispin® centrifuge (Eppendorf AG, Hamburg), sigma 6K15 centrifugate (Osterode am Harz, Germany), horizontal shaker and universal miller (IKA®-Werke GmbH, Staufen, Germany), MHR 13 incubator (HLC BioTech, Bovenden, Germany), reacti-therm™ N_2-drier (Thermo Scientific, Hennigsdorf, Germany) and a syringe pump (Antec® Scientific, Zeoterwoude, The Netherlands) were used.

2.3. Electrochemical Oxidation and Detection of TPs

2.3.1. Optimization of EC Parameters

Since electrochemical reactions are highly dependent on experimental conditions, optimisation of the parameters is a crucial step. Hence, working electrode type, organic modifier type and composition, electrolyte type and concentration, pH, flowrate and working potential were the main parameters optimised for each targeted compound. The following parameters were tested:

- Working electrodes: BDD, GC, Pt, and Au
- Organic modifiers: MeOH, H_2O, ACN, or their different composition
- Electrolytes: HFA (0.1 – 1%) and NH_4FA (0.1 – 15 mmol/L)
- pH: 3.5, 7.2 and 9.2
- Flow rate: 20, 50 and 100 µL/min

Optimal working potentials (maximum yield of oxidation products) were determined by scanning 0-2,000 mV for GC, Pt, and Au and 0-2,500 mV for BDD with a 20 mV/s scanning rate. A potential that yields a reasonable oxidative metabolite (type and intensity) was selected based on current *vs* applied potential (voltammograms) and the intensity of each oxidation product (mass voltammograms).

2.3.2. Generation and Detection of Phase I Oxidative Products by Online EC/MS

Mass voltammograms were recorded within the specified potential range (Table 1), using a Roxy™ potentiostat (Antec Scientific, Zeoterwoude, The Netherlands) coupled online to an ESI source of a single quadruple 6130 MS (Agilent Technologies GmbH, Waldbronn, Germany). Instrumental setups (online EC/MS, EC/LC/MS and EC offline LC-MS/MS, MS/MS or HRMS) and EC conditions for each compound are shown in Fig. 13 and Table 1, respectively. The potentiostat was equipped with an electrochemical flow-through cell (µPrepCell™, Antec Scientific) consisting of BDD WE, Pd/H_2 reference electrode (RE) and titanium counter electrode (CE). The WE and CE were separated by two 100 µm thickness spacers. Working standard solutions (0.1 mmol/L) were infused by a syringe pump at a specified flow rate (Table 1). 2D and 3D mass voltammograms were plotted against applied potential.

Table 1 Optimised conditions applied for the electrochemical oxidation of CPF and FLP using BDD WE in μPrepCell™

EC parameters	CPF	FLP	
		Indirect EC	Direct EC
Concentration (mmol/L)	0.1	0.1	0.1
Flow rate (μL/min)	50	40	40
pH	7.3	7.1	4.5
Scan rate (mV/s)	5 and 20	10	10
Working electrode type	BDD	BDD	BDD
Working potential (mV)	1,800 – 2,300	1,650 – 2,500	1,650 – 2,300
Organic modifier	ACN/MeOH/H_2O, 1:3:1 *v/v/v*	ACN/H_2O, 9:1 *v/v*	ACN/MeOH, 1:1 *v/v*
Electrolyte and concentration	1 mmol/L NH_4FA	0.1% HFA + 5 mmol/L NH_4FA	0.1% HFA

BDD – boron doped diamond, HFA- formic acid, ACN- acetonitrile, MeOH-methanol

Blank measurements were performed using the same solvent composition without the analytes. The working electrode was reactivated before each measurement by pulsing at E1 = 2,000, E2 = −2,000 and E3 = 0 mV for 100 ms on each step using solvents without analyte (50 μL/min), for a total of 5 min.

A nominal mass of 50 to 1,000 Da was scanned using ESI-MS (flow path A, Fig. 13) in both (+) and (–) ESI. MS parameters were 12 L/min drying gas; 35 psig nebulizer pressure; and 350 ^{0}C drying temperature, for both compounds and their oxidation products. Capillary voltages were +5,500 and –4,500 V for FLP and +5,000 and –4,250 V for CPF. Dialogue™ (Antec Scientific) and LC-MSD OpenLab ChemStation software (Agilent, Waldbronn, Germany) were used to control the potentiostat and the ESI-MS, respectively.

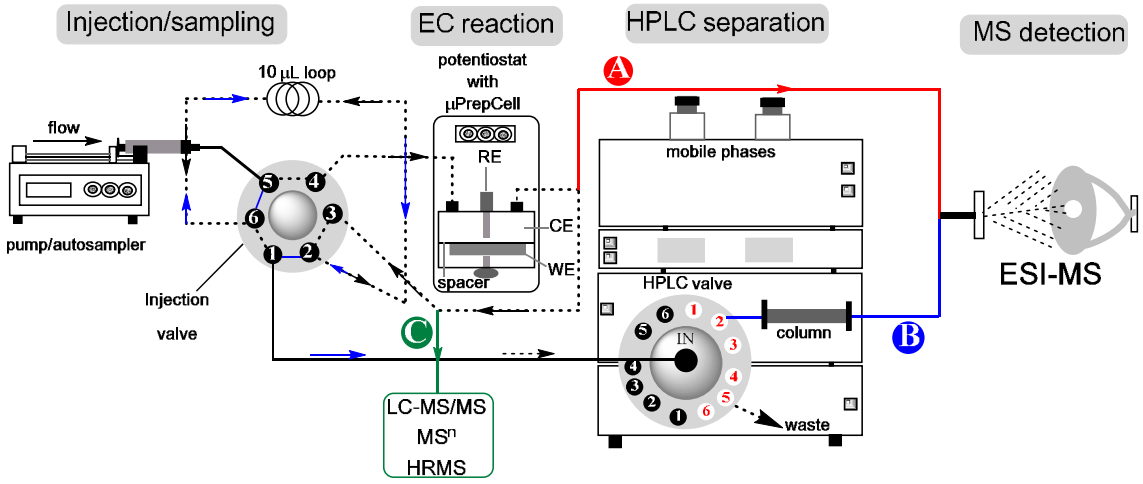

Fig. 13 General setup of the applied techniques: online EC/MS (flow path A), online EC/LC/MS (flow path B), and EC offline LC-MS/MS or HRMS (flow path C)

2.3.3. Phase I Oxidative Products by Online EC/LC/MS

In order to generate, separate and detect CPF and FLP oxidative products online, EC was coupled to LC/MS (Fig. 13, flow path B). Agilent 1200 series liquid chromatography consisting of a quaternary pump (1290 infinity) and an analytical column eclipse XDB C18 (150x4.6 mm, 5 μm, Agilent) for CPF or C8 (150x2.1 mm, 5 μm, Agilent) for FLP was coupled to the EC outlet by the external injection valve (Agilent 1290 infinity). Triplicates of 40 μL working standard solution (0.1 mmol/L, 120 μL in total) were injected by the autosampler into a flowing mobile phase (50 μL/min), which passes through the EC to the waste (the black arrow paths in Fig. 13). A direct current (DC) optimum potential (highest yield) of 2,100 mV for CPF and 2,000, 2,300, 2,500, 2,600, and 2,700 mV for FLP were applied for 30 s at each stage. Different potentials were applied to FLP as the aim of the analysis was to propose the hydroxylation sites (aliphatic *vs* aromatic positions). The HPLC valve was switched to the analytical column after EC oxidation and the products that were trapped by the external injection valve loop (10 μL capacity) were back-flashed (flow path B, blue line in Fig. 13) by the mobile phases. Mobile phases were water (A) and MeOH (B), both with 5 mmol/L NH_4FA and water (A) and ACN (B), both with 0.1% HFA, for CPF and FLP, respectively. Gradient profiles for CPF were 10% A for the first 8 min (EC reaction conditions), 40 → 0% A linearly for 12 min and isocratic for 2 min; then ramped to 80% A and kept for 2 min, linearly dropped to 0% A within the next 4 min and back to 40% A for 6 min re-equilibration. The total run time was 34 min (both EC and separation). For FLP, 10% A was isocratic for the first 15 min (EC reaction time), 60% A 15.1→23 min, 80% A 23.1→35 min, 0% A 35.1→45 min and finally 60% A for 5 min re-equilibration.

The flow rate was kept at 50 μL/min for the EC reaction step, then switched to 250 μL/min for CPF and 300 μL/min for FLP to separate oxidation products. Column compartment temperature was kept at 37 and 45 ^{0}C for CPF and FLP, respectively. The EC condition time was the time required for analytes to arrive on the WE surface from the autosampler, for the EC reaction to take place (30 s), to fill the loop and, finally, for generation of waste – which was calculated based on the dimensions of the capillaries and the flowrate. The MS conditions were identical to those in *sec 2.3.2*. To simulate EC oxidative products of CYP450 metabolites, both products were analysed using offline LC-ESI/MS and LC-MS/MS (flow path C in Fig. 13) parallel to blanks, control samples and standards (*look in sec 2.6.1*).

2.3.4. Phase II Conjugative Reactions by Online EC/MS

Glucosylation and GSH conjugation of CPF and FLP oxidative products were investigated by online EC/MS. Phase I oxidative products and intermediates were produced according to *sec 2.3.2* and trapped online by 0.5 mmol/L of GSH, or glucoside, which was pre-titrated to pH 7.2 using NH_4FA and HFA. The mixtures were allowed to react in a reaction loop (2.25 m) and infused to ESI-MS online (**Fig. 14**). Blank solvents (without analytes) and control samples (a mixture of CPF and GSH, E = 0 mV) were run simultaneously. For further structural elucidation by LC-MS/MS and triple quadrupole time of flight (TripleTOF)-HRMS, oxidative products were infused into an Eppendorf tube containing 0.5 mmol/L biomolecule (pH 7.2) and vortexed for 1 min. The mixture was incubated for 2 h (800 rpm, 37 ^{0}C) before LC-MS/MS analysis. The final 150 μL supernatant solution was analysed by LC-MS, LC-MS/MS and TripleTOF (Table 4). The effect of pH adjustment to 3.5, 7.1, and 9.2 using HFA and NH_4FA was investigated. The effect of transferase enzyme was studied in a similar way, except for the addition of 0.1 μmol/L GST to the biomolecule.

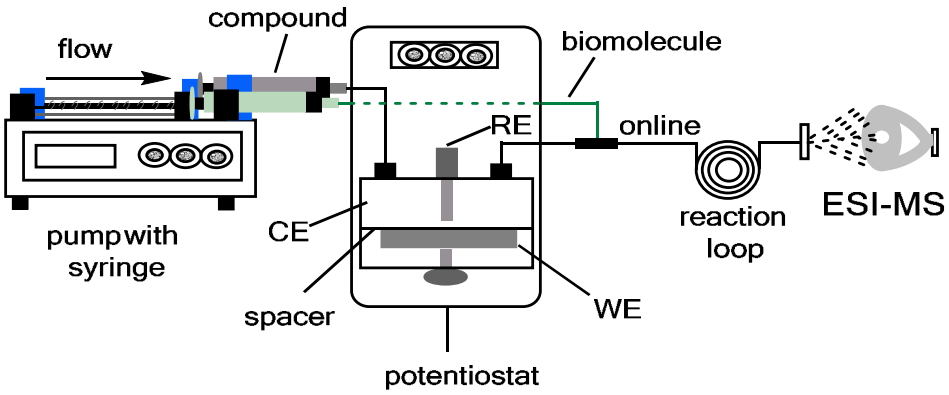

Fig. 14 Online EC/MS system for mimicking of oxidative products conjugation with biomolecules (phase II metabolites)

2.4. Incubation of Liver Microsomal Assays

To identify CYP450-catalysed metabolites, a solution of standard CPF and FLP were incubated with either HLM or RLM. Potassium phosphate buffer (136 μL, 0.1 mol/L adjusted to pH 7.4) was added to a mixture of 20 μL microsomal protein (20 mg/mL) and 20 μL of $MgCl_2{\cdot}6H_2O$. After addition of a substrate (4 μL of 3.125 mmol/L of either of FLP or CPF), the mixture was vortexed for 5 s and pre-incubated for 5 min at room temperature. 20 μL NADPH was added to the mixture and incubated further for 90 min (800 rpm, 37 °C). To terminate the reactions,

50 µL of ice-cold ACN was added and centrifuged (11,828×g force) for 5 min. The final concentrations were 50 µmol/L of substrate, 0.1 mmol/L $MgCl_2$, 1.6 mg/mL microsomal protein and 0.5 mg/mL NADPH in 250 µL of final volume for both RLM and HLM. Three negative controls (without either one of microsomes, substrate or cofactor) were incubated and analysed simultaneously. Incubations with substrate were performed in triplicate. The final 150 µL supernatant solution was analysed by LC-MS/MS and HRMS. A similar approach was used for phase II metabolites, except in this case GSH and GST were added after the substrate in order to allow conjugation with reactive species.

2.5. Photodegradation of CPF and FLP

To investigate PPs, a UV reactor equipped with a water-cooling system and medium pressure mercury lamp (TQ 150 W, Heraeus Noblelight GmbH, Hanau, Germany) that emits light in the UV-C wavelength range (λ = 200 – 280 nm) was used. The vessel was filled with 200 mL of 0.1 mmol/L working solution (FLP in 0.1% ACN *v*/*v* or CPF in 20% MeOH *v*/*v* aqueous solution) and stirred constantly by a magnetic stirrer (700 rpm). After cooling down the system to 12.5 ^{0}C, the UV lamp was switched on (255 mW/cm^2 irradiance) and aliquots (1 mL) were collected after 2, 5, 10, 20, 40, 60, 120, 180, 360 and 420 min for FLP and 5, 10, 30, 60, and 120 min for CPF. The aliquots were investigated by LC-MS/MS and HRMS. The overall setup is depicted in Fig. 15.

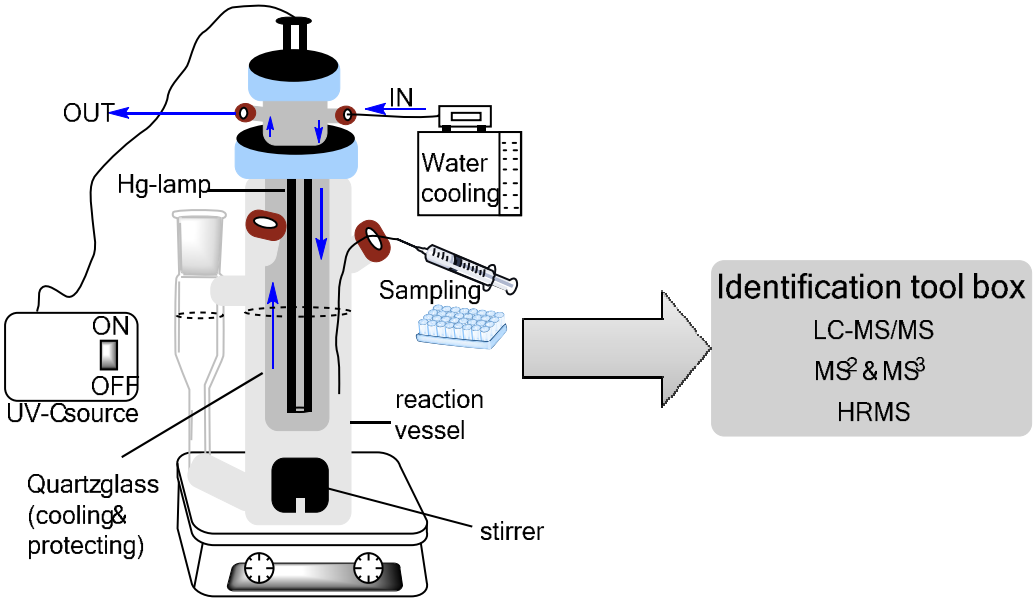

Fig. 15 Schematic diagram of the photoreactor used for investigation of PPs of FLP and CPF by UV-C irradiation (adopted from Mekonnen et al. [147])

2.6. General Strategies for Structural and Mechanism Elucidation of TPs Using EC Offline LC-MS, LC-MS/MS, and HRMS

Transformation products from EC, liver microsomes (LMs) and UV-C were structurally elucidated using different MS techniques (Fig. 13, flow path C). The first information on the oxidation products' mass-to-charge ratio (*m*/*z*) was derived from EC/MS by comparing offline and online mass voltammograms (for EC oxidative products). The mixtures infused from the EC flow-through cell may contain oxidative products, intermediates (radicals and reactive species), an unreacted portion of the parent compound, electrolyte and modifier molecules or adducts with the oxidation products and polymers (dimers, trimers). Hence, successive screening of unbiased metabolites was performed by a series of steps depicted in Fig. 16. Based on the available information (databases and literature) either targeted, suspected, or non-targeted screening approaches have been followed to assign a possible structure and avoid false positives. Similarly, LM incubates and PPs contain many interfering and, as yet, unknown transformation products. Thus, nominal *m*/*z*, isotopic patterns and their ratio (e.g. ^{35}Cl:^{37}Cl approximately 3:1), as well as adducts with NH_4^+–, Na–, and K–, were sought using EC/MS (for EC products) or from LC-MS^n, MS^n and HRMS (for all EC, LMs and UV products). Further confirmation was obtained using online EC/LC/MS (only for EC products) or offline LC-MS (for EC, LMs, and UV products) by scanning in a specified *m*/*z* range to gain information based on their retention time. Transformation products from all the three methods were fragmented using data-dependent product ion (PI) scan mode (MS^2). This enables the identification of the fragmentation pattern, precursor ions and isotopic peaks. Then, multiple reaction monitoring methods were developed to increase selectivity for retention time comparisons.

In the case of conjugative phase II metabolites, fragments with the suspected moiety and sulphur have been used exclusively to check whether the conjugative site is between the thiol group of -Cys- and the cofactor. Furthermore, the product ions of the cofactor or the biomolecule moiety were fragmented at the third quadrupole (MS^3) to compare the spectra with the standard. EC products that did not match with LM metabolites in their fragmentation pattern, isotopic configuration and retention time were not considered as metabolites. The final structural assignment for the suspected molecules was based on accurate mass and molecular formula measurement by HRMS. Absolute mass error ($\delta m/m$) = ($m_{measured}$ –

$m_{theoretical})*10^6/m_{theoretical} \leq 5$ ppm was considered as a threshold value to assign accurate structure of the TPs.

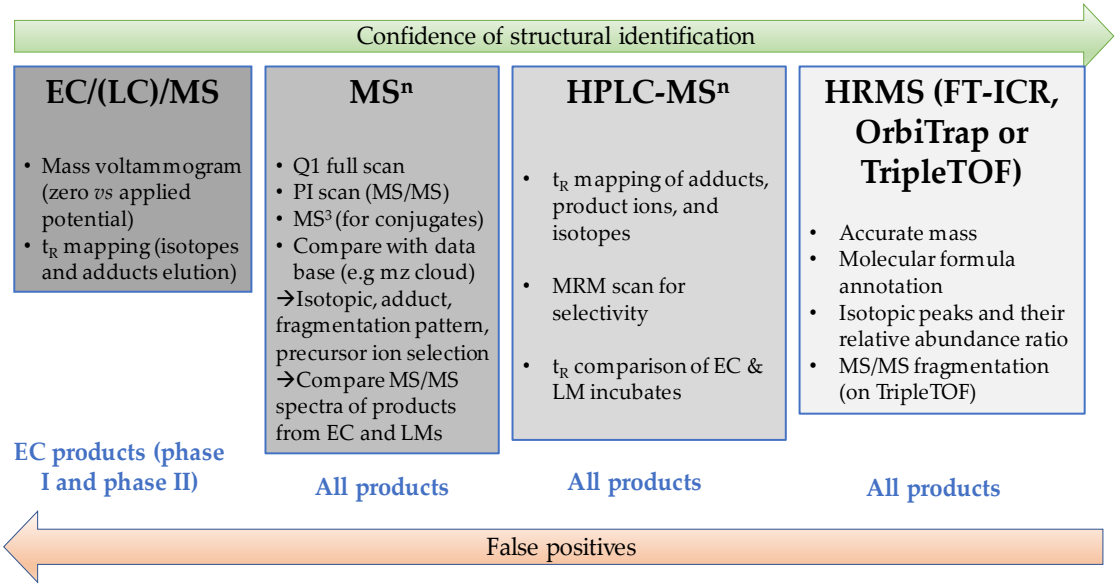

Fig. 16 Work-flow for structural and mechanistic elucidation of TPs from EC, LMs and UV-C direct photolysis (Q1 – first quadruple, tR– retention time, MRM – multiple reaction monitoring)

2.6.1. LC-MS/MS of EC Oxidative Products and LM Incubates

Agilent 1200 series HPLC hyphenated to an AB Sciex 4000 QTRAP® MS/MS (Foster City, USA) was used to further characterise the TPs from all the three methods. Standard solutions of CPF or FLP (80 mL, 0.1 mmol/L) with similar modifiers and electrolytes (as in *sec 2.3.2*) were oxidized by a SynthesisCell™ (Antec Scientific). The cell was equipped with a BDD WE (4.5 x 4.5 x 0.2 cm dimension), Pd/H_2 RE and coiled Pt-wire inside a glass spacer with a porous frit as CE. A DC current of 2,100 and 2,300 mV was applied for CPF and FLP, respectively. The other experimental conditions are identical to online EC/MS experiments (*sec 2.3.2*). 1 mL aliquots were collected after 0, 3, 30, 60, 120 and 180 min (for CPF) and 0.5, 1, 3, 6 and 24 h (for FLP) of synthesis. 5 µL of the aliquot was injected into the LC-MS/MS autosampler and analysed in parallel to standards, controls and LM incubates. Similar chromatographic conditions (columns, mobile phases and gradients) to the online EC/LC/MS analysis (*sec 2.3.3*) were applied for offline analysis of EC effluents and LM incubates (HLM and RLM), except for a few modifications for FLP products. Briefly, the following parameters were used: 60% A isocratic for the first 8 min, 60→0% A linear decreases in 2 min and kept for 5 min, linear increase 0→50% A in 5 min and kept for the next 5 min and, finally, 10 min re-equilibration elution gradients with 350 µL/min flow rate. The MS/MS conditions are listed in Table 2.

Table 2 QTRAP-MS/MS parameters for investigation of TPs from EC, LMs and UV-C

MS/MS parameters	CPF	FLP
Ion source voltage (IS)	+5,000 and -4,250 V	5,500 V
Source gas (GS)	GS1 = 20; GS2 = 60 psi	GS1 = 60; GS2 = 20 psi
Curtain gas (CUR)	35 psi	30 psi
Collison gas (CAD)	7	5
Source temperature	450 ^{0}C	500 ^{0}C
Dwell time (DWT)	200 ms	300 ms
Interface heater	ON	ON

Fragmentation experiments on MS^n:- To obtain structural information for each product from EC, LMs and UV-C, the MS/MS spectra of targeted precursor ions were collected by linear ion trap (LIT) with dynamic fill time (DFT) in both (–) and (+) ESI polarities. The products were infused to the ESI at 10 μL/min and spectra were recorded for 3.5 min with 4,000 Da/s scan rates and 30 s delay time. The MS/MS parameters are shown in Table 2 and Table 3. Data was acquired using Analyst® 1.5.2 software (AB Sciex, Foster City, USA).

MRM method development for selected TPs:- After the identification of the possible structures of TPs, the LC-MS/MS method was developed based on MRM scanning for targeted analysis of selective TPs in real samples. From the product ion (PI) scan of each TP in MS/MS, the quantifier and qualifier product ions were selected from the most abundant precursors. The optimised MS/MS parameters for each *m/z* transition are listed in Table 3. The chromatographic conditions were the same as in *sec 2.3.3* and *2.6.1.*

Table 3 Mass transitions (m/z) for simultaneous analysis of selected oxidative phase I metabolites of CPF and FLP

Compounds	Abbreviation	Q1→Q3	DP (eV)	CE (eV)	CXP (eV)	EP (eV)
Fluopyram	FLP	397→**208**, 173	80	45, 45	13	10
2-trifluoromethyl benzamide	M2	190→170, 130	65	37, 32	13	10
7,8-dihydroxyl FLP	M5	429→411, 391	95	42, 33	14	10
7-/8-monohydroxyl FLP	M7b/M7a	413→395, 145	95	40, 33	14	10
Triphenylphosphate	TPP*	327→**215***, 77	+80	35, 35	13	10
Chlorpyrifos	CPF	350→**198**, 115	+80	40, 35	13	10
Diethylthiophosphate	DETP	169→141, **95**	-60	-33, -25	-11	-10
Diethylphosphate	DEP	153→79, **125**	-60	-30, -25	-13	-10
Trichloropyridinol	TCP	196→181, **35**	-60	-40, -31	-10	-10
Desethyl chlorpyrifos	Des-CPF	320→196, **306**	+80	40, 35	13	10
Chlorpyrifos oxon	Oxon	334→278, **145**	+80	40, 31	13	10

***Q1** –precursor ion*, ***Q3** –product ion*, ***DP** –declustering potential*, ***CE** –collision energy*, ***CXP** –cell exit potential and* ***EP** – entrance potential, *–internal standard. Bold m/z's are more intense transitions used for quantitation*

2.6.2. LC-MS/MS Analysis of UV-C Products and Bioconjugates

The same instrumentation type and MS/MS conditions as *sec 2.6.1* (although with modified chromatographic methods) were used to investigate UV degradation products and bioconjugate samples. Similar mobile phases and injection volume as in *sec 2.6.1* and 45 ^{0}C column compartment temperature were used to analyse bioconjugates and PPs. Other chromatographic parameters are listed in Table 4. After gaining information on the probable conjugative products from online EC/MS (**Fig. 14**), targeted precursor ions were investigated by product ion scan (PI) on (+) ESI (*look Fig. 16 and sec 2.6.1.*). Precursor ions that contain -S- (from the Cys-) and phase-I oxidative product were used to check the formation of conjugates via the thiol groups of Cys. Additionally, the moiety from the expected oxidative products was selectively fragmented on the third quadrupole (MS^3), in order to compare with the standard MS/MS spectra.

Table 4 Analytical columns, flow rate and elution gradients for separation of CPF and FLP bioconjugates and PPs

Parameters	Bioconjugates				UV-C degradation products		
	CPF		FLP		CPF	FLP	
Analytical column	Luna Omega polar C18 (250x4.6 mm, 5 μm)		Luna Omega polar C18 (250x4.6 mm, 5 μm)		Eclipse XDB C18 (150x4.6 mm, 5 μm)	Eclipse XDB C8 (150x2.1 mm, 5μm)	
Flow rate (μL/min)	250		250		250	300	
Gradient	time (min)	%A	time (min)	%A	Similar to sec 2.6.1	time (min)	%A
	0→20	80→0	0→15	80		0→8	60
	20→25	0	15→20	80→0		8→10	60→0
	25→35	60	20→25	0		10→15	0
	35→45	20→0	25→35	60		15→20	0→50
	45→60	80	35→45	20→0		20→25	50
			45→60	80		25→35	60

2.6.3. Confirmation by HRMS

A hybrid linear quadrupole ion trap (LTQ) 7T high-resolution Fourier transform ion cyclotron resonance mass spectrometer (FT-ICR-MS) (Thermo Scientific, Bremen, Germany) was used to acquire HRMS data for accurate mass determination of EC oxidation products and CYP450-based metabolites (flow path C in Fig. 13). The FT-ICR-MS was equipped with an ESI source, operated at a spray voltage of +5,000 V for CPF and +5,500 V for FLP products. Aliquots from SynthesisCell™ (24 h for FLP and 3 h for CPF) were diluted tenfold using 50% MeOH (for

CPF) and ACN (for FLP) containing 0.1% HFA. 10 µL of the diluted solution was injected into a static nano-ESI emitter and scanned from 100 to 650 *m/z* for CPF and 100 to 1,000 *m/z* for FLP with 100,000 nominal mass resolutions.

UV products were identified using an Exactive™ orbitrap mass spectrometer (Thermo Fisher, Bremen, Germany). The Orbitrap was equipped with an ESI source, operated at +5,000 V spray voltage. Aliquots from 2 h-irradiated samples were diluted by a thousand-fold using 50% ACN containing 0.1% FA and infused to the ESI source using a microsyringe (5 µL/min flow rate). A full scan using (+) ESI within a 120 to 2,000 *m/z* range and 100,000 nominal mass resolutions (5 Hz scan rate) was performed.

For phase II conjugative products, an AB Sciex TripleTOF® 6600 (Foster City, USA) was used. The samples were infused at 7 µL/min. For TOF-MS experiments (Q1 scan) the conditions were: +5,000 V ion spray voltage floating (ISVF), 400 ^{0}C temperature, +80 eV DP, 10 eV CE, 20 psi GS1, 15 psi GS2, 25 psi CUR and 7 CAD. Ions were accumulated for 2.5 sec and scanned in the range of 100 – 2,000 Da. For TOF-MS/MS experiments (PI scan), the same experimental conditions were used, except for 40 psi GS2, 40 eV CE with 5 eV collision energy spread (CES), 30 ms ion release delay (IRD) and 15 ms ion release width (IRW) were fixed. Data was acquired using XCalibur™ 4.0 (ThermoFisher Scientific) for FT-ICR and Orbitrap and Analyst® 1.7.1 (AB Sciex) for TripleTOF. Additionally, open sources of MZmine-2.33 [148] and ProteoWizard [149] were used for further manipulation of MS data.

2.7. Investigation of TPs in Food Samples

2.7.1. Synthesis and Stability of Reference Standards

For application to food samples, TP reference standards were synthesised using an EC cell especially designed for this purpose. TP standards of CPF and FLP were synthesised using a BDD (4.5 x 4.5 x 0.2 cm dimension) electrochemical SynthesisCell™ (from Antec Scientific, Zoeterwoulde, The Netherlands) based on the method stated in *sec 2.3.2* and *2.6.1.* Before each measurement, the WE was pulsed at E1 = 2,000, E2 = -2,000 and E3 = 0 mV (for 100 ms on each step) for 5 min and rinsed using solvents without the analyte. Aliquots of synthesised products after 3 h for CPF (2,100 mV) and 24 h for FLP (2,300 mV) were collected and analysed by the developed LC-MS/MS methods (*see sec 2.6.1*). Three batches of synthesis (80 mL each)

were performed and mixed together. The solvents were evaporated by N_2-stream at 35 ^{0}C, until complete dryness, and re-dissolved to 5 mL by the mobile phases before using for real sample investigation. The overall work flow is illustrated in Fig. 17.

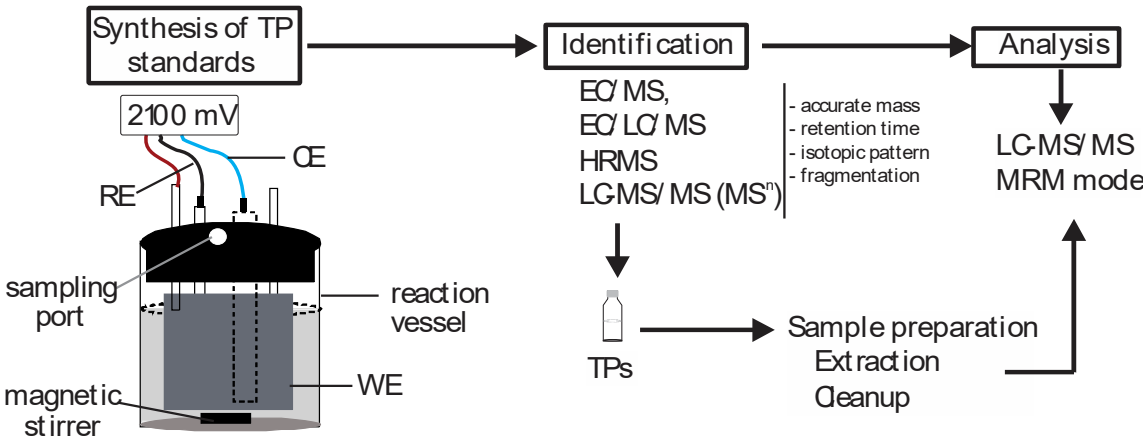

Fig. 17 General outline of TP standard synthesis, identification and application for real sample investigation (reused from Mekonnent et al. [150], license number (LN) 4442490416941)

Stability studies:- Since storage time and sample processing temperature could potentially cause loss of analyte, the investigation was carried out on CPF-synthesised products. Triplicates of synthesised samples stored at 4 ^{0}C were analysed after 0, 10, 40 and 50 days of storage in 20% MeOH *v/v* aqueous using LC-MS/MS and compared by peak area. Meanwhile, possible adsorption to glass containers was also investigated by rinsing the empty glass after 0, 10, 40, and 50 days of storage. Furthermore, the effect of temperature on sample processing was investigated by drying triplicate of mixed EC-synthesised standard at 23, 35, 45 and 65 ^{0}C using N_2-stream at 2 bar constant pressure.

2.7.2. Sample Collection and Preparation

Foodstuff samples were collected randomly between January and April 2017 (four samples each month) from four local markets in Berlin, Germany. Samples were collected from spices (black pepper, cinnamon, coriander, fenugreek seed, fragrant chili, hot chili pepper, curry and star anise (n = 32 samples)) and fresh fruits (grape (red and white), lemon (green and yellow), potato, tomato, strawberry and sweet pepper (green, yellow, and red) (n = 33 samples)). In total, samples from 12 different countries were purchased. FLP was investigated exclusively in fruit samples and not in spice samples. Spice samples were stored at dry room temperature while fruit samples were stored at -35 ^{0}C until use. Samples were homogenised using a blender and stored at 4 ^{0}C prior to analysis. 5 g of spice or 10 g of fruit samples were extracted

using a Quick Easy Cheap Effective Rugged Safe (QuEChERS) protocol (Fig. 18). MeOH was added to spice samples to extract polar TPs and double cleaned due to a high oil content. The final extract was filtered through PTFE and analysed by LC-MS/MS in MRM mode.

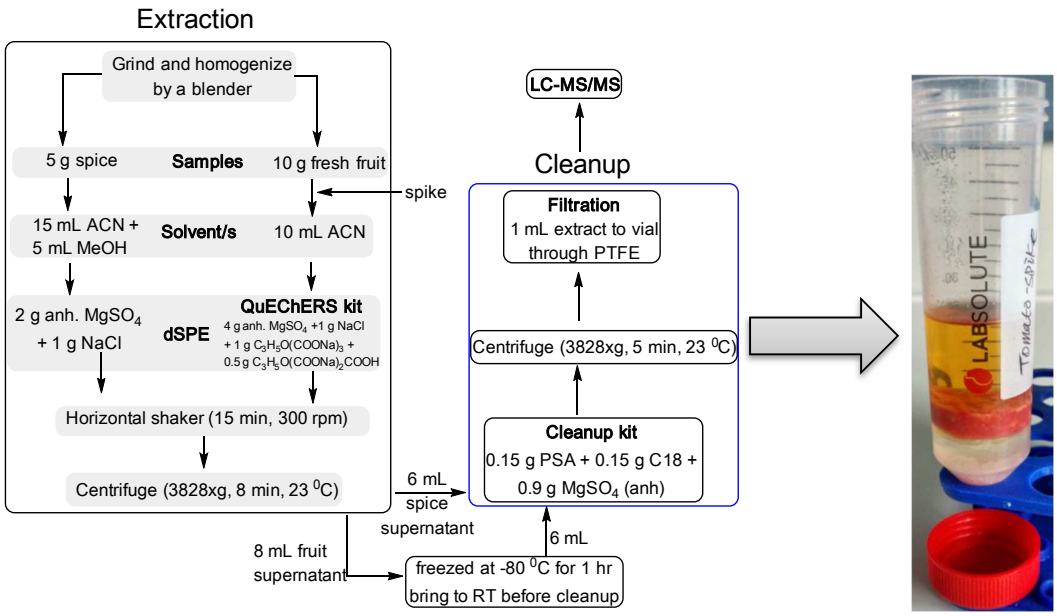

Fig. 18 Schematic diagram for extraction and clean-up of fruit and spice samples (dSPE – dispersive solid phase extraction, PSA – primary secondary amine, PTFE – polytetrafluoroethylene)

2.7.3. Analysis of TPs in Food Samples by LC-MS/MS

Extracted fruit and spice samples were analysed using a TripleQuad LC-MS/MS system (sec 2.6.1). The analytical columns, mobile phases and gradient elution profiles were the same as in *sec 2.6.1*, except in this case they were preceded by 4x3 mm of the same stationary phase security guard columns (Agilent). The gradients for CPF and its TPs were modified slightly as interfering peaks were detected in the matrices – especially in spice extracts. The analysis started at 40% A, then linearly dropped to 10% within 8 min and was kept isocratic for 4 min, switched to 100% B for 2 min, decreased to 20% B at 14 min and kept isocratic for 2 min, linearly dropped to 0% A in 16→20 min and raised to 40% A in 20→26 min and, finally, kept at equilibration for 6 min. The total analysis time was 32 min. Other chromatographic conditions were: 250 µL/min flow rate, 45 ^{0}C column temperature and 5 µL injection volume. After each of the five consecutive injections, blank samples were injected to control for the carry-over effect, which was not observed. The MS/MS conditions and *m/z* transitions were identical to those in Table 2 and Table 3 (*sec 2.6.1*).

2.7.4. Method Validation

The performance of the analytical method was validated using blank fruit and spice samples. A 7-point matrix-matched calibration curve (with triplicates for each point) was constructed by spiking blank samples at 20, 50, 75, 100, 200, 500 and 1,000 μg/kg levels. The blank samples were from hot chili pepper and strawberry for CPF and grapes and strawberry for FLP. The presence of the analyte of interest was pre-checked in the blank samples. The calibration solutions were prepared by serial dilution of a 1,000 μg/L working standard solution. The spiked samples were passed through the extraction protocol in Fig. 18. Triphenylphosphate (TPP) was added to each sample as an internal standard at the 500 μg/kg level. Only two matrix-matched calibration curves (one for fruits and one for spices) were constructed for CPF and extrapolated for other samples. For FLP, only fruits were used.

Linearity, limit of detection (LOD) and quantitation (LOQ):- Linearity was shown in terms of the regression coefficient (R^2). LOD and LOQ were determined as a signal-to-noise ratio of 3:1 and 10:1, respectively. In the case of TPs, LOD and LOQ were not calculated, as the EC-synthesised products were not fractionated. A preparative HPLC approach was tested; however, due to structural similarities and stability differences of the products, fractionation of single product was not achieved.

Reproducibility:- Inter-day (RSD_R) and intra-day (RSD_r) repeatability were assessed by spiking triplicate blank samples (n=3) at a 200 μg/kg level for CPF and FLP for three consecutive days, with triplicate extractions per day. The coefficient of variance between analyses performed on a single day, and between the three consecutive days, were considered as RSD_r and RSD_R repeatability, respectively.

Trueness (%R) and matrix effect (%ME):- Three sets of samples were used: pre-spiked by standard mixtures (n = 3) before extraction (a), blank samples (n = 3) post-spiked after extraction (b), and standard mixtures without matrices (c). These were dried at 35 ^{0}C and reconstituted to 1 mL by the mobile phase. The extracts were filtered through PTFE and analysed simultaneously by LC-MS/MS. Trueness and %ME (signal suppression or enhancement) of TPs were calculated by peak area (PA) ratio as:

$$\%R = (PA_a/PA_b) * 100 \quad (2.1)$$

$$\%ME = (PA_b/PA_c) * 100 \quad (2.2)$$

Where, PA_a, PA_b, and PA_c are peak areas of the sample set a, b, and c, respectively. The spiking level was 2 mL of unknown concentration of standard mixtures. The same is true for the parent CPF and FLP, except, in this case, a pure standard solution (200 µg/kg spiking level) and concentration ratios were used.

Investigating pesticides and their TPs in spice and fruit samples:- Triplicates of blank spice (5 g) and fruit (10 g) samples were subjected to an extraction protocol (Fig. 18). Triplicate injection of each extract was performed. The autosampler needle was washed three times in acetone/ACN/MeOH (1/1/4 *v/v/v*) before injecting extracts of different sample categories. Samples containing traces of CPF or FLP were selectively investigated for the presence of TPs of the respected parent residue by comparing with the reference standard synthesised by EC. Since FLP was not detected in any of the investigated samples, its TPs were not searched for in the fruit samples.

3. RESULTS AND DISCUSSION

The results and discussion chapter of this thesis is divided into six parts: general optimisation of EC/MS experiments; biotransformation processes (phase I and II) of CPF and FLP; abiotic transformation products (photodegradation) of CPF and FLP; and TPs detection in foodstuff samples. Simulation of phase I oxidative products by EC/MS is highly dependent on the reaction conditions of the EC cell. Hence, different parameters were optimised for effective oxidation of the intended pesticides. Biotransformation products and their formation mechanisms were investigated by EC/(LC)/MS and liver microsomal assays (human or rat liver). A large part of the photodegradation product identification phase focused on FLP, as many novel PPs were identified. On the other hand, investigation of pesticide residue TPs in foodstuff samples mainly focused on CPF and its TPs, as the parent FLP was not detected in any of the investigated samples.

3.1. General Optimization of EC Conditions

3.1.1. Organic Modifiers, Working Potential, and Scan Rate

Electrochemical oxidation takes place when a current is transferred through a solution by movement of ions/charges and through electrodes by movement of electrons. Appropriate solvent composition is also important for stable current flow and reproducibility of the products. Furthermore, the solvents should be electrochemically inert at the working potential. In Fig. 19a, the same concentration of FLP was scanned with different organic solvent compositions and potential scan rates, using 0.1% HFA as an electrolyte. Regardless of the scan rate, there was reproducible oxidation with ACN/MeOH, 1:1 *v*/*v* using 0.1% HFA as electrolyte. However, in the presence of H_2O >20%, FLP did not reveal any oxidation products (Fig. 19a). Attempting to oxidise with only MeOH also did not show oxidation of FLP, which could be due to lack of charge carriers. Nevertheless, FLP shows slight oxidation with ≤ 5% aq. solution of ACN/MeOH composition. This was not the case with CPF, which showed effective oxidation even with 50% aq. modifiers and the same WE. One hindering factor in the presence of H_2O is the possibility of formation of gaseous molecules due to water electrolysis ($2H_2O \rightarrow 2H_2 + O_2$) at a higher working potential (around 2,500 mV). This can be easily observed on the voltammogram, which would demonstrate a highly unstable current flow. On the other hand,

the presence of small amounts of water is necessary as it provides a source of hydroxyl and other ROS species for indirect electrochemical oxidation of the intended molecules (e.g. hydroxylation and hydroxyl derivative metabolites). Depending on the electrode materials used, some hydroxyl products show a stronger adsorption effect on the electrode surface, which reduces the available surface area for subsequent oxidation. This could be the reason why FLP shows no oxidation in the presence of a higher water content.

The scan rate is also important in generating a high enough yield of TPs, as well as a variety of TP types. Each TPs has its own specific potential for formation; thus, a slower scan rate helps a molecule remain for longer on the surface of the electrode at its preferred potential. In Fig. 19a, scans are shown at 20, 10 and 1 mV/s. While chemical composition and WE are the same, different humps could be observed at a slower scan rate, which provides information about oxidation at a different potential. At a rapid scan rate (e.g. 20 mV/s in Fig. 19a), it is difficult to visualise potential peaks where oxidization takes place. Regarding working potential, either direct current (DC) at constant potential, linear sweep (DC with constant increasing potential), scanning (either half, full or continuous scan between two potentials; E1 and E2 with specified scanning rate) or pulsing (sweeping between three potential points; E1→E2→E3) could be applied. However, it is practically challenging to simulate every oxidation product at a specific potential because of differences in stability and formation mechanism. For instance, Fig. 19b shows an intensity variation of 0.1 mmol/L FLP and three of its oxidative products (metabolite 2: M2, M3, and *m*/*z* 173) by applying different DC potential using BDD. FLP significantly decreases, while other products increase when a potential is applied. However, here more M2 and M3 were produced at around 2,000 mV, while *m*/*z* 173 was produced at around 1,800 mV (Fig. 19b). Thus, optimisation of working potential is vital for both the type and quantity of produced oxidative products. In summary, two working conditions for FLP (i) direct EC in ACN/MeOH, 1:1 *v*/*v* with 0.1% HFA and E_{max} = 2,300 mV; and (2) indirect EC in ACN/H_2O, 9:1 *v*/*v* with 0.1% HFA + 5 mmol/L NH_4FA and E_{max} = 2,500 mV have been used. In the case of CPF, ACN/MeOH/H_2O, 1:3:1 *v*/*v*/*v* with 1 mmol/L NH_4FA and E_{max} = 2,300 mV was used.

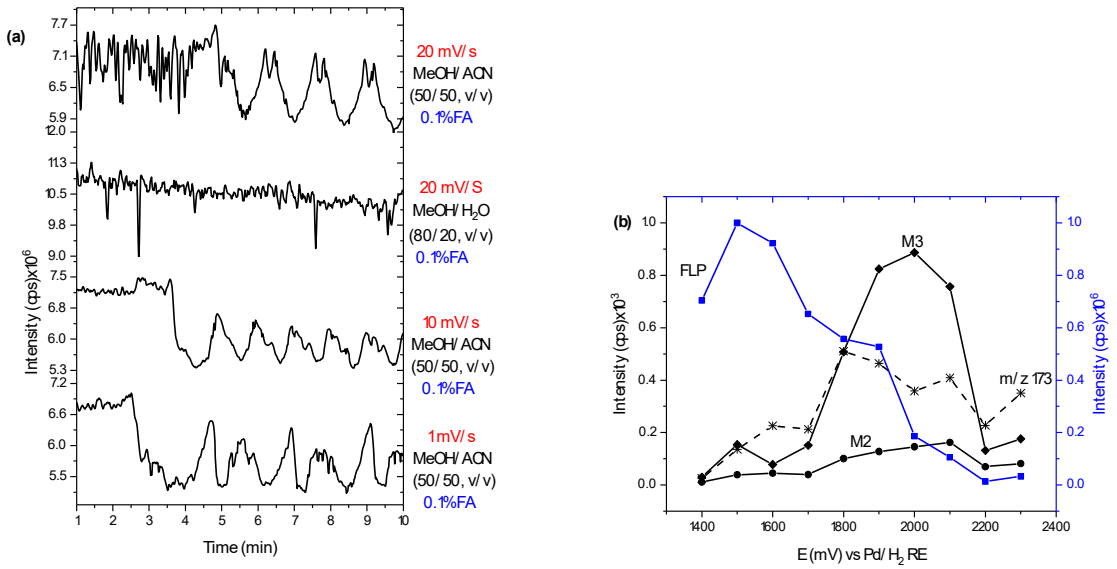

Fig. 19 Mss voltammograms of FLP with different organic modifiers and scan rates (a) and stability of 2-trifluoromethylbenzamide (metabolite 3: M3), 2-trifluoromethylbenzoic acid (M2), intermediate m/z 173, and FLP *vs* applied potential (1,650 – 2,300 mV) using BDD WE (b)

In order to determine optimal oxidation potential (amount and type), continuous scanning was performed for both CPF (full scan in Fig. 20a) and FLP (Fig. 20b). The voltammograms indicated a hump and an increase in current at around 1,800 mV for CPF and 1,650 mV for FLP, which ensures the oxidation of the molecules. The applied potentials are only for oxidation (positive mode) and the EC is a flow-through cell; thus, only the first half-cycle shows effective oxidation (no peak observed on scanning from E2→E1). On the other hand, oxidation of targeted molecules depends on the availability of an accessible WE surface. As evidenced in Fig. 20b, in five continuous scans of FLP, the oxidation potential peak shifted from 1,650 mV (first scan) to nearly 2,000 mV (2nd-5th scans). This is explained by the unavailability of the WE surface for these scans and signifies that the rate of electron transfer between the surface of WE and the molecule becomes slower, with the rate of oxidation also decreasing. As a practical note, the WE surface needs cleaning and reactivation (flushing with organic solvents and pulsing with appropriate potential) after two or three continuous scans (*Appendix Fig. A1a*). However, this depends on the modifier, WE, organic molecules and scan rate. For instance, a slower scan rate and relatively fast flow rate could help prolong surface activation; however, the faster flow rate can result in a small amount of oxidation products. Solvents like ACN are useful for reproducibility of the oxidation processes (type and amount) in continuous scanning.

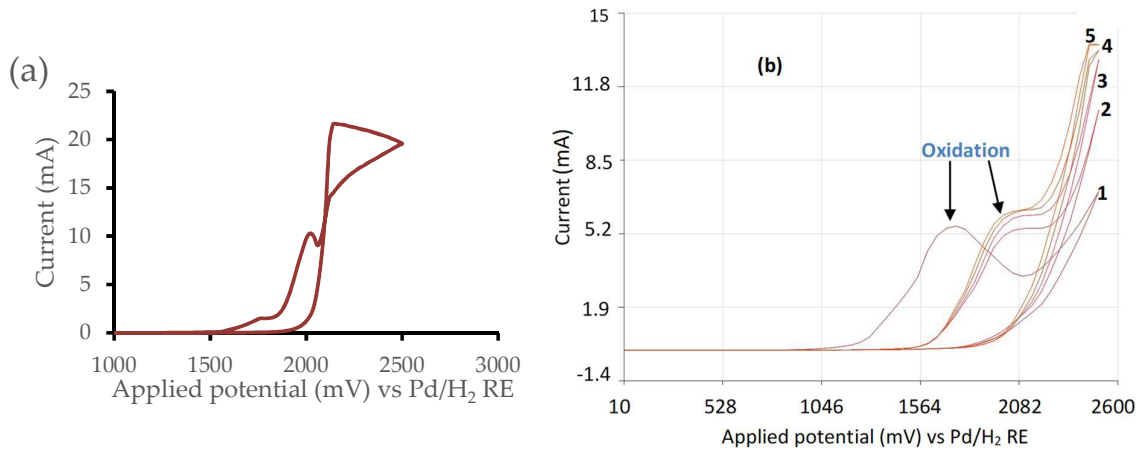

Fig. 20 Voltammogram of 0.1 mmol/L of CPF in ACN/MeOH/H_2O, 1:3:1 v/v/v and 1 mmol/L NH_4FA (a) and FLP in ACN/MeOH, 1:1 v/v and 0.1% HFA (b) with 20 mV/s scan rate using BDD as WE in µPrepCell

3.1.2. Type of WE and pH

Aside from the above chemical aspects, the nature of the WE used also plays an important role in the oxidation of compounds. In Fig. 21a, CPF with the same chemical composition and potential was analysed on GC, Pt, Au, and BDD WEs. Conversion efficiency was calculated as:

$$Conversion\ (\%) = (I_{E=0} - I_{E=t}) * 100/I_{E=0} \qquad (3.1)$$

where $I_{E=0}$ and $I_{E=t}$ are intensities on zero potential and after potential applied for time 't', respectively.

Regardless of the type of TPs, nearly 100% oxidation was observed using the BDD electrode. Using BDD as a WE also led to better oxidation of FLP. Furthermore, the BDD electrode enables a wider working potential window (as much as 3,500 mV), lower background currents and chemical inertness compared to other electrodes. Roser *et al*. also reported that BDD is an ideal WE for hydroxylation reactions [151]. Hence, BDD was used for all EC/MS experiments here. However, interfering products with organic modifiers, such as adducts and proton bound dimers/ trimers, were observed at a higher applied potential. For example, oxidation products of FLP generated by BDD at 2,700 mV with MeOH/ACN, 1/1 *v/v* and 10 mmol/L NH_4FA yielded methoxy FLP (δm/m = 0.4 ppm from HRMS) and carboxyl-conjugated FLP (δm/m = 2.2 ppm). At the specified organic modifier and BDD electrode, the mixtures were adjusted to pH 3.5, 7.2 and 9.2 using HFA and NH_4FA and oxidized at a 2,000 mV DC potential (Fig. 21b).

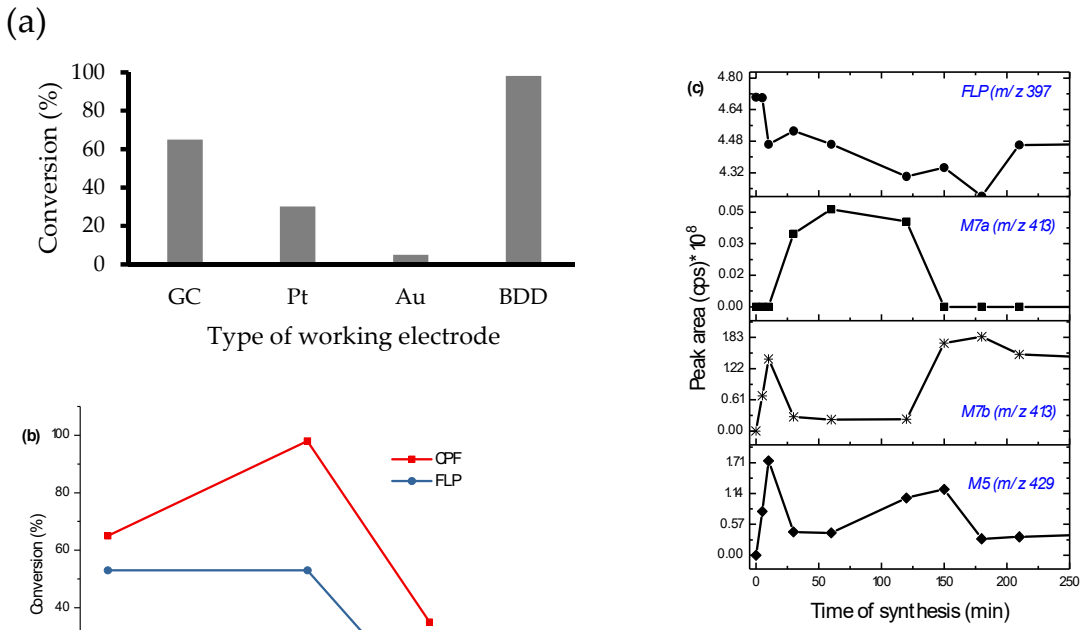

Fig. 21 Percentage of oxidation of CPF after two full cycles in 0-2,000 mV, 20 mV/s with different WEs (a), CPF and FLP with respect to pH using BDD as WE at a 2,000 mV DC potential (b), and stability of FLP and some of its oxidative products with respect to synthesis time on BDD WE at a 2,300 mV DC potential (c)

Maximum oxidation of CPF was observed at neutral pH, while FLP was similar under acidic and neutral pH. As a result, all oxidation experiments were performed at neutral pH. When a DC potential is applied to the SynthesisCell™, the time of synthesis plays an important role for both stability of the synthesised products and inactivation of the WE surface. Despite this, there is always a decay in the current through time (Fig. A1b). Therefore, to avoid potential loss of metabolites, the intensity of oxidative products *vs* synthesis time was investigated at 2,000 mV (Fig. 21c). A detailed account of product interconversion will be provided in the next section (*sec 3.3.2.*). Here, the importance of knowing the synthesis time for both the type and quantity of oxidative products should be noted.

3.2. Biotransformation of CPF (Phase I)

3.2.1. CPF Oxidative Products by EC/MS

Initially, EC/MS experiments without LC-column (Fig. 13 flow path A) were performed to obtain information on the electrochemical oxidation behaviour of CPF. The 2D and 3D mass voltammograms in Fig. 22a and b show that the oxidation of CPF ($[M+H]^+$ 350) starts at around 1,800 mV, indicated by a decrease in signal intensity with increasing potential. Contrarily, intensities of *m*/*z* ratios 155, 171, 198, 306 and 334 increased, indicating production during electrochemical oxidation (Fig. 22a). These *m*/*z* could be potential oxidative metabolites, likely formed by *in vivo* during phase I metabolism. Furthermore, *m*/*z* 113, 141, 184, 214, 228, 379 and 395 showed increased intensity with potentials above 2,000 mV (Fig. 22b). After obtaining first evidence of the suspected oxidative products, further elucidation of the structure and potential oxidation pathways were proposed based on the fragmentation pattern of targeted precursor ions analysed by MS/MS (Fig. 13 flow path C). Mass spectra of all oxidation products and metabolites from RLM were recorded by direct infusion into ESI-MS/MS. The spectra and fragmentation mechanisms are shown in the appendix (Fig. A2a – e). In a study by Choi *et al*. [72], similar metabolites were found in human hepatocytes.

The precursor ion at *m*/*z* 171 (product 1: P1 in Fig. 22b) was fragmented to *m*/*z* 153 ($–H_2O$), 143 ($–C_2H_4$) and 115 ($–C_4H_8$) in both EC and RLM. Similarly, in (-) ESI, *m*/*z* 169 fragmented to *m*/*z* 141 and 95, which can be considered as the subsequent neutral loss of C_2H_4 and C_2H_5OH, respectively (Fig. A2a). Additionally, *m*/*z* 171.0239 (0.0 ppm deviation from theoretical) on the HRMS spectrum supports P1 to be assigned for DETP. Another intense oxidative product of CPF was observed at *m*/*z* 334 (P5 in Fig. 22b). As evidenced in Fig. A2b, the MS/MS spectra show a product ion at *m*/*z* 316 ($–H_2O$), 306 ($–C_2H_4$), 198 and 137 (from –P – O– cleavage). Furthermore, the four peaks with the Cl-isotopic pattern on the HRMS measurement (Table 5) confirm that oxidation product P5 could have been formed through oxidation of CPF to oxon. CPF is primarily oxidised to P5 (CPF oxon, *m*/*z* 334) by P-oxidation and to P1 (DETP, $[M-H]^-$ *m*/*z* 169 or $[M+H]^+$ *m*/*z* 171) by dearylation. Although *m*/*z* 113 and 141 signals increase with increasing potential (Fig. 22b), they may originate from DETP by fragmentation at the ESI-MS interface (subsequent loss of C_2H_4 leads to 28 and 56 amu variation from the molecular ion peak, *m*/*z* 169). Redox reactions at the electrospray ionisation interface are well known and used to study

oxidative products of xenobiotics [125]. Although in-situ electrochemical oxidation is negligible on its own, it cannot be ignored when ESI is preceded by EC cells. Many active species and intermediates that can be easily oxidised at the ESI interface are produced in the EC cell. Further confirmation by chromatographic retention time and fragmentation profile of the precursor ion *m*/*z* 169 or 171 supports this assumption.

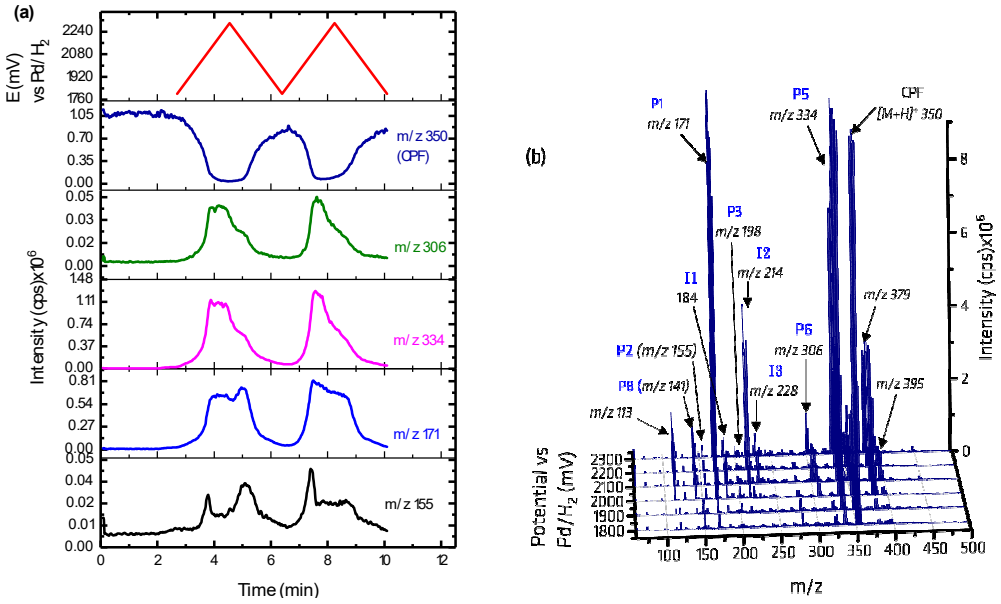

Fig. 22 2D (a) and 3D (b) mass voltammograms of CPF and its oxidation products (+ESI) using BDD WE (reused from Mekonnen et al. [152] with LN 4442490864684)

Both *m*/*z* 113 and 141 were the product ions of P1 (Fig. A2a). However, FT-ICR HRMS measurement (full scan without fragmentation) detected *m*/*z* 141 (δm/m = 5.6 ppm deviation) but not *m*/*z* 113 (Fig. A3a). Hence, *m*/*z* 141 could be desethyl DETP (P8). Meanwhile, two signals at *m*/*z* 379 and 395 arose during EC oxidation from formate adducts with oxon (P5) and CPF (45 amu increase from precursor ion), respectively. Product ion *m*/*z* 180 and 163 (Fig. A2c) from MS/MS spectra of *m*/*z* 198 (P3 in Fig. 22b) confirm the loss of H_2O and Cl^- from TCP, respectively. Due to the stability of the pyridinium cation, more fragments were not detected. Furthermore, Cl-isotopic peaks at 197.9274, 199.9245 and 201.9215 clearly indicate the formation of TCP (Table 5).

It is likely that subsequent oxidation of electrochemically-generated P1 (DETP) and P5 (oxon) yielded *m*/*z* 155 (P2 in Fig. 22b); its ESI-MS/MS spectrum shows product ions of *m*/*z* 137 (–H_2O), 127 (–C_2H_4), 109 (–C_2H_5OH) and 99 (–C_4H_8) (Fig. A2e). Although it was not detected by HRMS

analysis due to its low formation rate (Fig. 22b) and lower sensitivity of HRMS, compared to ESI-MS/MS or ESI-MS, further investigations by EC/LC/MS and LC-MS/MS showed that oxidation product P2 is DEP (*look in sec 0 and 3.2.3*). Similarly, O-dealkylated products by desethylation of CPF (Des-CPF) and oxon (Des-oxon) were detected at *m/z* 322 (P4) and 306 (P6 in Fig. 22b), respectively. The recorded MS/MS and FT-ICR spectra are plotted in Fig. A2d and A3b, respectively.

Meanwhile, the oxidation products P1, P3, P4, and P6 are also assumed to result from fragmentation of oxon and/or CPF in the ESI-MS source. However, further chromatographic analysis using LC-MS/MS and EC/LC/MS showed distinctively different retention times compared to the parent CPF or oxon (Fig. 23 and *sec 3.2.3*).

3.2.2. Production, Separation, and Detection of CPF TPs by Online EC/LC/MS

A chromatographic separation was performed using a RP column to glean more structural and mechanistic information on each of the oxidation products (Fig. 13 flow path B). For automation purposes (production, separation, detection and characterisation), online EC/LC/MS was developed using an external valve to separate the EC reaction and LC separation steps. The mobile phase containing the analyte flows through the EC cell and becomes waste during the EC reaction. The valve was switched to the analytical column and the oxidation products trapped by the external valve loop (10 μL) were flashed back to the analytical column (Fig. 13 flow path B*)*. After a 2,100 mV DC potential was applied for 2 seconds, 7 oxidation product peaks and CPF (16.1 min) were eluted at different retention times (

Fig. **23**). At 9.6 min, P1; 10.7 min, I1 (*m/z* 184); 12.0 min, P3; 14.1 min, P5; 14.8 min, P6; 15.7 min, P2; and 15.9 min, P4 was eluted. The P-oxidation (-S- to -O-) slightly increased the polarity, which could be attributed to the early elution of P5 from CPF and P6 from P4. However, P8 and *m/z* 228 and 214, which increased with increasing potential (Fig. 22b) during online EC/MS measurements, were not separated with EC/LC/MS.

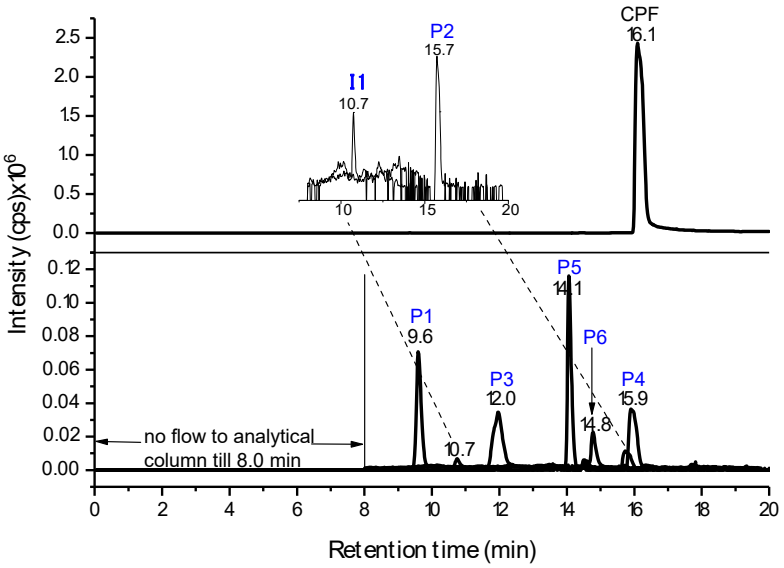

Fig. 23 Extracted ion chromatograms (EIC) of CPF and oxidation products by online EC/LC/MS at a constant potential of 2,100 mV using BDD as WE (modified from Mekonnen et al. [152]

P2 elution at 15.7 min during online EC/LC/MS was unexpected, as this product has a lower molecular weight and is more polar than P1. Additionally, offline LC-MS/MS that uses identical chromatographic conditions and analytical column elutes P2 as early as at 1.8 min (Fig. 24). This may be explained by two reasons: first, the rate of conversion of online EC/LC/MS, the WE surface area and the composition of reaction mixtures may delay the arrival of analytes (e.g. P2) to the LC column. In contrast, in the offline LC-MS/MS offline protocol, all oxidation products are injected at the same time. Second, adsorption of P2 to the surface of the WE electrode could result in a longer elution time, as previously reported [153]. The same is true for oxon and Des-CPF.

3.2.3. *In Vitro* Assay Metabolites *vs* EC/MS Oxidative Products of CPF

Although the above EC/MS oxidative products were successfully identified here, comparison to natural biotransformation products, produced via enzymes such as CYP450 *in vitro* or *in vivo* is a necessary step for annotating unbiased metabolites. CPF was incubated in RLM and HLM assays and the metabolites were investigated by LC-MS/MS. EC/MS effluent composition was changed to LC-mobile phase composition and investigated together with liver microsome incubates in MRM mode to compare retention times. The products P1, P2, P3 and P4 were identified in (-) MRM, while P5 and the parent CPF were identified in (+) MRM mode (Fig. 24).

Except for a 0.1 min deviation in the early eluted product, all P1-P5 products from both EC/MS and RLM analyses were perfectly matched. Previous studies using HLM and blood plasma showed that DEP, DETP and TCP are phase-I metabolites of CPF [73, 75]. In this study, P5, which is one of the main biotransformation products of RLM and EC, was not detected during HLM (female pool sample) incubation with CPF (Fig. A4). This may be explained by fast enzymatic hydrolysis of oxon to TCP and DEP, or that the activation of CPF to oxon occurs in the nervous system and not the liver – as suggested by Choi, *et al.* [72]. Tang *et al.* [74] also showed that metabolism of CPF to oxon varies widely between individual HLMs, based on *in vitro* levels of CYP2B6 and CYP3A4 (the CY isoforms responsible for desulfuration reactions).

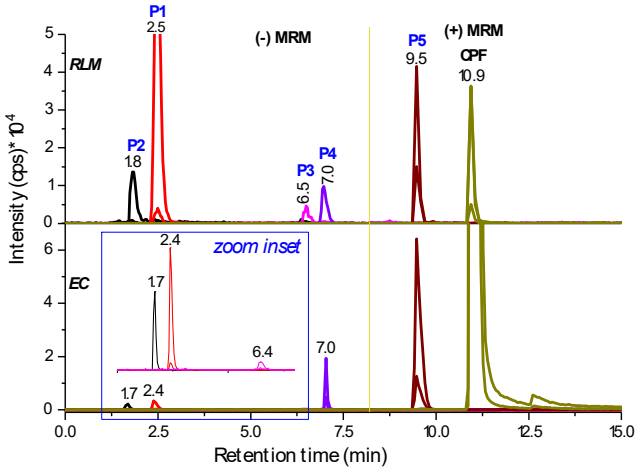

Fig. 24 EIC of CPF metabolites from RLM and EC oxidation products using LC-MS/MS (from Mekonnen *et al.* [152] with LN 4442490864684)

The metabolism of most organophosphate pesticides into their oxons is initiated by SET from -S-lone pair electrons by forming a subsequent epoxide-like intermediate between -S-O-P-. This intermediate is unstable and undergoes oxidative desulfuration to oxon. CPF and oxon could also be converted to their O-dealkylated product by hydrolysis (Fig. 25a). Like CYP450, EC prefers electron abstraction from -S-lone pairs, as other heteroatoms (O, N, and Cl) are more electronegative. Hence, in a similar mechanism, CPF is oxidised to P5 by EC/MS.

In support of this, the peak at *m/z* 157 (Fig. A3a) was determined as an intermediate during the desulfuration oxidation of P1 to P2. Thus, P2, P5 and P6 are formed via epoxide-like (bearing sulfoxide) intermediates, which leads to spontaneous desulfuration of most organothiophosphate compounds. Furthermore, O-dealkylation can occur through HAT as

long as a proton is available on the α-carbon (Fig. 25b). Since the high valent ferric-heme complex abstracts a proton from the α-carbon, O-dealkylation could lead to the production of P1, P4, P6 and P8. In the case of P3, hydrolysis cleavage (Fig. 25a) accounts for the product's formation. In the case of EC/MS-based oxidation, electron abstraction from -O- requires a high potential to be applied, which leads to hydrolysis of water (if available in the modifier). It is, therefore, difficult to simulate by EC/MS, as stated by Jurva *et al*. [118]. In this experiment, hydrolysis of water was observed above 2,300 mV (ACN/MeOH/H_2O, 1:3:1 *v*/*v*/*v* composition). P1, P4, P6 and P8 were also discovered from the 1,800 – 2,100 mV potential (Fig. 22a, b). Hence, the most likely EC oxidation mechanism may be indirect nucleophilic hydroxyl (HO•) and proton (H•) radical formation from water, which attacks -P- and ethoxy, respectively.

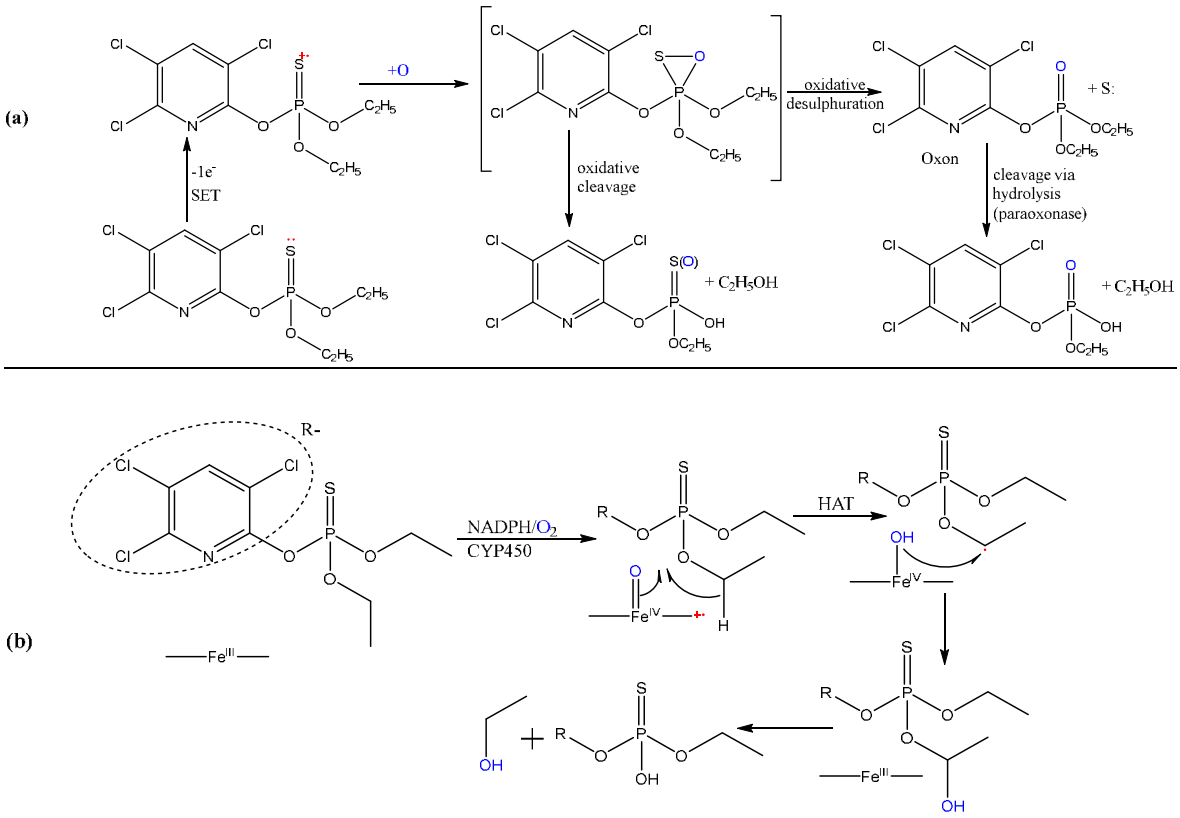

Fig. 25 Proposed reaction mechanisms of CPF metabolism by SET (a) and HAT (b), involving CYP450

Meanwhile, the oxidation products analysed by online EC/(LC)/MS at *m*/*z* 113, 184, 214 and 228 were not detected by offline LC-MS/MS (Fig. 13, flow path C). This may be caused by their short-living characteristics. Although, in this study, P6 was only detected using online EC/(LC)/MS (and not in LMs), previous findings in human lymphocytes indicate that this product is one of the metabolites of oxon [72]. It can, therefore, be concluded here that EC/LC/MS produced the

same oxidative metabolites as those produced by CY during oxidation metabolism, as well as the short-lived oxidation products. On the other hand, EC/MS can also reveal electronic transfer mechanisms of xenobiotic metabolism. For instance, *m*/*z* 214 and 228 were not detected here during the LMs incubation experiment, even though the ESI-MS conditions were the same.

It seems that unstable intermediates are formed by SET from the pyridine N-lone pairs (Fig. A5). Targeted fragmentation of m/z 214 and 228 was observed, with at least two or three -OH groups, respectively. An interesting additional observation was fragmentation of -CO from both m/z 214 and 228. The m/z 184 product, on the other hand, did not undergo such fragmentation. All three short-lived intermediates also demonstrated the Cl-isotopic pattern feature. As a result, m/z 214 and 228 are postulated quinone-like intermediates (Fig. 27b), resulting from modification of the pyridine ring (Intermediate 2 and 3; I2 and I3). Similarly, m/z 184 represent H-radical attack on *N*-pyridinyl, rather than a hydroxyl radical (I1).

3.2.4. Confirmation of CPF Phase I Metabolites by HRMS

The final structural assignments of each metabolite were carried out after confirming the accurate *m*/*z* and molecular formulae by HRM. Typical spectra of CPF oxidative metabolites were measured by FT-ICR-MS, as depicted in Fig. 26a-b and A3a-c. The theoretical *m*/*z* of P1 is 171.0239, which provides strong evidence that the measured peak at *m*/*z* 171.0239 (0.0 ppm deviation from theoretical value) corresponds to DETP (Fig. 26a). Furthermore, the 197.9274 (δm/m = -0.5 ppm) peak with typical Cl-isotopic patterns at *m*/*z* 199.9245 and 201.9215 annotated P3 as TCP. As evidenced in Fig. A3b, P4 at *m*/*z* 321.9022 (δm/m = -0.3 ppm) and P6 at *m*/*z* 305.9251 (δm/m = 0.0 ppm) were matched to desalkylated CPF and oxon, respectively. Similarly, the most common metabolite of CPF (oxon), was also confirmed by its accurate mass and Cl-isotopes at 333.9564 (δm/m = -0.3 ppm, oxon in Fig. A3c). The Structures and potential mechanisms of each product are shown in Fig. 27a.

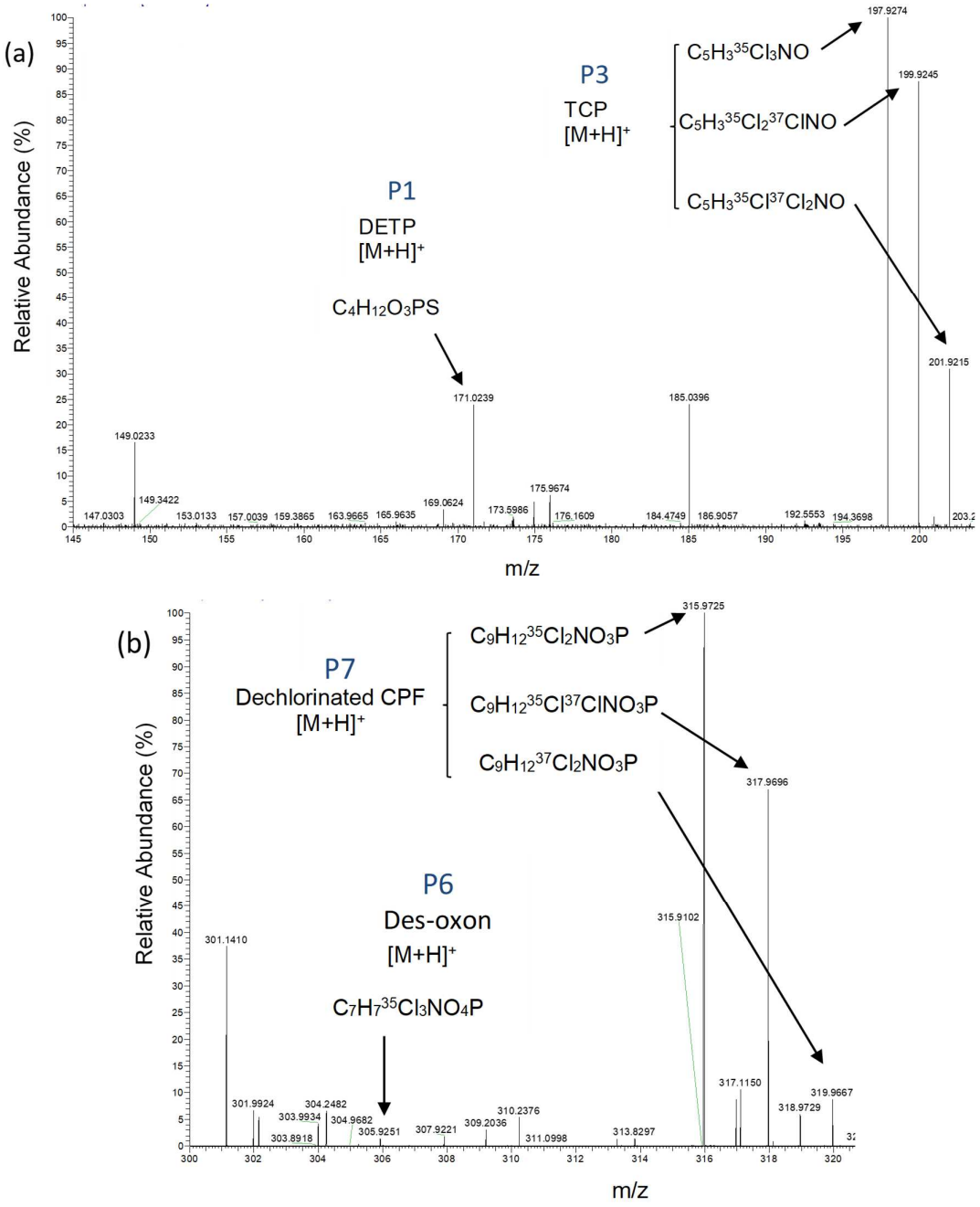

Fig. 26 FT-ICR-MS spectrum of DETP and TCP (a), des-oxon (P6) and monodechlorinated CPF (P7) (b) recorded on (+) ESI after 3 h of synthesis at 2,100 mV vs Pd/H$_2$ DC potential via BDD WE

Moreover, monodechlorination of CPF (P7 in Fig. 27a), which was not detected in the *in-vitro* assays here, was identified at *m/z* 315.9725 (δm/m = 0.0 ppm, Table 5) from electrochemically generated oxidation products (Fig. 26b). Different studies show that CPF phase-I metabolism occurs mainly through desulfuration and hydrolysis, while phase-II metabolism involves conjugation with GSH and Glc [72-73, 75]. DEP (P2) can either be derived from DETP by P-oxidation or from oxon by indirect HO• nucleophilic attack on the phosphate group (e.g. P1

formation from CPF). From the mass voltammogram in Fig. 22a, DEP (*m*/*z* 155) varies like DETP (*m*/*z* 171) in the first full cycle; however, in the second cycle, it increases similarly to oxon (*m*/*z* 334), again behaving like DETP (Fig. 22a). Thus, DEP could be produced from both oxon dearylation and DETP oxidation (-P=S to -P=O). On the other hand, desalkylated oxon (*m*/*z* 306) shows similar signal variation as oxon in both cycles, signifying that it is distinctively formed by O-dealkylation of oxon (Fig. 22a). The potential metabolic pathways of each identified oxidation product, along with their measured mass deviations from theoretical, are summarised in Table 5.

Table 5 Detected CPF oxidation metabolites with their retention time, mass deviation and proposed pathways (from Mekonnen *et al.* [152] with LN 4442490864684*)*

Compounds	t_R (min) on EC/LC/MS	Molecular formula	Measured *m*/*z*, $[M+H]^+$ by HRMS	δm/m (ppm)	Proposed oxidation pathways	Confirmed by	Detected in experiments
CPF	16.1	$C_9H_{11}Cl_3NO_3PS$	349.9334	0.6	-	-	-
Oxon (P5)	14.1	$C_9H_{11}Cl_3NO_4P$	333.9563, 335.9533, 337.9543, 339.9515	-0.3	P-oxidation of CPF	LC-MS/MS, HRMS, EC/LC/MS	EC, RLM
Des-CPF (P4)	15.9	$C_7H_7Cl_3NO_3PS$	321.9022, 323.8993, 325.8965	-0.3	O-dealkylation of CPF	LC-MS/MS, HRMS, EC/LC/MS	EC, RLM, HLM
DETP (P1)	9.6	$C_4H_{11}O_3PS$	171.0239	0.0	CPF dearylation	LC-MS/MS, HRMS, EC/LC/MS	EC, RLM, HLM
DEP (P2)	15.7	$C_4H_{11}O_4P$	155.0*	-1.9	P-oxidation of P1, P5 dearylation	LC-MS/MS, EC/LC/MS	EC, RLM, HLM
TCP (P3)	12.0	$C_5H_2Cl_3NO$	197.9274, 199.9245, 201.9215	-0.5	CPF dearylation	LC-MS/MS, HRMS, EC/LC/MS	EC, RLM, HLM
Des-oxon (P6)	14.8	$C_7H_7Cl_3NO_4P$	305.9251	0.0	Deethylation of P5	EC/LC/MS	EC
I1	10.7	$C_5H_4Cl_3N$	184.0*	-36.0*	Dearylation	EC/LC/MS	EC
DeC-CPF (P7)	-	$C_9H_{11}Cl_2NO_3PS$	315.9725, 317.9696, 319.9667	0.0	CPF dechlorination	HRMS and EC/MS	EC
P8	-	$C_2H_7O_3PS$	141.9854	5.6	P1 O-dealkylation	EC/MS, HRMS	EC

*t_R – retention time, *- measured by QTRAP-MS/MS, ppm – parts per million, EC – measured by EC/MS, I1-intermidate 1*

In summary, six main oxidative metabolites of CPF (P1 – P6) were successfully identified by EC/(LC)/MS and compared with *in vitro* assay metabolites. The products of CYP450 incubates and EC/MS-synthesised products were compared in terms of retention time, MS/MS spectra (fragmentation), accurate mass from HRMS and isotopic pattern. Another interesting feature of EC/MS is that it is able to determine fast reactive species/intermediate metabolites. In line with this, I1, I2 and I3 were intermediates determined here by online EC/MS.

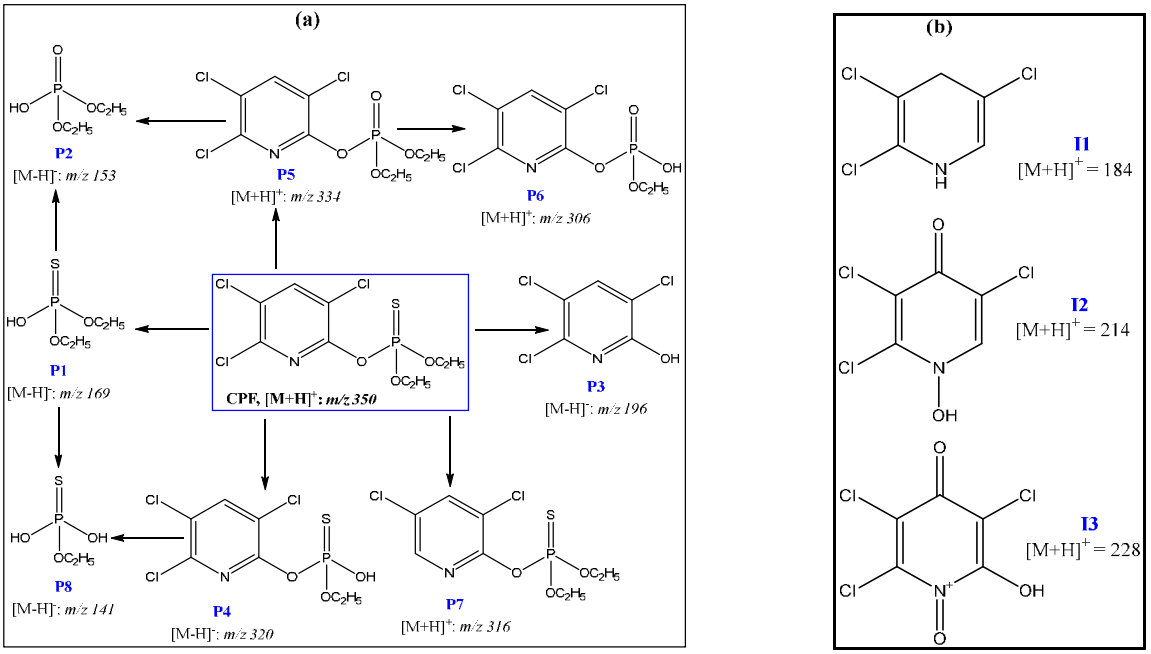

Fig. 27 Proposed phase I oxidative metabolism of CPF (modified from Mekonnen *et al.* [150]) (a) and structures of short-lived intermediates detected by EC/MS (b)

3.3. Biotransformation of FLP (Phase I)

Unlike CPF, FLP electrochemical oxidation was achieved using two different experimental approaches: direct EC (in ACN/MeOH, 1:1 *v*/*v* with 0.1% HFA and E_{max} = 2,300 mV) and indirect EC (in ACN/H_2O, 9:1 *v*/*v* with 0.1% HFA + 5 mmol/L NH_4FA and E_{max} = 2,500 mV). This was done to mimic as many metabolites as possible by EC/MS. In addition, we observed reproducible oxidative TPs (both in type and quantity) with stable current flow by direct EC (Fig. 28a five continuous full cycles); however, it was impossible to predict oxidative metabolites by hydroxylation and related mechanisms. Conversely, using indirect EC with aqueous media, prediction of oxidative metabolites by hydroxylation is easier than other metabolites, such as N-dealkylation or dehydrogenation. As a result, two experimental designs were followed to predict TPs via N-dealkylation, lactam formation, oxidation via dehydrogenation (direct EC) and hydroxylation and successive dehydrogenation or N-dealkylation (indirect EC). The 2D mass voltammograms recorded by EC/MS (without HPLC-column) are shown in Fig. 28a and b for direct and indirect EC, respectively. The oxidation of FLP (*m*/*z* 397, $[M+H]^+$) can be easily identified by a reduction in signal intensity at a potential ≥1,650 mV. Conversely, generation of TPs is evidenced by increasing signal intensities when the potential is applied (Fig. 28a,b).

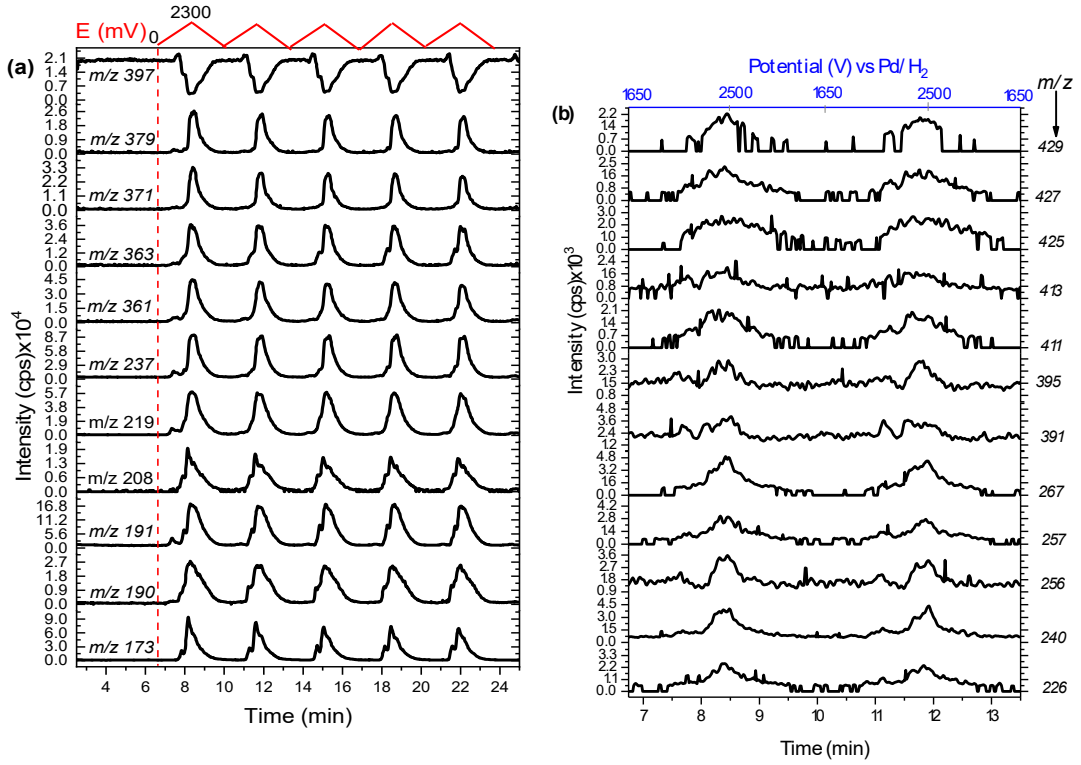

Fig. 28 Mass voltammograms of FLP in ACN/MeOH, 1:1 *v*/*v* with 0.1% HFA (direct EC) scanned 0 – 2,000 mV, 10 mV/s (a) and in ACN/MeOH/H_2O, 40/50/10 *v*/*v*/*v* with 0.1% FA and 5 mM NH_4FA (indirect) scanned from 1,650 – 2,500 mV, 10 mV/s using BDD as WE (b)

As shown in Fig. 28a, products such as *m*/*z* 173, 190, 191, 208 and 363 show additional miner peaks/shoulders. These indicate that a specific TP could be formed at several different maximum potentials or from two different oxidative pathways. The exact masses of several EC and HLM-derived products measured by FT-ICR HRMS and the corresponding modifications of the parent FLP are listed in Table 6. Some of the transformation products (EC and LMs) were not confirmed by HRMS. This may be due to either the unstable nature of the products or the differences in the sensitivity of the techniques itself. However, from a combination of EC/MS, MS/MS fragmentation, isotopic patterns and retention time analyses, the possible structure of some of the products were proposed and tabulated in Table 7.

Table 6 Transformation products of FLP with the corresponding modification, exact masses and deviations measured by HRMS after incubation with HLM and oxidation by EC (from Mekonnen et al. [154] with LN 4347550440858)

Transformation products	Molecular formula, $[M+H]^+$	Calculated *m/z*, $[M+H]^+$	Measured *m/z*, $[M+H]^+$	δm/m (ppm)	Proposed modification	Formed by
FLP	$C_{16}H_{12}ClF_6N_2O$	397.0535	397.0535	0.0	-	-
M1a/M1b	$C_{16}H_{10}ClF_6N_2O_3$	427.0279	427.0267	-2.8	+2O, -2H	EC, LM
M2	$C_8H_6F_3O_2$	191.0314	191.0317	1.6	N-dealkylation, +OH	LM
M3	$C_8H_7F_3NO$	190.0474	190.0475	0.5	N-dealkylation, +H	EC, LM
M4	$C_{16}H_{13}F_6N_2O_2$	379.0881	379.0880	-0.2	-Cl•, +HO•	LM
M5	$C_{16}H_{12}ClF_6N_2O_3$	429.0435	429.0441	1.4	+2O	EC, LM
M6	$C_7H_4ClF_3NO_2$	225.9877	225.9874	-1.3	C-dealkylation, +2O	EC, LM
M7a/M7b	$C_{16}H_{12}ClF_6N_2O_2$	413.0491	413.0489	-0.5	+O	EC, LM
M10	$C_{16}H_{13}F_6N_2O$	363.0932	363.0932	0.0	-Cl•, +H•	EC, LM
M11 (olefin)	$C_{16}H_{10}ClF_6N_2O$	395.0380	395.0380	0.0	-2H	EC, LM
M15	$C_{16}H_{11}F_6N_2O$	361.0776	361.0786	2.7	-HCl	EC
E1	$C_8H_6ClF_3N$	208.0135	208.0135	0.0	N-dealkylation, -2H	EC
E2	$C_8H_6ClF_3NO_3$	255.9983	255.9975	-4.3	N-dealkylation, +3O	EC
E3	$C_8H_6ClF_3NO_2$	240.0034	240.0032	-0.8	N-dealkylation, +2O	EC
E5	$C_{16}H_8ClF_6N_2O_3$	425.0128	425.0115	-3.0	+2O, -4H	EC
Intermediate	$C_8H_4F_3O$	173.0208	173.0209	0.6	N-dealkylation	EC

***M** –metabolites detected in LMs and EC, **LM** –liver microsome, **E** –products produced by EC but not by LM, **δm/m** – relative mass deviation error*

The fungicide FLP shows several metabolic pathways in both EC/MS oxidative stress and *in vitro* assay (RLM and HLM) incubates. The main phase I metabolites produced via dehydrogenation, N-dealkylation, hydroxylation and dehalogenation were identified; these will be discussed in *sec 3.3.1* to *3.3.4.* For clarity, the metabolites produced from EC-based oxidation and/or CYP450 incubation were assigned with the letter 'M', while those produced only from EC were assigned the letter 'E'.

3.3.1. Dehydrogenation and N-dealkylation of FLP

Structural and oxidation pathway analyses are shown in **Fig. 30**. The known olefin metabolite of FLP was detected by HRMS in both EC and LMs experiments at *m/z* 395 (δm/m = 0.0 ppm, Table 6), although the former produced a low yield (Fig. 28b) likely through oxidation via hydrogen abstraction from C_7- and C_8- (FLP structure shown in Fig. 8). Activation of aliphatic hydrocarbons is especially problematic with EC/MS. Indirect oxidation due to involvement of a supporting electrolyte (i.e. mediated redox reaction) could produce olefins (M11). The anion (e.g. formate) forms a radical that subsequently attacks C-H bonds in the electron transfer process [155]. On the other hand, electron abstraction from -NH-lone pairs could lead to the formation of imines with C_8- (**Fig. 30**a). In support of this, oxidative products of *m/z* 190 and 208

were detected by EC/MS (Fig. 28a). According to previous EFSA and APVMA studies, FLP is metabolised to Z- and E-olefin isoforms by *in vitro* and *in vivo* [88-89].

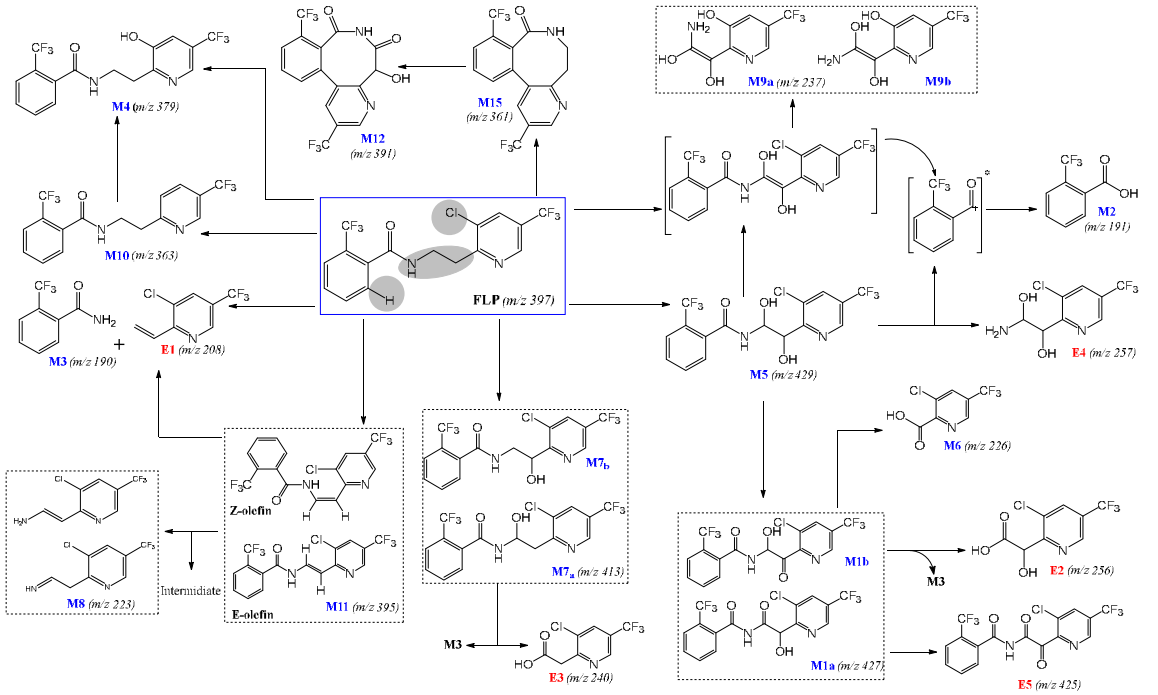

Fig. 29 Proposed oxidation products of FLP generated after electrochemical oxidation by direct and indirect EC conditions (modified from Mekonnen *et al.* [154] with 4347550440858)

The likely isomeric compounds, whose structures were predicted by the applied techniques, are highlighted with dashed rectangles.

Further investigations by FT-ICR-MS (Table 6), EC/LC/MS and LC-MS/MS proved that *m*/z 190 and 208 signified a 2-trifluoromethylbenzamide metabolite (M3 in Fig. 29) and a 3-chloro-2-ethenyl-5-trifluoromethylpyridine oxidative product (E1 in Fig. 29), respectively. The accurate masses were then fitted with their theoretical values (δm/m = 0.5 ppm for M3, and 0.0 ppm for E1 in Table 6). Oxidation product E1 ($C_8H_6ClF_3N$) was not detected in LMs, which led to the conclusion that M3 is produced by N-dealkylation of olefin FLP in EC and parent FLP by CYP450. Both E1 and M3 were detected at a lower potential (around 1,800 mV), which agrees with previous reports that N-dealkylation products are readily formed by EC [156-157]. Hence, the formation of olefin and imine is the crucial step for further hydroxylation and N-dealkylation of FLP, as radially undergo oxidation by generated epoxide intermediates.

3.3.2. Hydroxylated TPs of FLP by Online EC/LC/MS and Offline LC-MS/MS

Another observed important oxidative metabolism of FLP was hydroxylation. Both mono (*m/z* 413) and dihydroxylated FLP (*m/z* 429) oxidative products were formed at around 2,000 mV by indirect EC (Fig. 28b). The presence of Cl-isotopic peaks and adducts (Na- and K-adducts) helped to determine the possible modification of FLP. The FT-ICR HRMS data with a mass error of 0.5 ppm (M7a/b: $C_{16}H_{12}ClF_6N_2O_2$, Table 6) and 1.4 ppm (M5: $C_{16}H_{12}ClF_6N_2O_3$, Table 6) ensured the formation of mono- and dihydroxyl FLP, respectively. The proposed oxidation mechanism of hydroxyl FLP is shown in **Fig. 30**a,b and could be formed either via SET or HAT. Electrochemically, the lone pairs on the amine (-NH-) are radially available for exchange with the BDD surface (by SET), which could form imine (between -N=C_8) instead of olefin (-C_8=C_7-). The detection of E1 by EC/MS supports this mechanism.

Fig. 30 Mechanism of mono- and dihydroxyl FLP formation via epoxide and imoxide intermediates (a) and SET and HAT mechanisms of FLP hydroxylation (b)

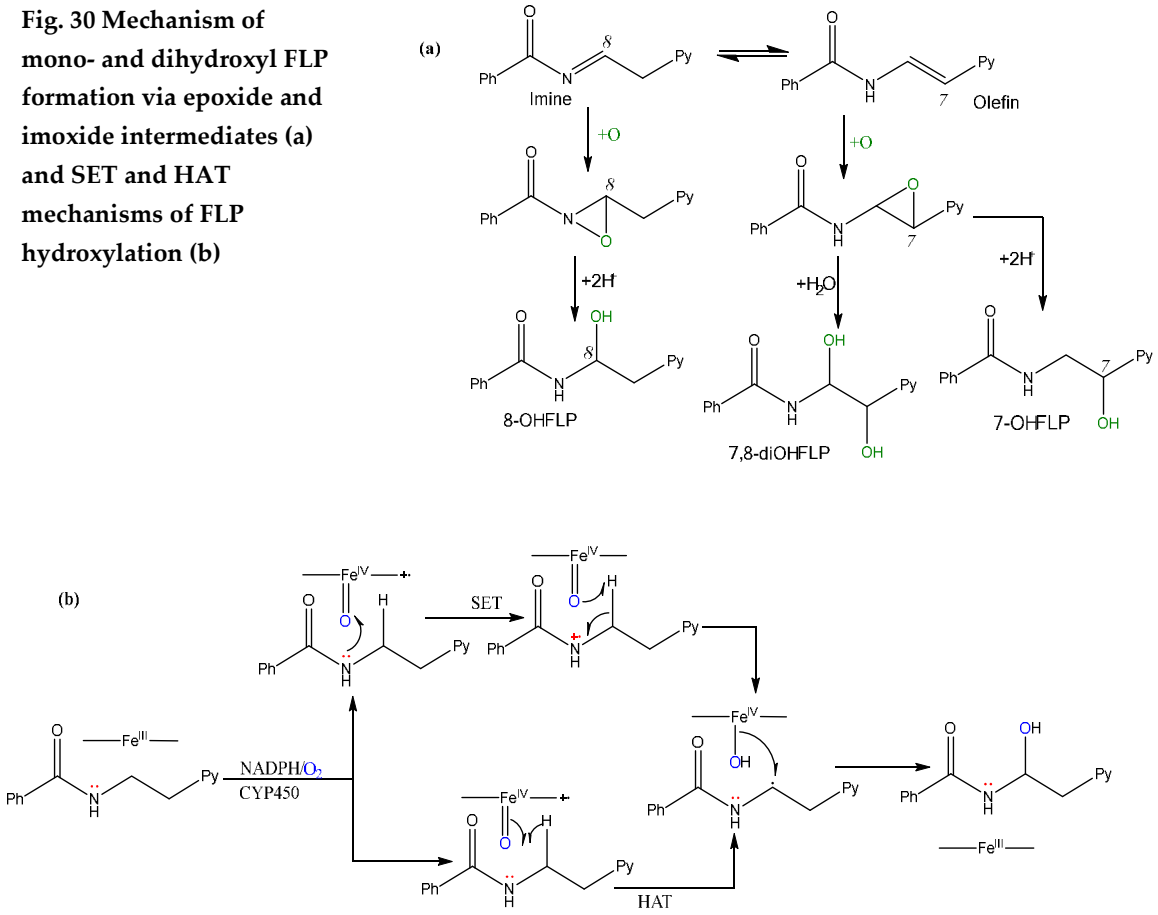

Regardless of whether imine or olefin are initially formed, both could easily form an epoxide intermediate together with ROS during the EC reaction (**Fig. 30**a). The unstable epoxide leads to diol formation (M5 in Fig. 29) by subsequent hydrolysis of 7- or 8-monohydroxyl FLP (M7a, b in

Fig. 29) through addition of active protons. On the other hand, in CYP450 metabolism the high valent [FeO^{4+}] heme complex could abstract an electron from -NH- (via SET), which bears a positive radical on the amine group and leads to H-abstraction from α-carbon to produce a carbon radical at C_8 and -Fe^{IV}-OH (**Fig. 30**b). This radical then abstract the •OH from -Fe^{IV}-OH and regenerates -Fe^{III}-by forming 8-OH FLP (M7). The carbon radical at C_8- could also abstract a proton to form a more stable carbocation on C_7- (due to electron delocalisation through the Py-ring), which finally yields 7-OH (M7). It is also possible that -Fe^{IV}=O could directly bear H-C_8 (HAT), leading to the same final product as SET (**Fig. 30**b). In terms of electrochemistry, SET is followed more commonly than HAT for the hydroxylation of FLP due to the availability of amine free electrons. The SET mechanism is similar to CYP450 reactions, in that it could yield two isomeric monohydroxyl FLPs (7-OH and 8-OH FLP). Thus, mono- and dihydroxyl FLP could be formed by SET via carboradical and epoxide intermediates, respectivel.

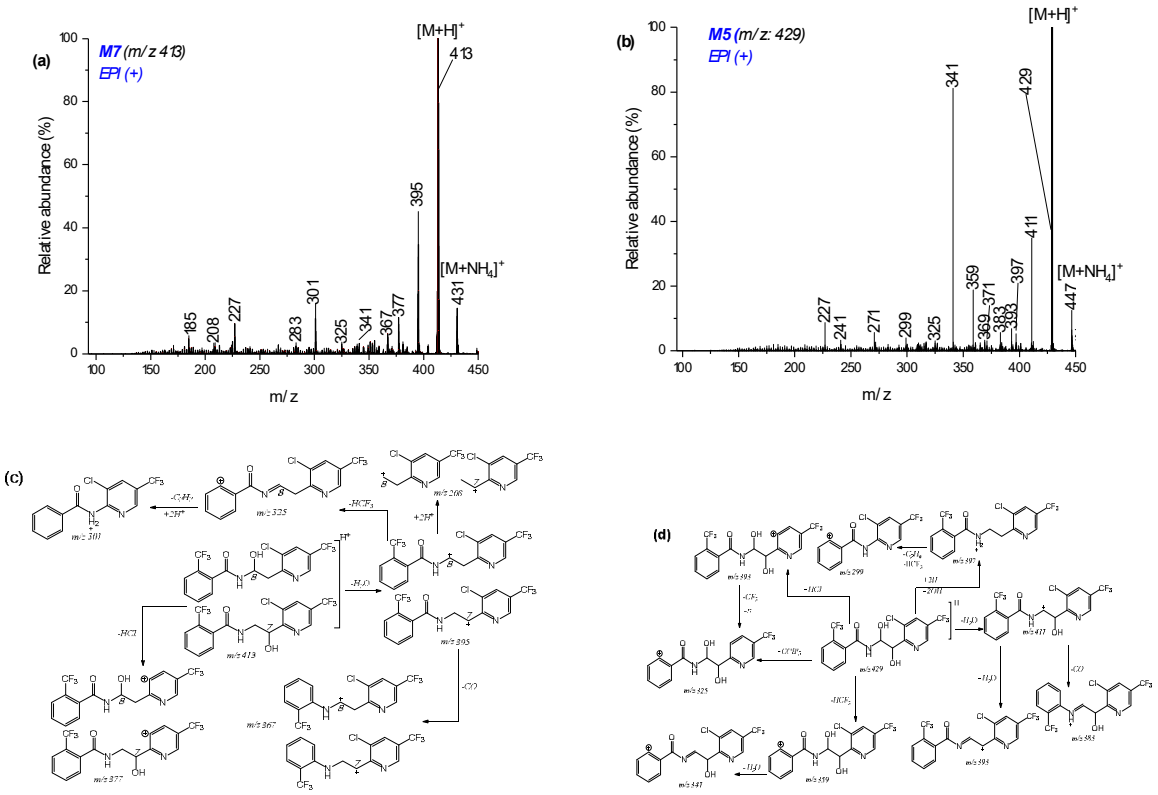

Fig. 31 (+) ESI-MS/MS spectra and the corresponding proposed fragmentation mechanisms of M7–monohydroxylated FLP (a, c) and M5 –dihydroxylated FLP (b, d). The figures are part of Mekonnen et al. [154] with LN 4347550440858.

In support of this, *m*/*z* 411 was detected by online EC/MS and could represent an epoxide intermediate (Fig. 28b). Acquired MS/MS spectra and proposed fragmentation mechanisms of M5 and M7 are presented in **Fig. 31**a-d. The precursor ion at *m*/*z* 413 (M7) was fragmented to *m*/*z* 395 (–H_2O) and 377 (–HCl). Similarly, *m*/*z* 429 (M5) was fragmented to *m*/*z* 411 (–H_2O), 397 (–2OH, +2H^+) and 393 (–HCl), which proves that 7,8-diOH FLP is formed. In both cases, the ammonium adduct (*m*/*z* 431 **Fig. 31**a and *m*/*z* 447 **Fig. 31**b) is produced due to the presence of 5 mM NH_4FA as an electrolyte in the EC reaction (enabling conductivity). A previous study showed that hydroxylation at C_7– and/or C_8– produces the main metabolites of FLP [88].

Thorough comparison between EC and CYP450-based metabolism by Jurva *et al*. [118] showed that hydroxylation of aliphatic carbons is more difficult compared to aromatic rings. To elucidate the hydroxylation mechanismis of FLP, different constant potentials were applied and the products were monitored by online EC/LC/MS. The chromatograms are shown in Fig. 32. At 2,000 mV two monohydroxylated peaks of *m*/*z* 413 (M7a and M7b) and one dihydroxylated peak of *m*/*z* 429 (M5) were separated and characterised alongside other oxidative products (Fig. 32). The more hydroxylated metabolites are eluted earlier in the RP column due to higher polarity (M5, then M7); thus, all investigations point to M5 being 7,8-di OH FLP and the two peaks (M7a and M7b) representing 7- and 8-OH FLP isomers. This result contradicts the findings by Jurva *et al*. [118]; however, the relatively more abundant product ion at *m*/*z* 395 for the monohydroxylated FLP (**Fig. 31**a) and at *m*/*z* 341 for the dihydroxylated FLP (**Fig. 31**b) suggest aliphatic hydroxylation of FLP. As additional proof, the N-dealkylated metabolite of imine or olefin at *m*/*z* 223 (M8), as well as E1 and M11, (look structures in Fig. 29) support the modification of FLP in the aliphatic region. As the potential was increased to above 2,300 mV, both 2-trifluoromethylbenzoic acid (M2 in Fig. 29) and M3 were not stable enough, while products such as M7a and M7b persisted up until 2,700 mV (Fig. 32).

Interestingly, a single M5 peak at 2,000 mV split into two peaks (M5a and M5b) at 2,500 mV and then into four peaks (M5a-d) at 2,700 mV (Fig. 32); these peaks could be isomers produced from further hydroxylation of the two aromatic rings at the higher applied potentials. Further investigation of specific hydroxylation sites (*ortho, para* or *meta*) was not carried out.

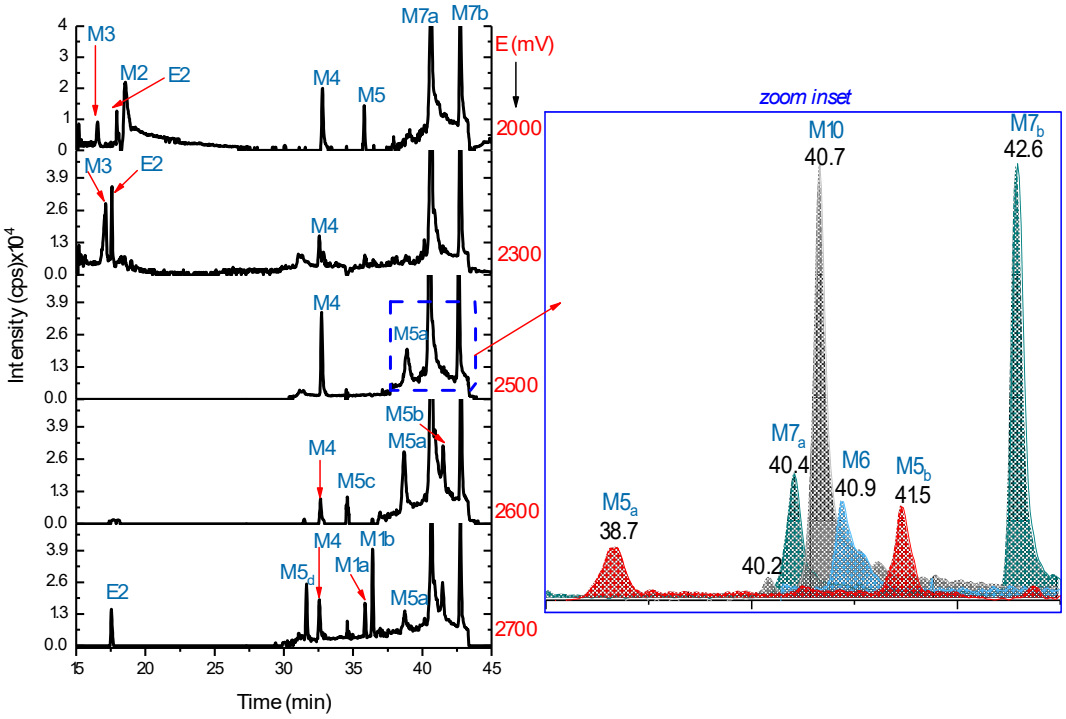

Fig. 32 TIC (left) of FLP oxidation products at different potentials and EIC of selected products at 2,500 mV (right) measured by online EC/LC/MS in ACN/H_2O, 9:1 *v/v* with 0.1%FA and 5 mmol/L NH_4FA (modified from Mekonnen *et al.* [154] with LN 4347550440858)

The M5 disappeared at ≥2,300 mV and two new peaks, 2 Da lower than the corresponding 7,8-diOH FLP at *m/z* 427 (M1a and M1b: $C_{16}H_{10}ClF_6N_2O_3$, δm/m = -2.8 ppm in Table 6) appeared at 2,700 mV. Targeted fragmentation of *m/z* 427 by MS/MS (*see Fig. A7a*) showed product ions at *m/z* 409 (–H_2O), 173 (Ph–CO) and 145 (Ph-). Thus, M1a and M1b could be hydroxylimide derivatives of M7a and M7b, produced by electrochemical oxidation of alcohol (-CH-OH → -C=O). Similarly, both -C_7-OH and -C_8-OH oxidation products were detected at *m/z* 425 by EC/MS and HRMS (E5 in Table 6, δm/m = -3.0 ppm) but not by *in vitro*. Electrochemical oxidation of alcohol into ketone or aldehyde is a widely observed mechanism in EC/MS-based oxidation reactions [120]. The observation of M1 and E5 products at 2,700 mV agrees with the requirement for a higher potential to abstract an electron from oxygen. In general, M1, M5 and M7 are FLP metabolites formed by hydroxylation in both LM assay incubates and non-enzymatic EC/MS experiments. On the other hand, too many oxidative products by successive N-dealkylation of hydroxylated products were detected in both EC and *in vitro* assay incubates.

To understand the possible correlation between M5, M7a and M7b, indirect EC oxidation at 2,300 mV DC potential was performed using SynthesisCell™ for 250 min. Aliquots were collected (1 mL) at different time intervals and analysed by LC-MS/MS. As shown in Fig. 21c, M7b and M5 were abundantly synthesised for the first 20 min but their production then decreased after 25 min. The M7b revealed constant intensity at around $3x10^7$ cps until 125 min, following which the dihydroxyl M5 intensity slightly increased. Conversely, M7a was not produced until the 20th min and then significantly increased in yield after 25 min. Unlike M5 and its isomer M7b, M7a showed steady production from 25 to 125 min of the experiment. This shows that M7a and M7b were not produced at the same time; instead, their synthesis was negatively correlated. It corroborates the proposed mechanism in **Fig. 30**a, b. Furthermore, when the synthesis time exceeded 150 min, M7a, M7b and M5 intensities all decreased, which may be explained by their oxidation to M1a and M1b (alcohol to carboxyl).

3.3.3. TPs by N-dealkylation of Hydroxyl FLP

After mono- and dihydroxylation of FLP, extensive modification by N-dealkylation was observed both during EC/MS oxidation and *in vitro*. As evidenced by HRMS and EC/(LC)/MS measurements (Table 6 and Fig. 32), hydroxylated FLP was further oxidised via N-dealkylation. The oxidative metabolites M2 (δm/m = 1.6 ppm in Table 6), M3 (δm/m = 0.5 ppm), monohydroxyl-[3-chloro-5-trifluoromethylpyridyl]acetic acid (E2, δm/m = -4.3 ppm) and (3-chloro-5-trifluoromethylpyridn)-yl carboxylic acid (M6, δm/m =-1.3 ppm) were identified at 2000 mV (Fig. 32 and 29). N-dealkylation of the parent FLP could have yielded M2 and M3, which are known metabolites of FLP in fruits and animals [90]. Depending on synthesis time and chemical composition, a single product could be produced from several mechanisms in principle. For instance, M3 seems to be produced from N-dealkylation of one or more compounds by EC/MS: from olefin FLP together with E1; from 8-OH FLP alongside with pyridyl acetic acid (E3); and from hydroxylimide (M1) in parallel to E2 (Fig. 29). In support of this, a 2-trifluormethlybenzoyl intermediate (*m*/*z* 173) that was later hydroxylated to M2 was detected by both EC/MS (*m*/*z* 173 in Fig. 28a) and HRMS (δm/m = 0.6 ppm, Table 6). The detection of the benzoyl intermediate could have resulted from electron delocalisation stability (through the Ph-ring). Another oxidation product of *m*/*z* 257 (Fig. 28b) yielded *m*/*z* 279 (+Na-adduct), 239 (–H_2O) and 259 (Cl-isotope) product ions (Table 7). This may represent 1-amino-2-[3-chloro-5-

trifluoromethylpyrdiyl]ethan-1,2-diol (E4 in Fig. 29) formed together with M2 by N-dealkylation of 7, 8-diOH FLP. During CYP450 catalysed metabolism, FLP could have unmasked its amine group by SET or HAT. Similarly, the lone pairs on the amine group are freely available for electrochemical abstraction (SET) to initiate HAT from the α-carbon (Fig. 33a). Subsequently, hydrolysis and HO• nucleophilic attack on the carbonyl radical may have yielded amide and carboxylic acid metabolites. Thus, the metabolites M2, M3 and 3-chloro-5-trifluoromethylpyridinyl ethanimine (M8), as well as the electrochemical products E1, E2, E3 and E4, should have been formed via N-dealkylation of the parent FLP and/or its TPs. Recorded MS/MS spectra and their respective fragmentation pattern of selected TPs are depicted in Appendix Fig. A6a – e and Fig. A7a,b.

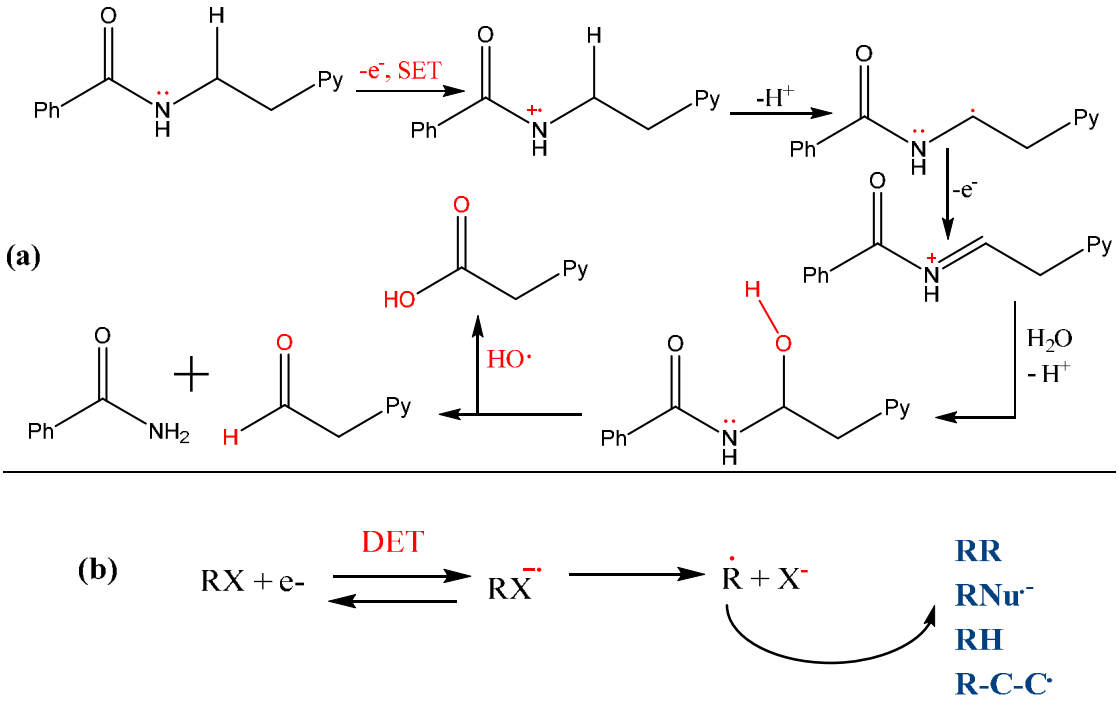

Fig. 33 Mechanism of FLP oxidation via SET N-dealkylation to produce Ph-amide and Py-carboxylate metabolites (a) and via DET dehalogenation oxidation (b) using EC/MS

However, several products of both EC and LMs were not detected by HRMS and their possible structures were, therefore, assumed only from EC/(LC)/MS and LC-MS/MS data (Table 7). Further investigation is also required to identify the possible competitive products of identical *m/z*. For example, M8 could be its isoform, (3-chloro-5-trifluoromethylpyridyl)-ethenamine, both of which show *m/z* 223 (Fig. 29). Similarly, in LMs, Py-carboxylic acid and Py-ethanol are

known metabolites of FLP [88] and are analogous to each other (i.e. they share same molecular formula $C_7H_4ClF_3NO_2$ and are of equal *m/z = 226*).

3.3.4. Oxidative Dehalogenation of FLP

In addition to hydroxylation and N-dealkylation, HO- and H- substitution of -Cl were identified in both LM incubates and EC/MS oxidative experiments. The *m/z* at 363 and 379 in Fig. 28a were also separated in HLM incubates at 40.7 and 32.8 min (Fig. 34a), respectively. As additional evidence, both peaks were eluted together with their respective +Na-adduct (*m/z* 385 and 401), without the Cl-isotopic pattern. MS/MS spectra of *m/z* 379 is shown in Fig. A6e. These findings confirm the modification of FLP by HO- and H-substitution of -Cl, generating *m/z* 379 and 363, respectively. During FT-ICR HRMS, both *m/z* 363 and 379 were detected with 0.0 and -0.2 ppm deviation from the theoretical value (Table 6), respectively. Consequently, M4 ($C_{16}H_{13}F_6N_2O_2$) was assigned for the HO-substituted and M10 ($C_{16}H_{13}F_6N_2O$) for the H-substituted metabolites (Fig. 29). Aside from -Cl substitution by H- or HO-, two oxidative products were formed by cyclisation between C_3- and C_{16}- after loss of neutral HCl (*m/z* 361 in Fig. 28a and *m/z* 391 in Fig. 28b). Similar mechanisms of EC-based oxidation by dechlorination of aromatic rings were reported elsewhere [131, 152]. In particular, direct SET and HAT are not mechanisms that favour this because of the high electronegativity of -Cl and a lack of α-halogen. Often, dissociation electron transfer (DET) is responsible for dehalogenation oxidation of xenobiotics through formation of an intermediate $RX^{-\bullet}$ (where X is a halogen). After an electron is exchanged to the BDD, the intermediate $RX^{-\bullet}$ is unstable and dissociates by attaching a radical to the molecule (R•) and an anion to the halogen (Fig. 33b). The R• radical can then undergo different reactions, such as bonding with nucleophiles (Nu:), dimerisation to itself (RR), protonation (RH) or polymerisation, depending on the molecular structures (Fig. 33b).

3.3.5. *In Vitro* Metabolites *vs* EC/MS Oxidative Products of FLP

All TPs generated by liver microsome incubation and EC oxidation were analysed by LC-MS/MS in parallel to a FLP standard solution, so as to compare the feasibility of each approach for simulation of FLP biotransformation products. Although one-to-one comparison is impossible, many identical biotransformation products were detected in both systems. A typical chromatogram of FLP metabolites from HLM is shown in Fig. 34a. As there were no

differences between HLM and RLM metabolites, only the HLM metabolite chromatogram was pictured. The hydroxyl metabolites M5, M7a and M7b were eluted at 23.4, 24.3 and 24.6 min (Fig. 34), respectively. Elution of their +Na-adduct at *m*/*z* 435 and 451, +K-adduct at *m*/*z* 451 and 467, and Cl-isotopic pattern at *m*/*z* 415 and 431 occurred at the same retention as M7 and M5, which assured the mono- and dihydroxyl FLP metabolites, respectively. Moreover, the accurate *m*/*z* in Table 6, their MS/MS spectra and fragmentation in **Fig. 31**a-d and A7b and their elution order in Fig. 34a, b (with di-OH eluted first) confirmed that EC/MS can successfully mimic *in vitro* metabolites. The two peaks, M7a and M7b, also confirmed formation of isomeric monohydroxylated products in EC/MS. To differentiate between 7-OH and 8-OH FLP, a (+) MRM method was developed for targeted analysis of FLP, M3, 7-OH, 8-OH and 7,8-diOH by LC-MS/MS (Fig. 34b). The MRM transitions and instrumental conditions are listed in Table 3. The 7,8-diOH FLP (M5) at 19.2 min and the two monohydroxyl FLPs (M7a and M7b) at 19.9 and 20.6 min were detected. The M3 peak (15.9 min) appeared to give rise to another two peaks corresponding to FLP (20.9 min) and to monohydroxyl FLP (19.6 min). Since the Py-ring cation can easily stabilise by the -OH free electrons, 8-OH can fragment into *m*/*z* 190 (the same ion product as M3 molecular ion) more easily than 7-OH FLP. Hence, the peak at 19.6 min is most likely 8-OH FLP (M7a), while the one at 20.6 min is 7-OH FLP (M7b). Another interesting observation was the significant difference in intensities between EC/MS-synthesised products and those from liver microsome incubates (M7a and M7b in Fig. 34a *vs* b). In HLM, M7b showed the highest intensity, while the M7a produced in EC agreed with the synthesis mechanism (imine by EC and olefin by CYP450). Hydroxylimide (M1) in HLM was also fragmented by the same mechanisms as 7,8-di OH FLP to produce *m*/*z* 409 and 391 (2 Da lower than M5, Fig. A7a); these were eluted at the same retention time, at *m*/*z* 429 (Cl-isotope) and 449 (+Na-adduct), while the M5 peak appeared at *m*/*z* 431 and 451 (Fig. 34a). Unlike EC/MS, only one M1 product was detected in microsomes.

As shown in Fig. 32, the hydroxylation sites can differ between electrochemical and enzymatic reactions and result in the same *m*/*z* but different structures. CYP450 enzymes are stereoselective and catalyse specific reactions, whereas electrochemical oxidation favours hydroxylation of electron-rich groups. In line with this, oxidative products E1, E2, E3 and E4 (all by N-dealkylation) are only confirmed in EC synthesized products.

Table 7 Retention time (t_R), mass fragments and proposed mechanisms of miscellaneous TPs after LMs and EC experiments analysed by LC-MS/MS (from Mekonnen et al. [154], LN 4347550440858)

Products	(+) ESI (*m*/*z*)	t_R (min)	Product ions, Q3 (*m*/*z*)	Proposed mechanisms	Formed by
E4	257	n.d.	279, 259, 239, 153	+2O, N-dealkylation	EC
M8	223	24.9	225, 209, 196, 187, 167, 91	-2H, N-dealkylation	EC, HLM
M9	237	24.8, 26.1	220, 219, 162	-2H, +2O,N-dealkylation	EC, LM
M12	391	26.9	413, 373, 321	+2O, -3H	EC, LM
M13[u]	317	27.2	251, 219, 201, 185, 170	-2CO, -HCl	EC, LM
M14[u]	371	27.6, 29.1, 31.8	353, 297, 253, 213, 223, 171, 97	-2CO, +2O	EC, LM
M16[u]	493	28.55	475, 457, 198, 273, 221	+6O	LM

***n.d.** – not detected, **U** – unknown, **LM** – liver microsome*

An EC major product of *m*/*z* 237 (Fig. 28a) appeared together with two minor peaks at 24.8 and 26.1 min (M9 in Fig. 34a) during *in vitro* experiments. These peaks could represent Z-/E-hydroxylated olefin isomers of E2, formed by N-dealkylation of the 7,8-dihydroxyl olefin FLP intermediate (Fig. 29).

Metabolites M2 and M3, produced by N-dealkylation of FLP, were shown at 22.1 min and 22.4 min in microsomal assay incubates (Fig. 34a), respectively. An intense peak, M8, at 25.0 min (Fig. 34a) yielded an ion product 225 (Cl-isotope), 196 (–C_2H_2), 167 (–Cl), as well as other characteristic peaks (Fig. A6c and Table 7); this corresponds to the N-dealkylation of M11 (olefin). The metabolite M6 at 24.1 min (Fig. 34a) with a -1.3 ppm deviation, produced by FT-ICR HRMS (Table 6), was fragmented into *m*/*z* 208 (–H_2O) and 190 (–HCl) peaks. This could reflect formation of 3-chloro-5-trifuoromethylpyridyl carboxylic acid or its isoform, 2-(3-chloro-5-trifuoromethylpyridylethan)-1-ol. However, from the fragmentation pattern of precursor ion *m*/*z* 226, product ion *m*/*z* 194 is specific to the alcohol, while the most abundant fragment at *m*/*z* 208 suggests carboxylic acid (Fig. A6b).

Although lactam FLP formation by photodegradation was studied before [91], the detection of products (generated via dechlorination in liver microsomal incubates), such as M4, M10, M12 and M15 (at 23.1, 25.0, 26.9, and 28.0 min in Fig. 34a) was novel data, as these have not been previously reported as FLP mechanisms. Mani, *et al*. [158] have also reported the dechlorination and subsequent hydroxylation of aromatic-Cl from chlorotyrosine *in vivo*. Moreover, the hydroxylimide products (M1, M12 and M15) are new metabolites here that, to our knowledge, have not been previously reported.

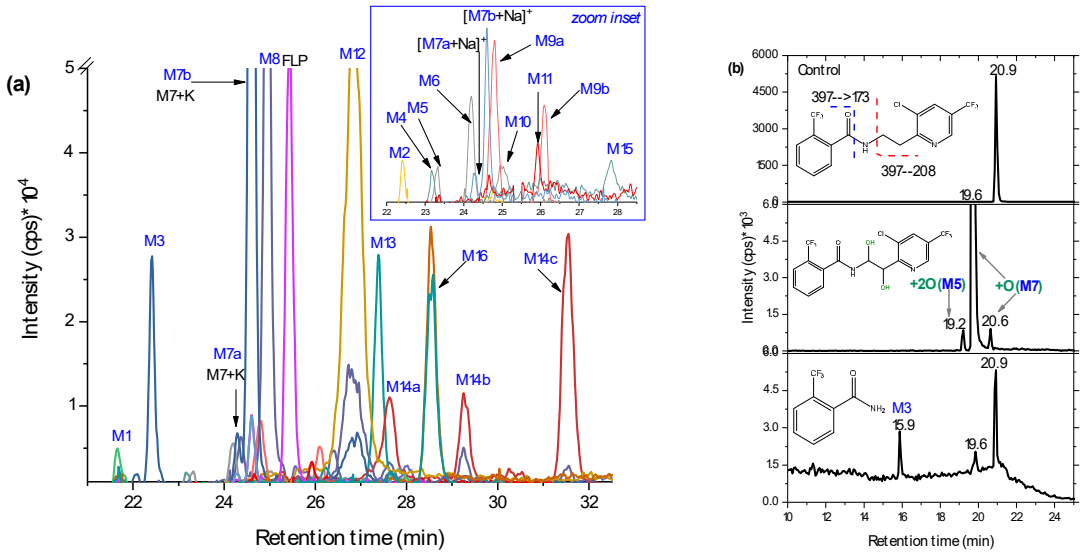

Fig. 34 EIC of FLP metabolites in HLM (a) and MRM chromatograms of hydroxylated FLP and M3 from EC (b) measured by LC-MS/MS on (+) ESI (modified from Mekonnen *et al.* [154], LN 4347550440858)

In this thesis, a combination of different MS-techniques was employed to identify the possible metabolic mechanisms of the compounds of interest. However, some metabolites or oxidative products were not identified in both liver microsome incubates and EC. A high-intensity metabolite of *m/z* 493 (M16 at 28.6 min in Fig. 34a) was detected only in *in vitro* by LC-MS/MS analysis. From MS/MS fragmentation and (+) MRM scans, the product ions *m/z* 475 (–H_2O), 457 (–HCl) and 198 (with a ^{37}Cl isotope pattern) eluted at the same retention time as M16 (Table 7). This could reflect multiple hydroxylations of FLP (both aliphatic and the two aromatic rings, Ph- and Py-) or polymers of other metabolites. Similarly, two major metabolites at *m/z* 317 and 371 (M13 and M14, Fig. 34a) were detected in both EC and *in vitro* experiments. M14 appeared with three isomeric peaks at 27.6, 29.1 and 31.8 min (M14a-c, Fig. 34a). All three peaks gave rise to the product ion *m/z* 223 (Table 7) and could represent oxidative products from unusual rearrangements of mono- and dihydroxylated FLP, whereby 2xCO neutral molecules were lost and formed imines. However, due to insufficient data, M13, M14 and M16 were not structurally determined – a limitation of this work.

EC/MS is useful for identifying reactive or short-lived species, such as benzoyl (*m/z* 173 in Fig. 28a) and epoxide (*m/z* 411 in Fig. 28b) intermediates, which fosters more comprehensive understanding of oxidation mechanisms. Moreover, EC/(LC)/MS saves both time and cost and

is relatively matrix-free. Although the selectivity of EC-based oxidation is incomparable with enzymatic metabolism, it could still provide a useful complimentary tool for simulation of biotransformation processes of xenobiotics.

3.4. Bioconjugation of EC Products (Phase II)

Active phase I metabolites are detoxified by phase II conjugative metabolism, which includes GSH conjugation, glucosylation, sulfation, acetylation, methylation and amination. The conventional *in vitro* and *in vivo* methods are not suitable for phase II metabolism investigations, as interference and long sample preparation times (especially for reactive species detection) pose major challenges. In this regard, online EC/MS could be a better approach, as it enables matrix-free conjugation or adduct formation of electrochemically generated reactive species in a short period of time. The current section of this thesis aimed to investigate glucosylation and GSH-conjugation of CPF and FLP TPs using online EC/MS.

3.4.1. GSH and CPF TPs Conjugation: Online EC/MS *vs* Liver Microsome

Several oxidation products of CPF from P-oxidation and O-dealkylation, as well as dechlorination products, were identified by EC/MS or in LMs (*sec 3.2.1*). The TPs and intermediates (reactive species) were trapped and reacted online in a loop before being entered into the ESI source (**Fig. 14**). As shown in Fig. 35a, the mass voltammogram of GSH and CPF were significantly decreased when the potential changed from 1,800 mV to 2,300 mV in all 4 subsequent full cycle scans. The reduction in CPF intensity was expected as it was oxidised into TPs at the optimal potential. However, GSH appeared to behave like CPF without any applied potential. This could be explained by the reaction of GSH with some of the TPs of CPF. Online EC/MS enables observation of the reaction products *m*/*z* in real time. Hence, in addition to the TPs of CPF *m*/*z* 453, 469, 533, 564, 593, 605, 621, 627, 639, many others were detected in the online EC/MS spectra after being trapped by GSH (Fig. 35b).

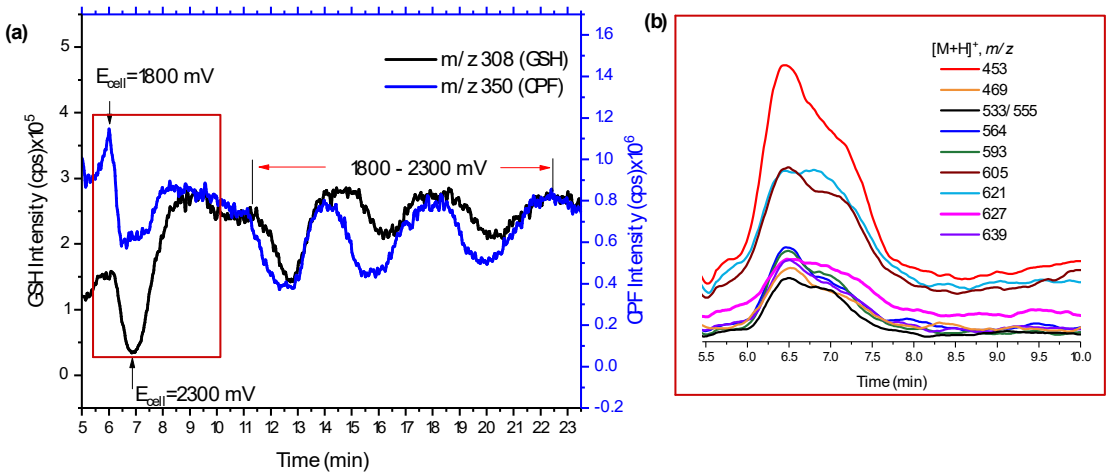

Fig. 35 Mass voltammograms of CPF (1,800→2,300 mV, 10 mV/s) and GSH (0 mV) (a) and intensity of possible conjugates (b) by BDD in µPrepCell™

The extracted mass voltammogram of the *m*/*z* observed between 5.5-10 min (Fig. 35b) showed an increase in the time when both CPF and GSH decreased (after the potential applied); this then returned to zero when the potential decreased below 1,800 mV. This provides important evidence that the observed *m*/*z* traces may be conjugative phase II products. However, some *m*/*z* traces could be H-bounded adducts or interferences formed during EC reactions, unless they were resolved by chromatographic separation. Therefore, effluents of GSH and TPs mixtures were investigated by offline LC-MS (Fig. 36a, b).

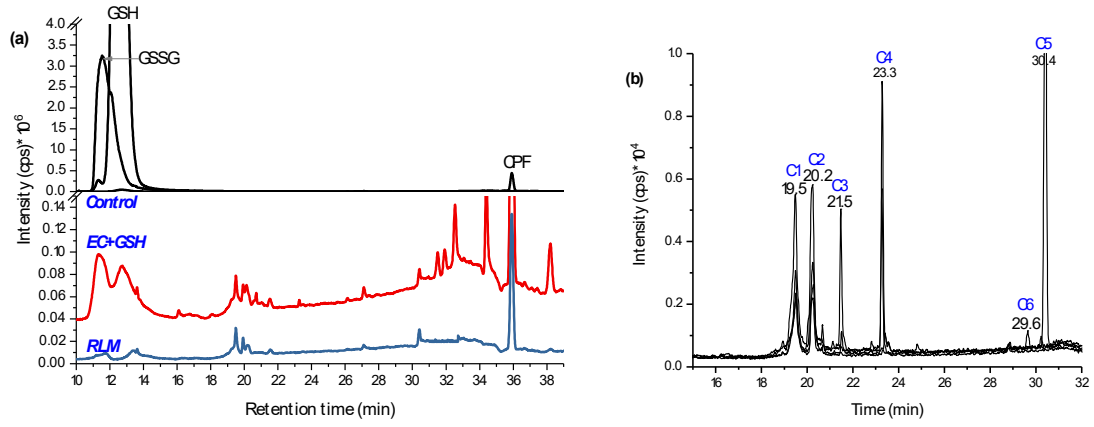

Fig. 36 TIC of GSH and CPF during control (black), at 2,100 mV DC applied potential (red), RLM incubates (blue) (a), and EIC of bioconjugates at 2,100 mV DC potential (b) using BDD WE recorded by LC-(+) ESI-MS

The control (Fig. 36a), which was the same mixture at zero potential, showed only three distinctive peaks at 11.4 (*m*/*z* 613, $[GSSG+H]^+$), 12.6 (*m*/*z* 308, $[GSH+H]^+$) and 36.0 min (*m*/*z* 350,

[CPF+H]$^+$). The peak at 11.4 min was confirmed as GSH-oxidized to GSSG (δm/m = -1.3 ppm in Table 8) by forming a disulfide bond (–S–S–) through the Cys-thiols. It is highly common for GSH to be oxidised to GSSG at room temperature [159]. When a potential of 1,800-2,300 mV was applied (red line in Fig. 36a), different peaks were observed and the intensities of both GSH and GSSG decreased. The substrate was then incubated in RLM together with GSH and GST. The supernatant was run alongside the EC effluents (blue line in Fig. 36a) and revealed 4 peaks that matched by retention time (19.5, 20.2, 21.5, and 30.4 min) and by the *m*/*z* to the EC/MS products. Traces of the *m*/*z* observed during online EC/MS experiments (Fig. 35b) were investigated using selected ion monitoring (SIM). At 19.5 min (conjugate 1: C1) *m*/*z* 487 and at 20.2 min *m*/*z* 469 (C2) were eluted. At 21.5 min (C3), *m*/*z* 621 and product ions 605 (–NH_2), 593 (–CO_2) and 564 were detected. At 30.4 min C5 elutes with the same *m*/*z* 621 were detected, but without the product ions. Furthermore, at 23.3 min *m*/*z* 605 and 564 (C4) and at 29.6 min *m*/*z* 627 (C6) were separated by LC-MS (Fig. 36b).

Table 8 Retention time (tR), MS/MS product ions and δm/m measured by TripleTOF of GSH and glucoside adducts of CPF and FLP oxidative products using BDD as WE

Abbreviation /symbol	t_R (min)	Calculated $[M+H]^+$	Product ions by QTRAP-MS/MS	Measured $[M+H]^+$	δm/m (ppm)	Type of conjugate
C1	19.5	487.0007	308, 291, 180, 179, 205, 233	487. 0030	4.7	TCP + GSH – H_2O
C2	20.2	469.0346	469, 451/453, 433, 437, 405	469.0312	1.3*	TCP + GSH – HCl
C3	21.5	621.0407	621, 603/605, 564, 593, 541,	621.0534	4.8	CPF + GSH – HCl
C5	30.4		469, 314, 288, 171, 154			
C4	23.3	605.0635	605, 564, 587, 573, 569, 555, 540, 339, 327, 298, 251, 154	605.0520	2.2*	Oxon + GSH – HCl
C6	29.6	626.9704	609, 538, 369, 322, 308, 231,	627.0068	-7.2*	U
C7	15.6	359.9803	360, 362, 364, 324, 198, 180	359.9891	-5.2*	TCP + Glc – H_2O
C8	18.4	478.0431	316, 163, 153, 137, 162	478.0410	6.5	Oxon + Glc – HCl
C9	20.5	494.0203	515, 314, 171, 163	494.0299	-3.2*	CPF + Glc – HCl
C10**	23.84	702.1280	705, 513, 429, 395, 308, 173, 145, 129, 291, 179, 162	702.1832	-5.1*	Hydroxyl FLP + GSH – H_2O
C11**	28.9	701.2423	703, 413, 395, 307, 289, 573, 173, 145, 129	701.2093	-4.3*	Hydroxyl FLP + n-Glc – H_2O

*U-unidentified, *–accurate mass error was compensated by the respective standards, **– conjugates of FLP TPs*

The TripleTOF measurement was not especially accurate, even for pure standards; thus, δm/m of the probable conjugates were compensated for by the deviations of the pure standards. In addition to the comparison of retention times, further confirmation was performed for each conjugate using the following two strategies: (1) selective fragmentation of the molecular ion peaks of the conjugate in MS/MS and checking whether the moiety from the expected TPs of the parent compound plus 34 Da mass (-SH_2^+) was present and; (2) fragmenting the moiety of

the substrate, or the biomolecule, in MS^3 and comparing the fragmentation pattern with the standard. For example, the molecular ion peak at *m/z* 621 was expected to be a conjugate of GSH and CPF through loss of neutral HCl. Hence, after fragmentation using MS/MS, product ion *m/z* 314 (Q3) was further fragmented at the third quadrupole (Fig. 37a). The peaks at *m/z* 314, 162 and 146 were lower than the corresponding dechlorinated CPF product (P7) by 2 Da. The other peaks also coincided with P7 (Fig. 27a). Similarly, the product ion of *m/z* 605, *m/z* 298 (P5 – Cl), was analysed. Thus, C5 could be a GSH and CPF conjugate formed after loss of a neutral HCl.

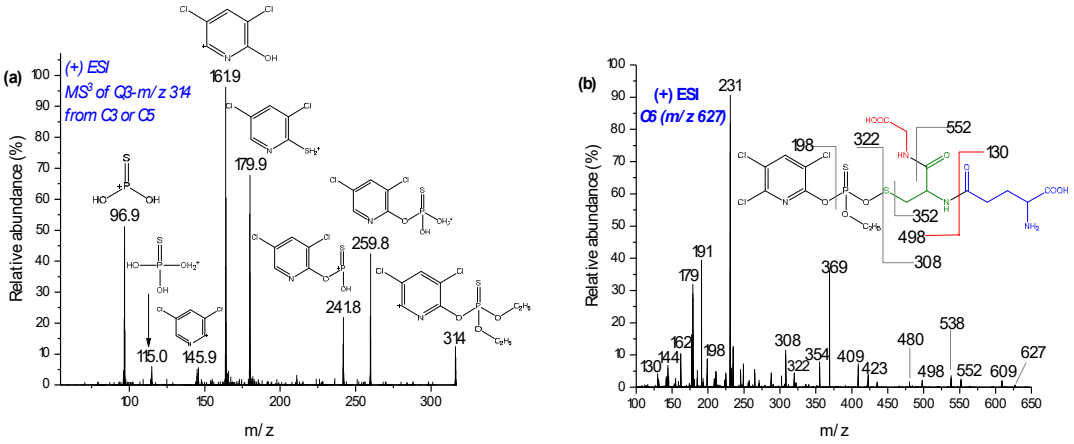

Fig. 37 Mass spectra of product ion *m/z* 314 from C3 on MS^3 (a) and C6 with its suggested fragmentation measured by MS^2 (b)

Two products of *m/z* 627 (C6 at 29.6 min) and 639 also increased in intensity (Fig. 35b). The *m/z* 639 chromatogram peak was not found by offline LC-MS investigation. MS/MS experiments and comparison of isotopic distribution with theoretical formula coincided with *m/z* 627, as a conjugate of dealkylated CPF with GSH. In Fig. 37b, the product ions of *m/z* 627 at *m/z* 322 and 308 may represent fragmentation of the -O–S- bond. Furthermore, product ions of *m/z* 130- 231 confirm the presence of GSH. The product ion at *m/z* 198 exclusively shows the presence of the pyridine ring. On the other hand, *m/z* 354 could be dealkylated CPF of 34 Da (+SH_2). Hence, C6 could be a conjugate with GSH and CPF after loss of C_2H_6 (Fig. A8d). On the other hand, *m/z* 639 yielded product ions at *m/z* 308 ($[GSH+H]^+$ and 334 ($[oxon+H]^+$), along with further characteristic peaks of GSH (*m/z* 130- 290). The MS-spectrum is shown in Appendix Fig. A8b. The peak at *m/z* 350 could also indicate the presence of oxon with 'O' (333+16+H). Although the appearance of *m/z* 484 could also signify GSSG (as *m/z* 484 is main stable product ion of GSSG), by comparing the isotopic distribution of the measured molecular ion peak with the theoretical,

it clearly shows the presence of Cl-isotopic patterns in the molecular formula. Therefore, the conjugate is suggested to be between oxon and GSH (Fig. A8d).

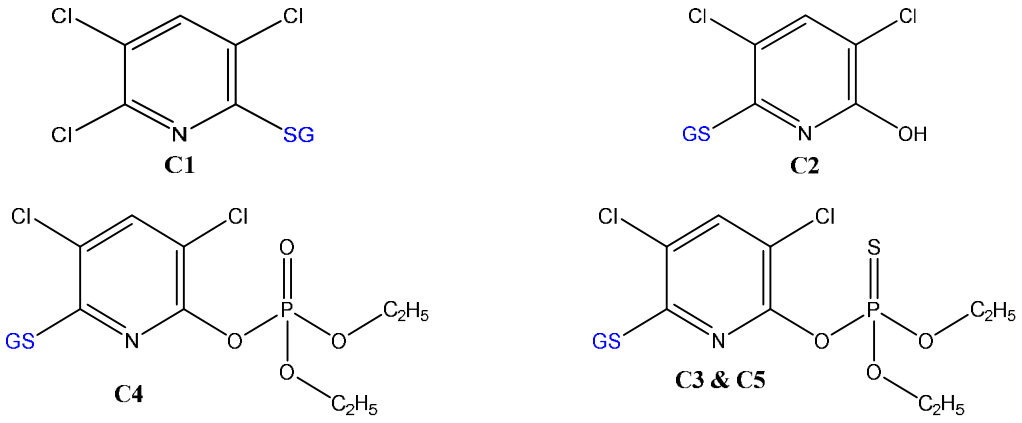

Fig. 38 Proposed molecular structures of GSH-conjugates with CPF oxidative products

Despite the benefit of matrix-free detection, a major issue of simulating conjugative phase II metabolites in such a non-biological system is the difficulty in determining the binding sites between TPs and the trapping agent. Often, the more nucleophile thiol is susceptible to bonding with the substrate. In the case of biological systems, the conjugation sites are more specific and selective because of their respective enzymes. Indeed, C3 and C5 may be conjugates of CPF at different sites of GSH (via -SH, -NH_2 or -NH-) or three Cl substituted by GSH. Meanwhile, regarding *m/z* 639, the appearance of product ions at *m/z* 350 and 320 does not suggest formation of -N-S- bond. Thus, the conjugation may take place between -N-lone pairs of the pyridine ring and -O- or -NH_2- of the GSH, instead of the thiol group.

In the case of TCP conjugates, two GSH conjugates were identified at *m/z* 487 (C1) and 469 (C2 in Fig. 36b). After fragmentation by MS/MS, the absence of product ions at *m/z* 155, 171 and 137 confirms that both *m/z* 469 and 487 (Table 8) are not TPs containing DEP or DETP. The conjugate C2 was previously reported by Choi *et al.* [72]. The peak at *m/z* 487 was observed to yield *m/z* 180 (TCP – OH) instead of *m/z* 162 (TCP – Cl). In addition, the product ions at *m/z* 308, 291, 179, 205 and 233 (Table 8) confirmed the presence of GSH. Hence, C1 and C2 could be conjugation products of GSH with TCP after loss of water and HCl molecules, respectively.

Many mass traces, including *m/z* 407, 453, 533, 564 and 593, were also produced during online EC/MS (their intensities increase with applied potential); however, their chromatographic separation was not successful. Some of the peaks (*m/z* 453, 407, and 533) were eluted at the same

retention time with GSSG, (*m/z* 564 and 593) C3 and C4, which are likely fragmentation products of GSSG in ESI. We, therefore, focussed on the peaks that coincided with those from LMs. As the formation of conjugates in online EC/MS depends on the reaction conditions (pH, temperature and organic solvents), more conjugation products can be predicted by EC/MS.

3.4.2. Glucosylation of CPF TPs by Online EC/MS

In addition to GSH conjugation, glucosylation is one of the main mechanisms of phase II metabolism for many xenobiotics. Pesticides, in particular, often come into direct contact with foodstuffs that contain glucosides. Thus, the glucosylation of CPF TPs was investigated here by trapping with Glc, instead of GSH. The resultant mass voltammograms and chromatograms are shown in Fig. 39a and b, respectively.

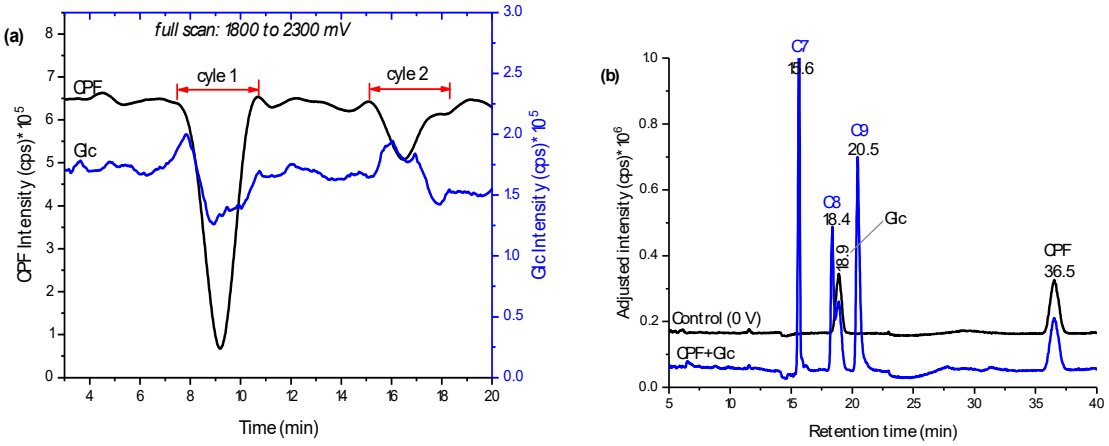

Fig. 39 Mass voltammograms of CPF and Glc after scanning in 1,800 – 2,300 mV (10 mV/s) using MD as WE (a) and TIC with and without applied potentials (b)

As evidenced in Fig. 39a, Glc intensity decreased in the first cycle when no potential was applied. In the second cycle, there was low variation in both CPF and Glc intensities, which could either signify adsorption of some products to the BDD surface or that more time was needed for the conjugation reaction to take place before infusing to ESI. Nevertheless, a slight decrease in Glc intensity could also be evidence of conjugate formation. Further separation of the effluents in offline LC-MS revealed an additional three distinctive peaks at 15.6 (C7), 18.4 (C8) and 20.5 min (C9), compared to control (the same composition at zero potential). Similarly, the intensity of Glc at 18.9 min instantly decreased when a potential was applied (Fig. 39b). The *m/z* eluted together with C7 were 360, 362, 364, which confirm Cl-isotopes of the TPs of CPF.

Furthermore, C7 did not show fragments of *m/z* 153, 137, 97 or 171; however, *m/z* 198 (TCP), 180 (TCP-OH), 163 (Glc-OH), and 324 (Table 8) peaks were observed. These findings are suggestive of formation of a conjugate, C7, between TCP and Glc after loss of a water molecule (C7 in Fig. 40). On the other hand, C8 *m/z* 478, 480 and 482 were shown to fragment to *m/z* 316, 163, 153, 137 and 162 (Table 8). The ion product at *m/z* 153 and 137 are characteristic of a dimethylphosphate group, while *m/z* 162 with Cl-isotopes suggest the presence of the pyridine ring. On the other hand, ion products *m/z* 316 and 163 may reflect formation of a dechlorinated oxon, with additional 'O' and Glc–OH, respectively. Moreover, analysis of the effluents using TripleTOF-HRMS revealed C8 with δm/m = 6.5 ppm. It is, therefore, reasonable to conclude that C8 is formed between oxon and Glc after loss of a neutral HCl (Fig. 40). According to Choi *et al.*, Cl- present at the *ortho* position of the pyridine ring is readily cleaved to form a conjugate [72]. Furthermore, C9 appeares with a molecular ion peak at *m/z* 494 and ion products at *m/z* 515 (+Na-adduct), 314 (CPF-Cl), 171 (DETP) and 163 (Glc – OH). Thus, as C8, C9 could be a conjugate of CPF and Glc through removal of a neutral HCl (Fig. 40). Confirmational LMs were not performed for this study due to unavailability of UDP-UGTs enzymes.

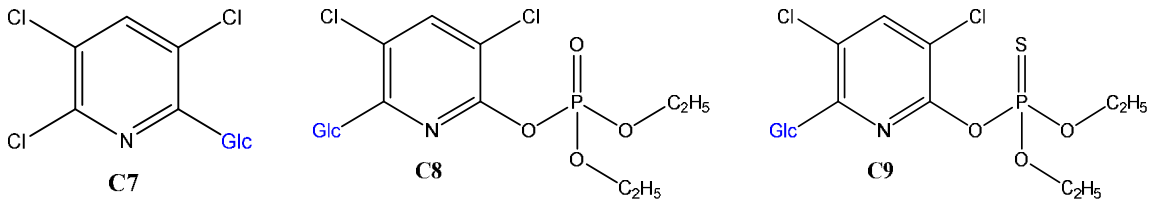

Fig. 40 Proposed structures of CPF TPs glucosylation products by online EC/MS

3.4.3. Glutathione Conjugation and Glucosylation of FLP TPs

For FLP, similar experiments were performed by trapping the EC effluents with GSH and β-nonyl-glucoside (*m/z* 307, n-Glc). Oxidation of FLP was performed using a BDD electrode in the presence of 5% water as a modifier. Only two conjugates (one for each of GSH and n-Glc) with hydroxyl FLP were formed. The peak at 23.8 min (C10 in **Fig. 41**a) and 28.9 min (C11 in **Fig. 41**b) appeared at *m/z* 702 and 701 after trapping with GSH and n-Glc, respectively. The ion products of C10 (*m/z* 702/705) at *m/z* 429 (FLP+SH), 395 (FLP–H), 308 (GSH+H), 173 (trifluoromethylbenzoyl ion), 145 (trifluoromethylphenyl), 129, 291, 179 and 162 (Table 8) are characteristic of both GSH and FLP. The conjugate C10 may have been formed between GSH and monohydroxyl FLP after losss of H_2O, or GSH and olefin FLP by addition reaction (C10 in

Fig. 42). However, C10 was not found in RLM incubations (**Fig. 41**a). Instead, the conjugate, C11, was shown at *m/z* 701 with Cl-isotope at *m/z* 703 when trapped by n-Glc.

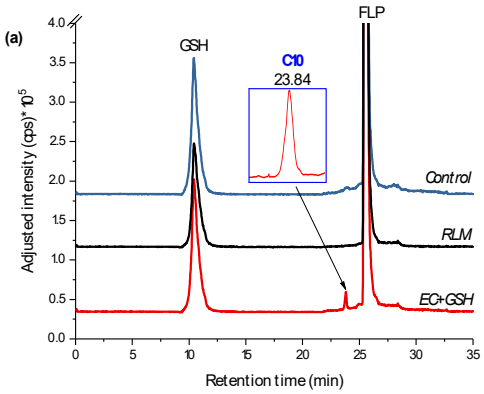

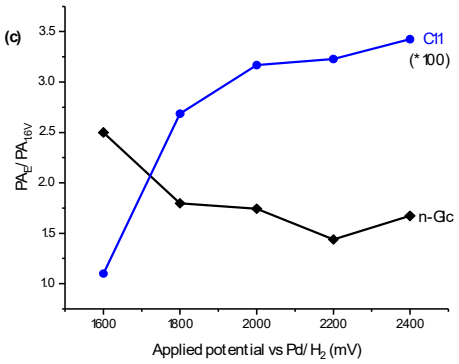

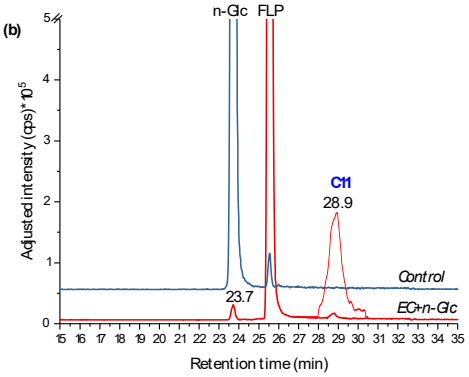

Fig. 41 EIC of FLP oxidative products effluent incubated with GSH (a), with n-Glc (b), and peak area ratios of selected conjugates at different applied potential (c) as measured by LC-MS/MS on (+) ESI

The peak area ratio between applied potential 'E' (PA_E) and 1,600 mV ($PA_{1.6\,V}$) was significantly increased for C11 and a decreased for n-Glc, with increasing potential (**Fig. 41**c). It is experimentally possible to detect a different conjugate by changing the working potential or reaction conditions, as a result of which the TPs would vary accordingly. The ion products were measured at *m/z* 573 (–nonyl), 413 (FLP+OH), 395 (FLP–H), 307 (n-Glc+H), 289 (n-Glc–O), 173 (trifluoromethylbenzoyl ion), 145 (trifluoromethylphenyl) and 129 (n-nonyl) (Table 8). The ion products *m/z* 395 and 307 could have been produced due to cleavage of the n-Glc–FLP bond, which features protonation with n-Glc. On the other hand, the ion product *m/z* 413 could represent monohydroxyl FLP, generated upon n-Glc cleavage of the -O–C- bond to yield *m/z* 289. Additionally, the peak at *m/z* 573 could be explained by n-nonyl (*m/z* 129) lost from C11. Thus, C11 could be a conjugate of n-Glc and monohydroxyl FLP following neutral water loss. FLP is also known to form imine and olefin intermediates, which could easily be conjugated

with n-Glc [89]. Nevertheless, the n-Glc-FLP conjugate formed through N-oxides (on the aliphatic -NH- or pyridine ring -N=) could still produce a molecular ion peak at *m/z* 701. With the observation of *m/z* 395, the most probable conjugation mechanism of C11 is n-Glc with monohydroxy-FLP through water loss (C11 in Fig. 42). Unlike CPF conjugates, several interfering adducts that are not real conjugates were found in the FLP oxidative product with n-Glc (Fig. A8c); these are *m/z* 635 (2*n-Glc+Na), 651 (2*n-Glc+K), 725 (n-Glc+FLP+Na) and 815 (2*FLP+Na).

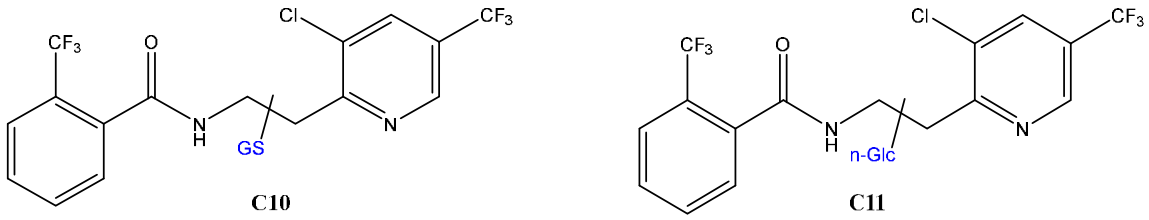

Fig. 42 GSH and glucoside conjugation products of monohydroxyl FLP

In summary, seven conjugates of CPF oxidative products, four with GSH and three with Glc, and two conjugates of hydroxyl FLP, with GSH and n-Glc, were identified using the intended method. However, the scope of this work did not permit a conclusion on the conjugation sites of the above (e.g. the sites at which Cl- of CPF, or HO- of Glc and n-Glc, were cleaved to form a conjugative bond). Additional conjugates of both compound's oxidative products with each biomolecule could be identified by modifying the electrochemical reaction (e.g. length and temperature of the reaction loop, chemical composition and EC cell potential).

3.5. Abiotic Transformation

In this section of the thesis, a UV-C light source of 200- 280 nm range was used to predict the abiotic TPs of the investigated compounds. Since the photodegradation products (PPs) and mechanism of CPF have already been investigated, more focus was given to FLP. Many industrial treatments use UV-C for effective germicidal treatment; thus, it was used here to investigate the PPs of the intended compounds.

3.5.1. Photodegradation of CPF

The photodegradation products of CPF have been extensively studied [81-83]. Nthumbi and Ngila previously found that DETP and TCP are the main PPs of CPF in the presence of a ferrous catalyst [160]. However, the focus of this thesis was to develop a method for producing TP

standards based on the photodegradation processes. After irradiation of standard CPF in aqueous solution with UV-C light, aliquots were run through LC-MS/MS in the same way as described in sec 2.6.1. The graph in Fig. 43a is the natural-logarithm (ln) of peak area ratio after irradiation to time 't' (A_t) and time zero (A_0). At t = 0 min, A_t and A_0 values for the PPs were considered as an arbitrary number ('unity') for simplification of the calculation.

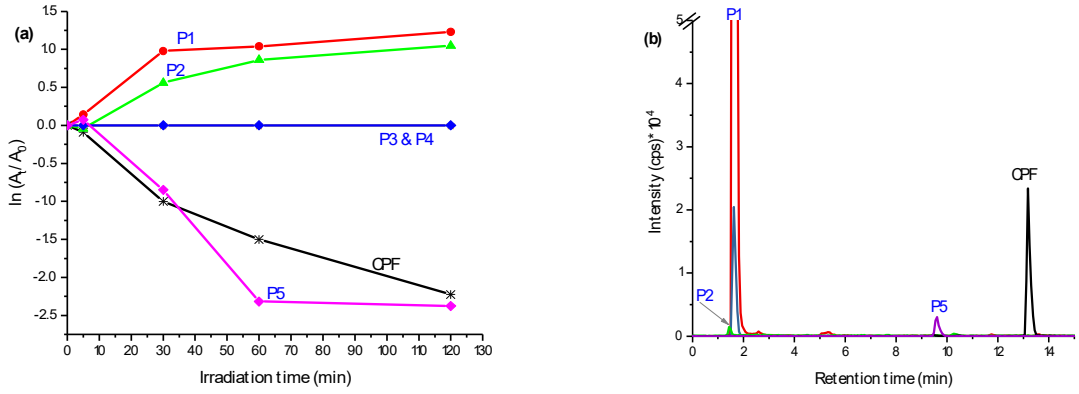

Fig. 43 Rate of CPF photodegradation and its PPs formation *vs* irradiation time (a) and their EIC running on MRM scan by QTRAP LC-MS/MS (b)

It was found that 97% of CPF was degraded to its PPs after 120 min of UV-C exposure. Formation of the two products, P1 and P2, increased, further demonstrating degradation of CPF. The increase in P5 in the first 10 min, followed by an abrupt decrease to zero, shows secondary degradation of oxon into other TPs. P3 and P4 (Fig. 27a) were not shown to be PPs of CPF. The structures of products were confirmed using the same procedure as with the EC and LMs products. Aliquots scanned by MS/MS (only Q1) revealed *m/z* 155, 171 and 334 (on +ESI) as the main PPs. Subsequent runs using the developed MRM chromatographic method (*sec 2.6.1*) and comparisons with the standards obtained from EC and LMs, confirmed the products P1, P2 and P5 as DEP, DETP and oxon, respectively. As evidenced in Fig. 43b, P1, P2 and P5 were eluted at the same retention time as the products in EC or RLM (Fig. 24). Further mass measurements and determination of molecular formulae by HRMS (Table 5) confirmed the structural assignments.

The pathways of the above degradation processes were next determined. Fig. 43a shows that P1 and P5 intensities increased in the first 10 min, whereas P2 was formed after 10 min of irradiation. This is suggestive of P2 formation from P5 (oxon) photodegradation by hydrolysis

or dearlylation (**Fig. 44**). However, the expected TCP was not observed after 120 min of irradiation, which may be explained by the unstable nature of TCP during the irradiation. In support of this, Zabar et al. showed that TCP is went through secondary photodegradation, via Cl-substitution by HO• and oxidation of -OH, in a photochemical reaction [76] ; this may account for why the product was not observed here.

Fig. 44 Photodegradation pathways of CPF in 0.1% MeOH aqueous solution after irradiated for 2 h by Hg-lamp (200 – 280 nm, 150 W, 255 mW/cm²)

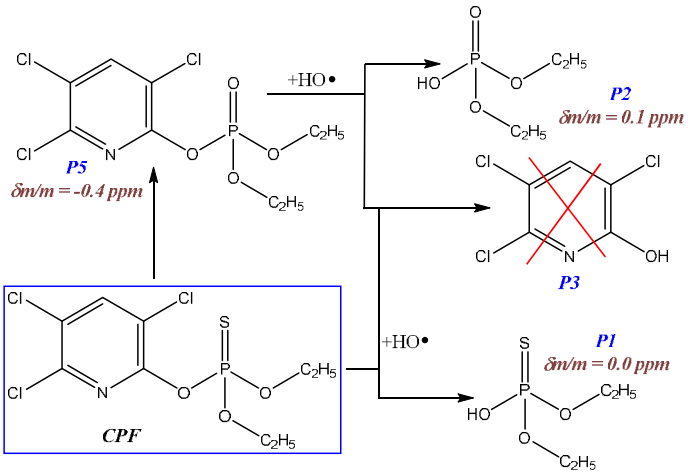

3.5.2. Photodegradation of FLP

Unlike for CPF, photodegradation processes of FLP have not been studied as of yet. The only available study, by Dong and Hu [91], showed only three TPs of FLP, all produced via dechlorination (proton and hydroxyl substitution of Cl- and lactam formation) by photocatalytic irradiation. To understand the transformation mechanisms in detail, the FLP standard solution was irradiated here using an Hg-lamp and the aliquots were investigated as previously. The degradation kinetics were investigated in aqueous media containing 0.1, 50, and 80% ACN, in parallel to the control (Fig. 45a). In all cases, FLP displayed relatively fast degradation in 0.1% of ACN. The control was the same amount of FLP in 0.1% ACN aqueous solution in a colourless glass container, exposed to natural sunlight for the same time interval. As evidenced in Fig. 45a, none or 93% of FLP was degraded after exposure to 7 h of sunlight or UV-C, respectively. After scanning the blank, control and UV-C irradiated samples by +Q1 of MS/MS, many *m*/*z* peaks appeared to be PPs. To discriminate possible adducts (+Na, +K, $+NH_4^+$) and isotopic peaks (C_3-Cl isotope), the *m*/*z* traces were separated by LC-MS/MS, without fragmentation, and the peaks appeared at different retention times were considered to be PPs.

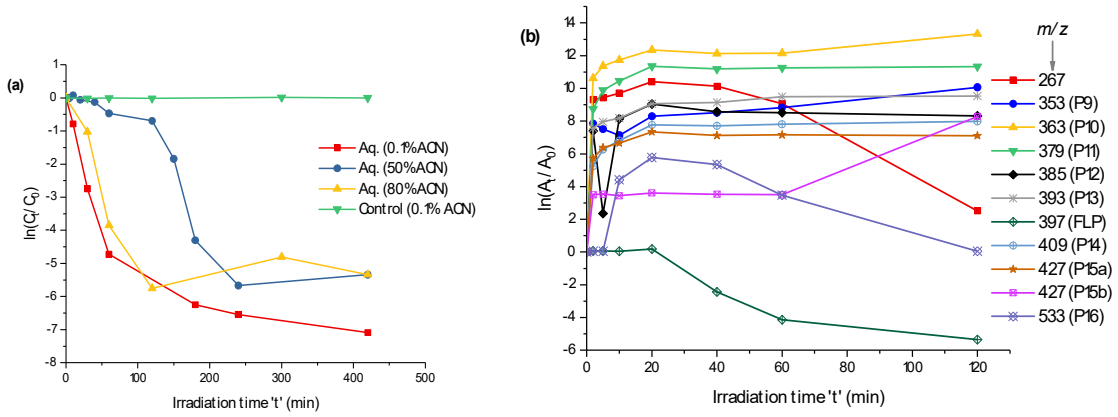

Fig. 45 Degradation kinetics of FLP with ACN content (a) and its PPs formed in 0.1% ACN aqueous solution (b), parts of Mekonnen *et al. [147])*

Although there many peaks were resolved by retention time, *m/z* 363 (P10), 379 (P11), 393 (P13), 409 (P14), 427 (P15), 429 (P17), 361 (P18) and 377 (P19), were identified as products of hydroxylation of FLP or lactam. Moreover, *m/z* 351 (P9) and 385 (P12) were identified as products of a rearrangement reaction and *m/z* 533 (P16) as a dimer. The kinetics of some of these PPs at different irradiation times are shown in Fig. 45b, as $\ln(A_t/A_0)$ *vs* time.

According to the APVMA report, FLP is cyclised to lactam (between C_3-Cl of the pyridyl and C_{16}-H of the benzamide aromatic rings, through loss of neutral HCl) under sunlight photolysis in aqueous media [89]. However, in this work, FLP was stable after exposure to natural sunlight for 2 weeks. Furthermore, Dong and Hu reported -Cl substitution by •OH and •H after exposure to UV in the presence of photocatalysts [91]. In both reports, the photo-initiator (the chloride site) was highly susceptible to UV irradiation and triggered hydroxylated and/or protonated substitution of -Cl. However, the final products could vary greatly, depending on irradiation time, chemical composition and UV intensity.

As shown in Fig. 45b, most of the products were formed in the first 20 min and then slightly increased, except for *m/z* 267 and 533, which rapidly decreased after 20 min. Needless to say, some of the products may be interchangeable; i.e. they may be products of another PP, rather than the parent compound. In line with this, P9 and P10 were increased after 20 min and P15b after 60 min. The higher formation kinetics of P10 and P11 confirm that FLP is preferably degraded through Cl-substitution. On the other hand, the intensities of the PPs of

rearrangement (P9 and P12) decreased at around 10 min and then increased, which confirms that the two products followed the same formation mechanism.

3.5.2.1. Identification of dechlorinated PPs

A Full scan of 100 – 1,000 *m/z* range (TIC in Fig. 46a) and selected ion monitoring in (+) ESI (Fig. 46b) were performed on aliquots of 2 h-irradiated samples using the QTRAP LC-MS/MS system. As evidenced in Fig. 46b, the many characteristic peaks helped identify the structures of the possible PPs. The three photodegradation products previously reported by Dong and Hu [91] were eluted at 25.7, 26.3 and 31.7 min (Fig. 46a), respectively representing Cl-substation by H• (P10 in Fig. 46b), Cl-substitution by HO• (P11) and lactam FLP (P18). Their structures were easily deduced from the lack of Cl-isotopes in their MS/MS spectra (see Appendix Fig. A6d,e). HRMS also showed that their accurate mass values only deviated by +2.7, 0.0, and -0.2 ppm, respectively, from theoretical (Table 9). As further evidence, the elution order in the RP analytical column was P11, P10 and P18, which corroborates the products' respective polarity profiles. The peak at 27.8 min is non-degraded FLP ([M+H] at *m/z* 397, +Na at *m/z* 419 and +K at *m/z* 435). However, the focus of this study was to identify novel PPs; as shown in Fig. 45b and 46b, many other peaks were indeed well separated and characterised by *m/z* eluted at the same retention time.

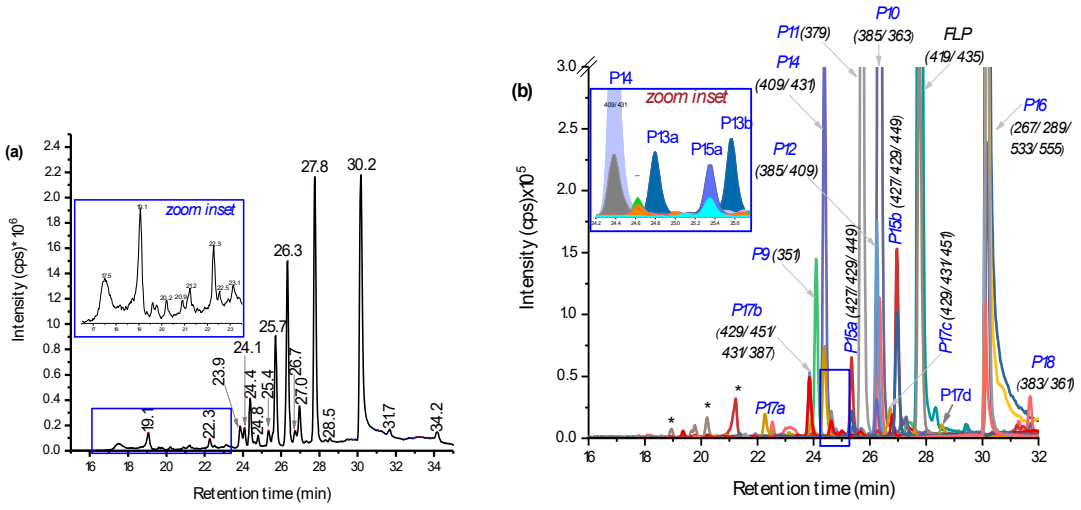

Fig. 46 TIC (a) and EIC (b) of photodegradation products of 0.1 mmol/L FLP measured by LC-MS/MS after irradiated for 2 h UV-C light (150 W, λ =200 to 280 nm). The peaks are assigned by retention time (a), *m/z* traces eluted at the specific time (b), * mean not identified (adopted from Mekonnen *et al.* [147]).

3.5.2.2. Characterization of hydroxyl FLP PPs

In addition to the known dechlorinated PPs (P10, P11 and P18), hydroxylation of the parent FLP was the main root of photodegradation. Different isoforms of dihydroxyl FLP (*m/z* 429: P17) were produced by UV-C irradiation. For instance, the peaks at 22.3 and 26.7 min (Fig. 46a) showed P17, including its Cl-isotope at *m/z* 431 and +Na-adduct at *m/z* 451/453 (Fig. 46b). The fragmentation pattern in Triple-TOF showed peaks at *m/z* 411 (-H_2O), 397, 240, 222, 173, 145, 131 and 115 (Table 9 and Fig. A7b). The ion products at *m/z* 173 and 145 confirm the presence of the trifluoromethylbenzoyl and *m/z* 397 confirms the structure of FLP. However, monohydroxylated FLP was not detected, which could be explained by high concentrations of HO• produced by UV-C leading to fast hydroxylation of all possible sites. As the experiment was performed in aqueous media, a higher concentration of reactive oxygen species, such as HO^- or HO•, is expected. Aside from this, longer irradiation appeared to produce different isomers of dihydroxyl FLP. In total, four dihydroxyl isoforms at 22.3, 24.1, 26.7 and 28.5 min (P17a-d in Appendix Fig. A11a) were found, although monohydroxylated FLP was not. Some of the dihydroxylated products could also be N-oxidation or hydroxylation at the aromatic ring, which generates the same *m/z*.

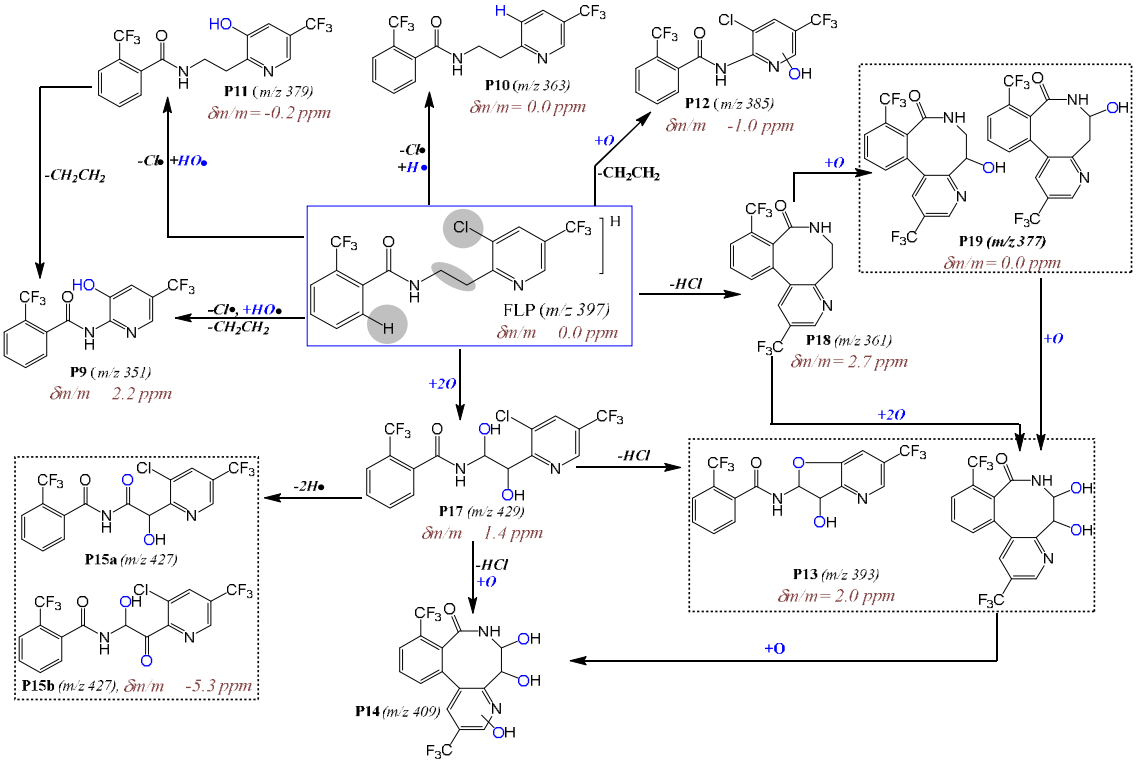

Fig. 47 Photodegradation mechanisms of FLP in 0.1% ACN aqueous media after irradiated for 2 h by 150 W, λ = 200 to 280 nm, 255 mW/cm² Hg-lamp (published in Mekonnen et al. [147])

Additionally, two isomeric peaks (P15a and P15b) at *m*/*z* 427 (2 Da lower than the dihydroxyl FLP) were eluted at 25.4 and 27.0 min (Fig. 46a). Including P15, its Cl-isotope at *m*/*z* 429, as well as the +Na-adduct at *m*/*z* 449 (Fig. 46b and A11a), were all eluted at the same retention time. Furthermore, the fragments gave peaks of *m*/*z* 409 (–H_2O), 380 (–CO), 238, 189, 173 and 145 (Fig. A7a). From the formation kinetics in Appendix Fig. A11b, the two products, P15a and P15b, suggest isomers that could be interchanged during irradiation. P15 could, therefore, be hydroxylimide formed by alcohol oxidation of the dihydroxyl FLP (P17). Alcohol oxidation into a carbonyl functional group by UV exposure was previously reported [76, 161]. The other product with *m*/*z* 427, which was eluted early at 21.2 min, was not confirmed by either Cl-isotope or Na-adduct (Fig. 46a and b). Both P15 and P17 were metabolites of FLP from EC/MS and *in vitro* studies. In terms of toxicity, it is possible that the imide is a toxic PP, as it produces reactive species that damage cellular activities [162]. In conclusion, two groups (dihydroxyl and hydroxylimide) of new hydroxyl PPs were identified here (Fig. 47).

3.5.2.3. Identification of hydroxyl lactam FLP PPs

After FLP was converted to lactam, secondary PPs formed via hydroxylation were found and represent another key photodegradation root of FLP. Mono- and dihydroxyl lactam (Fig. 47, P19 and P13) PPs were identified at *m*/*z* 377 (δm/m = 0.0 ppm, Table 9) and *m*/*z* 393 (δm/m = 2.0 ppm, Table 9), respectively. They eluted at 24.8 and 25.6 min (two isomeric peaks for P13a and P13b, inset in Fig. 46b). The MS/MS spectra of P13 appeared to be *m*/*z* 375 (–H_2O), 176, 188 and P19 at *m*/*z* 359 (–H_2O), 345, 176 and 188 (Fig. A9a and Table 9). Lack of Cl-isotopic peaks at *m*/*z* 379 and 395, and ion products *m*/*z* 145 and 173 in both P13 and P19 MS/MS spectra, confirm the presence of a lactam structure. The monohydroxylated lactam FLP (Fig. 47) could be formed at C7- or C8-positions, giving rise to the isomeric P13a and P13b. Another high-intensity PP with a lactam structure was found at *m*/*z* 409 and was eluted at 24.4 min (P14 Fig. 46a,b) with +Na-adduct at *m*/*z* 431 (Appendix Fig. A11a). P14 produced ion products at *m*/*z* 391 (–H_2O), 377 (lactam dihydroxyl), 359 (lactam), 202, 170, 131 and 115 (Appendix Fig. A9b), all without the Cl-isotope. Initially, this was supposed to be a hydroxylimide product, with HO• substation of -Cl; however, the absence of ion products at *m*/*z* 173 and 145 suggested a trihydroxyl lactam. Further hydroxylation could have occurred either in the Ph- or Py-ring. As reviewed by Burrows *et al*., different N-containing pesticides could produce N-oxide PPs when treated by UV [163].

In conclusion, five PPs, produced by hydroxylation reaction, were identified here: P13, P14, P15, P17 and P19. When aqueous solutions and molecular oxygen are irradiated by UV-light, this could lead to formation of many reactive oxygen species [24]. Radicals could be formed by direct photolysis of water (3.2):

$$H_2O + hv \rightarrow H\bullet + \bullet OH \qquad (3.2)$$

*Where **h** is Planck's constant (6.626x10^{-34} Js) and ν is frequency*. Furthermore, HO• radical could change to peroxides (3.3):

$$2HO\bullet \rightarrow H_2O_2 \qquad (3.3)$$

H• can also react with dissolved O_2 and produce different types of reactive species (3.4):

$$H\bullet + O_2 \rightarrow HO_2\bullet \rightarrow O_2^{\bullet -} \qquad (3.4)$$

These hydroxyl and superoxide radical species are highly short-lived and are capable of degrading many organic molecules. In particular, HO• could cause nucleophilic attack to produce hydroxyl products. Thus, the hydroxylated products of FLP and lactam could be formed in a similar mechanism.

Furthermore, other main PPs found in this work were *m/z* 351, 385, and 533 (P9, P12, and P16 in Fig. 45b and 47). The *m/z* 385 product eluted with *m/z* 387 (Cl-isotope) and 409 (+Na) and was then fragmented into *m/z* 198 (most abundant), 173, 162 and 145 (Appendix Fig. A10a and Table 9). The fragments at *m/z* 173 and 145 confirm the presence of the trifluorobenzoyl in the structure and the most abundant peak *m/z* 198 could be due to HO• hydroxylation of the Py-ring. Hence, P12 (δm/m = -1.0 ppm, Table 9) is suggested to be a rearrangement of PP after loss of $H_2C{=}CH_2$. Because of the peak at *m/z* 198 (Appendix Fig. A10a), the hydroxylation most probably occured at the Py-ring. P9 (δm/m = 2.2 ppm, Table 9) fragmentation into *m/z* 335 (–H_2O), 321, 173, 164, 145, 131 and 115 (*see Appendix Fig. A10b*) assures the presence of trifluoromethylbenzoyl, and at least one HO•, without -Cl. The intense peak at *m/z* 164 could be a fragment of the pyridine ring with HO• substitutes of -Cl. P9 varies from P12 by one -Cl atom. Hence, from the above findings it can be concluded that P9 could be formed due to rearrangement reactions from P11 after losing $H_2C{=}CH_2$. On the other hand, *m/z* 533, 555 (533+Na), 267 and 289 (267+Na) were eluted together at 30.1 min (Fig. 46a, b), whereas the fragmentation of P16 yielded only one ion product at *m/z* 267 (with Cl-isotope) and 249 (*see Appendix Fig. A11c*). This could be due to dimerisation of *m/z* 267 to P16 (2*267-H = 533).

Table 9 Transformation products of FLP with the corresponding modification, exact masses and deviations measured by HRMS (orbitrap) after incubation with HLM, oxidation by EC and photodegradation by UV-C (adopted from Mekonnen et al. [147])

Products	Molecular formula	Retention time (min)	Molecular ion, $[M+H]^+$	Product ions (Q3), $[M+H]^+$	Measured m/z, $[M+H]^+$	δm/m, ppm	Mechanism of formation from FLP
P9	$C_{14}H_8F_6N_2O_2$	24.1	351.0563	335, 321, 291, 173, **164**, 145, 115	351.0555	2.2	$-CH_2=CH_2$, -Cl•, +HO•
P10*	$C_{16}H_{12}F_6N_2O$	26.5	363.0927	385, 190, **173**, 145	363.0932	0.0	-Cl•, +H•
P11*	$C_{16}H_{12}F_6N_2O_2$	25.9	379.0881	417, 361, 208, **190**, 173, 152, 145	379.0880	-0.2	-Cl•, +HO•
P12	$C_{14}H_7ClF_6N_2O_2$	26.3	385.0173	387, 407/409, **198**, 173, 162, 145	385.0169	-1.0	$-CH_2=CH_2$, +O
P13	$C_{16}H_{10}F_6N_2O_3$	24.8[a], 25.6[b]	393.0674	409, 427, 449, 375, 176, **188**	393.0682	2.0	-HCl, +2O
P14	$C_{16}H_{10}F_6N_2O_4$	24.4	409.0618	431, 391, 377, 359, **220**, 202, 170, 150, 131	409.06899	3.8	-HCl, +3O
P15	$C_{16}H_9ClF_6N_2O_3$	25.6[a], 27.0[b]	427.0279	429, 449, 409, 353, 302, 206, 185, **173, 145**	427.0256	-5.3	+2O, -2H•
P16[U]	-	30.2	533	**267**, 279, 289, 555, 249	-	-	-
P17	$C_{16}H_{11}ClF_6N_2O_3$	22.3[a], 24.1[b], 26.7[c], 28.5[b]	429.0435	431, 451, 411, 397, **240**, 222, 190, **173**, 145, 131, 115	429.0441	1.4	+2O
P18*	$C_{16}H_{10}F_6N_2O$	31.8	361.0776	383, 343, **312**, 271, 190, 173, 145	361.0786	2.7	-HCl
P19	$C_{16}H_{10}F_6N_2O_2$	28.2	377.0719	359, 345, 331, 176, **188**	377.0716	0.0	-HCl, +O
FLP	$C_{16}H_{11}ClF_6N_2O$	27.8	397.0535	419, 435, 208, 173, 145, 131, 115	397.0535	0.0	-

Letters on t_R- isomers elution time, b*old Q3: most abundant peak, * known before this work, U-unidentified yet,* ***δm/m*** *–relative mass deviation error (ppm)*

To gain further data on the possible product structures and the correlation between *m/z* 267 and P16, the products' EIC and rate of formation were plotted in Appendix Fig. A11c, d. In the first 10 min of irradiation, only *m/z* 267 was produced. After 10 min, the peak area ratio of both *m/z* 267 and P16 behaved similarly, in that they were produced after 10 – 20 min and then reduced. Production of P16 after *m/z* 267 supports dimer production. However, the structure of P16 was not derived here, as the fragmentation experiment did not show any characteristic peaks of FLP.

In summary, seven new PPs of the fungicide FLP (mainly hydroxylated PPs from the parent FLP and lactam) were identified in this work. Although lactam was reported before, its mono-, di-, and tri-hydroxylated products were identified for the first time here. Depending on irradiation time, it seems that PPs with further hydroxylation at the two aromatic rings could be formed. Dihydroxyl, hydroxylimide and Cl-substitution (by HO• or H•) are also metabolites of FLP. However, N-dealkylation of FLP or hydroxyl FLP – suggested here as the main metabolic mechanism in EC/MS

and *in vitro* – were not formed with UV-C treatment. Furthermore, the TPs of dechlorination of FLP were rarely found in EC/MS studies, but were abundantly formed through UV-C irradiation. Both EC/MS or UV-C approaches could be used to synthesise TP reference standards for application to real sample analysis.

3.6. Investigation of TPs in Food Samples

After identification and structural analysis of biotransformation and abiotic TPs, the third objective of this thesis was to identify the TPs in real samples. However, one of the biggest challenges in such studies is lack of commercial available TP standards for real samples, such as foodstuffs, environment, and biofluids. Using EC or UV-based synthesis, in combination with fractionating analytical tools like preparative-HPLC, could be used to synthesise TP reference standards. However, TPs from a single compound can be nearly identical in structure and polarity, which makes chromatographic fractionation difficult. Other than this, synthesised TPs could be used for unbiased authentication of targeted TPs in real samples without quantitation and fractionation. Thus, this section is dedicated to the identification of TPs of CPF and FLP in fruit and spice samples.

3.6.1. Synthesis and Stability of TPs

As stated in sec 3.5.1, attempting to synthesise CPF TPs by UV was only successful for DETP (P1), DEP (P2) and oxon (P5). Using EC/MS, a representative mixture of standards containing eight TPs (P1-P8) of CPF could be produced. Additionally, the EC/MS oxidative mechanism is the same as the biotransformation mechanism in living organisms. Depend on the target TPs, a UV approach could also be used to simulate synthesis (e.g. environmental stressors); however, in terms of time and solvent consumption, EC/MS is superior. Thus, TP standards were synthesised using BDD WE in SynthesisCell™. Compared to μPrepCell in EC/MS, a wider surface BDD electrode was used to maximise production. The mass voltammograms in **Fig. 48** showed the peak area of each TP and CPF with respect to applied DC potential. Like online EC/MS, CPF starts at around 1,800 mV and can be easily identified by a decrease with increasing potential. In contrast, the intensity for the products of *m*/*z* 113, 141, 155, 171, 198, 306, 316, 322 and 334 increased, indicating TPs formation. Accordingly, representative TPs of CPF could be effectively produced with 2,000- 2,200 mV applied potential. Above 2,200 mV,

oxon-bearing TPs, P5 and P6, are shown to reduce in intensity, which may reflect their oxidation into other TPs. The possible oxidation mechanism of each of the TPs of CPF is shown in Fig. 27a. The well-known TP of CPF, P3 (*m/z* 198), could be produced by indirect HO• nucleophilic substitution during formation of P1 (*m/z* 171) from CPF or P2 (*m/z* 155) from oxon. One unusual TP of CPF produced in EC was monodechlorinated CPF (P7, *m/z* 316). It is not clear which -Cl was removed from the aromatic ring; however, its formation was confirmed by EC/MS and HRMS (δm/m = 0.0 ppm). Using SynthesisCell, greater production of P8 and thiophosphate (*m/z* 113) by O-dealkylation was observed (**Fig. 48**).

Aside from the versatility of the products, ease of handling and online characterisation (EC/MS and EC/LC/MS) make EC the method of choice for producing TP standard. Meanwhile, P6, P7 and P8 were not investigated in the real samples due to lower stability (P6), yield (P7) and early elution (P8). Hence, in this work, only five of the TPs (P1 to P5) and the parent CPF were assessed in real food samples.

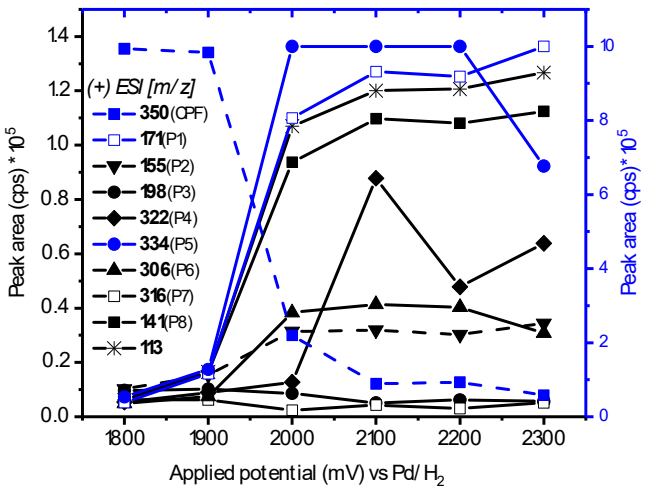

Fig. 48 Peak area of the TPs of CPF vs applied potential using BDD SynthesisCell™ in ACN/MeOH/H_2O, 1:3:1 v/v/v modifier and 1 mmol/L NH_4FA electrolyte after 3 h (from Mekonnen *et al.* [150] with 4442490416941)

Regarding FLP, both the EC and UV approach show versatile production of TPs. In particular, N-dealkylated TPs of the parent FLP and hydroxyl FLP could be effectively produced by EC. Using UV-C can be more effective, compared to EC, for production of hydroxyl FLP and lactam. FLP was not detected in any of the fruit samples here; thus, its TPs were not further investigated. In this thesis, parent compounds were investigated in all samples, while TPs were only investigated in the samples where the parent compounds were detected. The stability of TPs during sample processing is an important factor in the investigation. All

products were stable during 50-day storage at 4 ^{0}C, except for P3, which decreased by 40% after 20 days (Fig. 49a). The effect of temperature was evaluated by drying synthesised products immediately at 23, 35, 45 and 60 ^{0}C using N_2-stream (Fig. 49b). P4 and P5 were stable, while P1, P2, and P3 showed a significant decrease in 45 and 60 ^{0}C (23 – 33% lost); this could be due to evaporation. As evidenced in Fig. 49b, a slight increase in P1, P2 and P3 yield at 60 ^{0}C was due to thermal degradation of P4 and P5 (which slightly decreased). Hence, further sample treatments were performed on 35 ^{0}C.

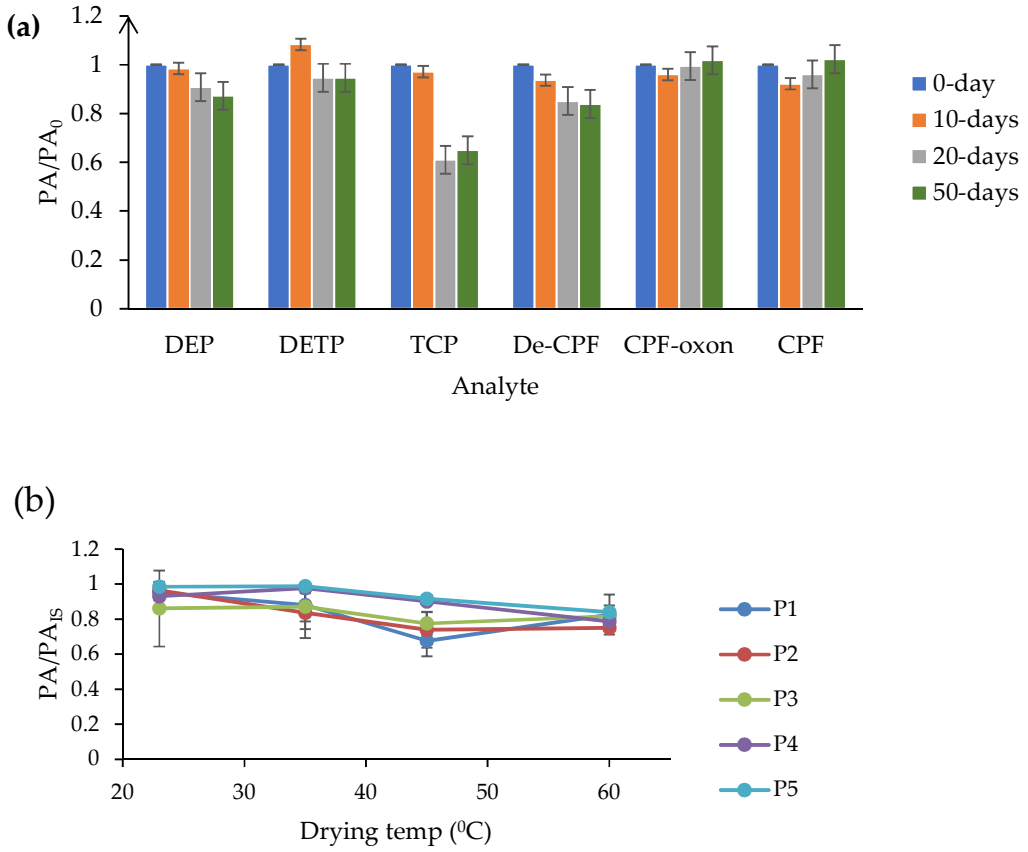

Fig. 49 Stability of synthesized TPs of CPF against storage time (a) and drying temperature (b) (n= 3)

3.6.2. LC-MS/MS Analysis

The chromatographic separation was achieved using the eclipse XDB RP C18 column for CPF and its TPs and C8 for FLP. The more polar and lower mass products, P1 and P2 (1.4 and 2.0 min in Fig. 50a), were eluted first. P1 and P2 are usually co-eluted, as they are structurally similar; however, they were detected by MRM scan, which is relatively free from

interferences. As shown in Fig. 50a, all five TPs (P1 – P5) and CPF were well separated (structures in Fig. 27a). P1- P4 were analysed in (-) MRM, while P5 and the parent CPF were detected in (+) MRM. The MRM transitions and MS/MS conditions are shown in Table 3.

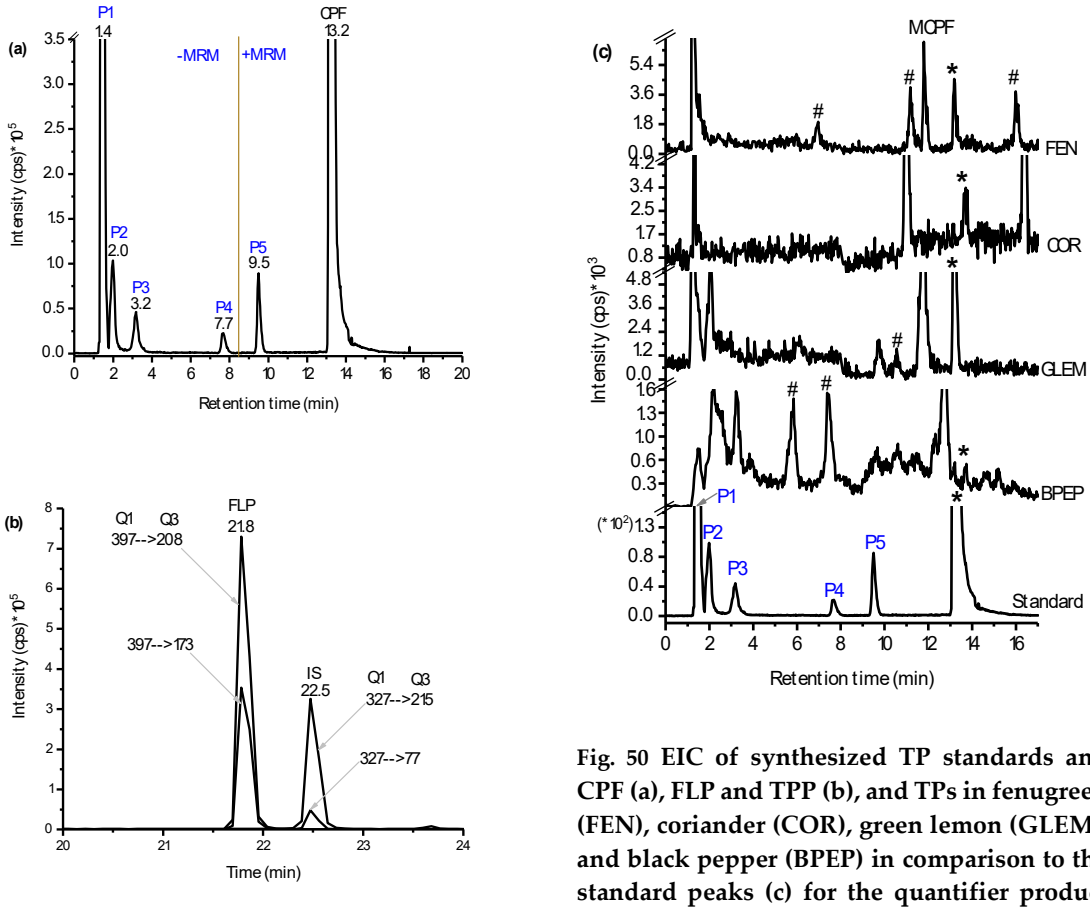

Fig. 50 EIC of synthesized TP standards and CPF (a), FLP and TPP (b), and TPs in fenugreek (FEN), coriander (COR), green lemon (GLEM), and black pepper (BPEP) in comparison to the standard peaks (c) for the quantifier product ions measured by LC-MS/MS on MRM mode (*-stands for CPF and #-for unidentified peaks). a and c are modified from Mekonnen *et al.* [150].

Few studies on the TPs of CPF have been performed, with only one or two TPs investigated simultaneously [57, 164]. However, the type of TPs in different food products could be vary due to different metabolisms and exogenic stresses (e.g. physicochemical, temperature and photodegradation). This method allows monitoring of five TPs and the parent compound CPF simultaneously in foodstuff matrices. In this study, all the TP standards were synthesised in-house, which saved time and money. Furthermore, the method could be used for investigation of other TPs of CPF, such as P6, P7, and P8 in the environment, industry (e.g. advanced oxidation processes), food and biological samples. Thus, EC/MS-based synthesis of TP

reference standards is easier, fast, matrix-free and cost-effective. Furthermore, it is a green chemistry approach for simulation of transformation mechanisms [165].

3.6.3. Method Validation

Limit of detections and linearity:- Method validation was performed using hot chili pepper and strawberry samples for CPF and its TPs, and strawberry and grapes for FLP. In the range of 20- 1,000 μg/kg spiked level, a good linearity of 0.9909 (in spices) and 0.9943 (in fruits) for CPF (Fig. A12a) and 0.9941 (fruits) for FLP were obtained (Fig. A12b). The method LODs and LOQs for CPF were 1.9 and 5.7 and 1.6 and 4.9 μg/kg in spices and fruits, respectively. In the case of FLP, 2.8 μg/kg LOD and 8.4 μg/kg LOQ were achieved. The LODs of the developed method were much lower than the EU-stipulated MRLs of both compounds in fruits (≥10 μg/kg CPF and 10 – 20,000 μg/kg FLP) and spices (≥100 μg/kg CPF) [68]. Hence, the LC-MS/MS method is sensitive enough to investigate CPF and FLP residues in fruits and spices.

Trueness and matrix effect:- Recoveries of TPs (65 – 85%) were slightly reduced compared to CPF (95%); nevertheless, they were in the acceptable range, with a repeatability of 2- 10% (Table 10). Lower recoveries of P2 could be due to more partitioning into the aqueous phase extract, as it is more polar than the other analytes. In contrast, P3 shows most recovery (111%) in the strawberry sample. This could be due to the acidic nature of the sample matrices, contributing to the hydrolysis of other TPs into P3 during sample preparation. The effect of the matrix was investigated by comparing the peak areas of post-spiked extracts with synthetic standards (without matrices). As shown in Table 10, signal suppression to less than 19% and 16% was observed in spices and fruits, respectively. In the case of FLP, the matrix effect is negligible. Foodstuff matrices are very complex and known to cause significant signal suppression or enhancement. However, in this method, all recoveries, the matrix effect and the repeatability are compliant with the commission's guideline [166].

Table 10 Trueness, matrix effect, and reproducibility (inter-day and intra-day repeatability) of investigated analytes in hot chili pepper and strawberry samples at 200 μg/kg spiking level by CPF (adopted from Mekonnen *et al.* [150], LN 4442490416941)

	%R (RSD), n = 6		%ME (RSD), n = 6		RSD_R (%), n = 9		RSD_r (%), n = 3	
Analyte	Pepper	Strawberry	Pepper	Strawberry	Pepper	Strawberry	Pepper	Strawberry
CPF	95 (2)	98 (8)	85 (6)	90 (1)	6	4	6	2
P1	79 (6)	78 (10)	81 (14)	89 (4)	21	15	10	11
P2	65 (10)	71 (9)	87 (8)	86 (5)	25	14	8	5
P3	73 (10)	111 (7)	84 (11)	84 (9)	35	11	15	12
P4	81 (6)	75 (5)	88 (5)	91 (5)	13	10	10	13
P5	85 (4)	83 (2)	95 (4)	90 (7)	10	8	9	7
FLP	Grape	Strawberry	Grape	Strawberry	Grape	Strawberry	Grape	Strawberry
	96 (10)	93 (0)	98 (8)	104 (2)	9	14	8	11

Reproducibility:- The method is rugged enough to detect TPs and the parent CPF residues in foodstuff matrices [166]. A higher deviation in RSD_R was observed compared to RSD_r (Table 10). In particular, P2 and P3 had shown 25 and 35% deviation in hot chili pepper, respectively. Good reproducibility (4 – 15%) was obtained in strawberry. Nevertheless, the RSD_r reproducibility is in the acceptable range in both fruit (2- 13%) and spice (6- 15%) matrices. Samples extracted from spice showed adsorption to the glass surface during long storage (10 days), thus requiring vortexing and re-filtering prior to further analysis.

3.6.4. Detection of CPF and TPs in Spices and Fruits by LC-MS/MS

Based on the protocol in Fig. 18, each sample was extracted and analysed by LC-MS/MS in MRM mode. The chromatograms and confirmed TPs in each sample are shown in Fig. 50c and Table 11, respectively. Many fruit and spice samples (n = 65), originating from different continents, were investigated. While CPF was abundantly detected (104 μg/kg), FLP was not. Traces of CPF (<LOQ) were also detected in coriander and cinnamon (Table 11). This detected CPF content was lower than the EU-stipulated MRLs in all samples [68].

Regarding the TPs, P1 and P2 were frequently detected in samples containing CPF. Conversely, P3 and P5 were detected only in black pepper and green lemon (Table 11 and Fig. 50c), respectively. This difference may be based on the origin of the samples or the transformation mechanisms in each foodstuff. The TPs may enter food after transformation in environmental, as a result of different stressors, or may be formed during plant metabolism.

The dealkylated product (P4) was not detected in any of the samples. An intense peak at 11.8 min (Fig. 50c) in lemon and fenugreek seed was identified as methyl chlorpyrifos (MCPF, *m*/*z* 326), which yielded the same product ion *m*/*z* 198 as CPF (from MS/MS fragmentation). MCPF is not expected to be a TP of CPF; rather, it appears as one of the residues detected in the samples. This occurs as using a mixture of CPF and MCPF is common practice in the agricultural sector. To date, there are no guidelines on the MRLs of TPs in respect to toxicity and health concerns in consumers. However, studies show that some TPs, such as P5, are more cytoactive than the parent CPF [75]. In addition to retention time, the parent *m*/*z* was fragmented in MS/MS and compared with the standard spectra produced by EC, to avoid false positives. For instance, the intense peaks at the same retention time as P4 in black pepper and fenugreek seed (*# at 7.7 min in* Fig. 50c) did not comply with the standard spectra (and are, therefore, not considered as TPs).

Table 11 Contents of determined CPF and confirmed TPs in the investigated real samples (from Mekonnen *et al.* [150], LN 4442490416941)

	No of	CPF (n = 3)	Detected TPs				
Samples	**samples**	**(µg/kg)**	**P1**	**P2**	**P3**	**P4**	**P5**
Fenugreek	4	39.8±0.3	√	√	n.d.	n.d.	n.d.
Green lemon	3	104.1±0.2	√	√	n.d.	n.d.	√
Black pepper	4	31.3±0.4	√	√	√	n.d.	n.d.
Coriander	4	<LOQ	√	n.d.	n.d.	n.d.	n.d.
Cinnamon	4	<LOQ	√	n.d.	n.d.	n.d.	n.d.

n.d. – not detected, √ - detected, No – number

Although studies on TPs of agrochemicals in foodstuffs are very rare, the presence of CPF and P3 in duck muscle [164] and tomato [57] were previously reported. It is likely that the multiple stressors and their effects vary with time and this can lead to formation of new TPs. This study reports a novel method of monitoring CPF and five of its main TPs in fruits and spices. Most importantly, the TP standards are made in-house; as mentioned, this saves money and time. However, the selectivity of the method could be improved as multiple interfering peaks were observed in the spice samples. For instance, the peak at 11.2 and 16.1 min in fenugreek seed and coriander revealed ion products at *m*/*z* 350→198 in MS/MS, but these did not match with the MS-spectra and the retention time of CPF. The same is true for the observed intense peak at 5.7 min in black pepper. It is known that pollutants undergo conjugative reactions with biomolecules (e.g. glucoside and lipid) in plant metabolism [167]; this may account for the observed peaks that had similar *m*/*z* transitions but a different retention time.

In summary, a novel method of investigating five TPs and CPF in foodstuff samples was developed here. Four of these TPs were detected in different fruit and spice samples. Although individual TP quantification was not successful in the scope of this work, a standard mix was used for unbiased confirmation of the TPs by MRM. There are currently no stipulated MRL limits for TPs.

4. CONCLUSIONS AND FUTURE PERSPECTIVES

4.1. Conclusion

In this thesis, biotransformation of the insecticide, chlorpyrifos (CPF), and the fungicide, fluopyram (FLP), was studied. For this purpose, an electrochemistry coupled to liquid chromatography-mass spectrometry (EC/LC/MS) method was established to simulate formation mechanisms and predict biotransformation products. Human and rat liver metabolites of CPF and FLP were annotated by targeted and untargeted MS-based approaches and thoroughly compared to non-microsomal EC/LC/MS oxidative products. By doing so, CPF metabolites derived from P-oxidation and O-dealkylation (initiated by electron abstraction (SET) from –S–) were identified. Similarly, FLP was metabolised via hydroxylation, N-dealkylation and dehalogenation. Most importantly, FLP metabolism appeared to be initiated by SET from the -NH- and hydrogen abstraction (HAT) from α-carbon, both of which led to the formation of imines, olefin (hydroxylated by epoxidation) and N-dealkylated metabolites. In this work, six new metabolites of FLP were identified using online EC/LC/MS. In general, 85% of phase I metabolites formed by CYP450 were predicted by EC/MS.

Furthermore, glucosylation and glutathione (GSH) conjugations (phase II) were studied by trapping reactive species prior to MS. A total of four GSH and three glucoside conjugates with CPF and two monohydroxyl-FLP conjugates were identified. Thus, online EC/LC/MS could be effectively used as a complimentary tool to predict phase I and phase II metabolites of xenobiotics. This enables matrix-free, fast (in seconds) and automated prediction of metabolites and their mechanisms.

In the second part of this work, abiotic transformation processes of CPF and FLP were investigated by photodegradation (UV light) as a model method. The photodegradation products (PPs) and their pathways were elucidated by LC-MS/MS and HRMS. Three main PPs of CPF, namely oxon, diethylthiophosphate and diethylphosphate were successfully identified. In the case of FLP, seven new PPs were identified for the first time: 7,8-didroxyl and hydroxylimide of FLP; mono-, di- and trihydroxyl lactam; and two rearrangement products. These were formed through loss of neutral $H_2C{=}CH_2$.

In the third part of this thesis, EC/MS was applied to produced transformation product (TP) standards for investigation of foodstuff samples. After TPs were synthesised in EC, they were successfully applied for unbiased authentication of TPs in fruits and spices. The versatility of electrochemical reactions enabled by the boron-doped diamond (BDD) electrode allows the synthesis of five representative TP standards of CPF – a green approach that saves costs, time and solvents. CPF was detected in a variety of samples in the 31-104 μg/kg range, while FLP was not detected. Regarding TPs, diethylthiophosphate and diethylphosphate were most frequently detected in foodstuffs. Oxon and trichloropyridinol were also detected in lemon and black pepper. Thus, EC/LC/MS could be applied to large-scale production of TP reference standards in other agrochemicals and pharmaceuticals to ensure food safety and quality.

In conclusion, EC/MS-based metabolomics has three main advantages compared to conventional *in vivo* and *in vitro* methods: (1) it saves time and money; (2) it enables matrix-free detection of metabolic products and allows the elucidation of their formation mechanisms; and (3) it can be scaled up for synthesis of metabolite reference standards for the development of new products and application to real samples.

4.2. Future Perspectives

Despite the many advantages of EC/MS, it is not experimentally straightforward. The following points should, therefore, be taken into consideration in EC/MS-based metabolomic studies.

1. **EC cell and ESI incompatibility**:- EC prefers relatively a slower flow rate (<10 μL/min), which is too slow for single quadrupole MS. This is especially pertinent when HPLC is included, as the products are diluted and extend the elution time by a couple of hours. The external injection valve is necessary to increase post-EC flow rate. Using nano-HPLC could be a solution to handling the low pressure flow rate.
2. **Chemical constituents**:- EC requires a relatively high concentration of analyte and electrolyte, which is not compatible with MS spectra quality. Furthermore, the electrolytes preferred for EC are not compatible with ESI (e.g. perchlorate, boric acid). Hence, using organic acids, such as formic and acetic acid, or their ammonium salts, is advisable.
3. **Interfering products**:- Although EC is matrix-free, it could cause formation of interfering products. As ESI is considered as a passive EC system, precise screening of real oxidation products from ESI degradation products should be performed. Cationic radicals/intermediates and charged products, that can be easily detected in ESI, are produced. Keeping the EC cell further from the ESI source helps to avoid this problem. On the other hand, proton-bound interferences (oxidative products, intermediates, electrolytes and organic modifiers), as well as dimers, usually appear in online EC/MS. Dilution post-EC reduces such chemical artefacts.

REFERENCES

[1] J. Hollender, H. Singer, D. Hernando, T. Kosjek, E. Heath, The challenge of the identification and quantification of transformation products in the aquatic environment using high resolution mass spectrometry, in: D. Fatta-Kassinos, K. Bester and K. Kümmerer (Eds.), Xenobiotics in the Urban Water Cycle: Mass Flows, Environmental Processes, Mitigation and Treatment Strategies, Springer Netherlands, Dordrecht, **2010**, pp. 195-211.

[2] A.-C. Macherey, P.M. Dansette, Chapter 25 - Biotransformations leading to toxic metabolites: Chemical aspects, in: C. G. Wermuth, D. Aldous, P. Raboisson and D. Rognan (Eds.), The Practice of Medicinal Chemistry (Fourth Edition), Academic Press, San Diego, **2015**, pp. 585-614.

[3] A.K. Ghattas, F. Fischer, A. Wick, T.A. Ternes, Anaerobic biodegradation of (emerging) organic contaminants in the aquatic environment, Water Res, 116 (**2017**) 268-295.

[4] H. Mestankova, A.M. Parker, N. Bramaz, S. Canonica, K. Schirmer, U. von Gunten, K.G. Linden, Transformation of contaminant candidate list (CCL3) compounds during ozonation and advanced oxidation processes in drinking water: Assessment of biological effects, Water Research, 93 (**2016**) 110-120.

[5] C. Boix, M. Ibanez, J.V. Sancho, J.R. Parsons, P. Voogt, F. Hernandez, Biotransformation of pharmaceuticals in surface water and during waste water treatment: Identification and occurrence of transformation products, J Hazard Mater, 302 (**2016**) 175-187.

[6] B. Testa, S.D. Krämer, The Biochemistry of Drug Metabolism – An Introduction Part 4. Reactions of Conjugation and Their Enzymes, Chemistry & biodiversity, 5 (**2008**) 2171-2336.

[7] P.A. Egner, J.D. Groopman, J.-S. Wang, T.W. Kensler, M.D. Friesen, Quantification of Aflatoxin-B1-N7-Guanine in Human Urine by High-Performance Liquid Chromatography and Isotope Dilution Tandem Mass Spectrometry1, Chemical Research in Toxicology, 19 (**2006**) 1191-1195.

[8] B.I. Escher, J. Hackermüller, T. Polte, S. Scholz, A. Aigner, R. Altenburger, A. Böhme, S.K. Bopp, W. Brack, W. Busch, M. Chadeau-Hyam, A. Covaci, A. Eisenträger, J.J. Galligan, N. Garcia-Reyero, T. Hartung, M. Hein, G. Herberth, A. Jahnke, J. Kleinjans, N. Klüver, M. Krauss, M. Lamoree, I. Lehmann, T. Luckenbach, G.W. Miller, A. Müller, D.H. Phillips, T. Reemtsma, U. Rolle-Kampczyk, G. Schüürmann, B. Schwikowski, Y.-M. Tan, S. Trump, S. Walter-Rohde, J.F. Wambaugh, From the exposome to mechanistic understanding of chemical-induced adverse effects, Environment International, 99 (**2017**) 97-106.

[9] A. Parkinson, B.W. Ogilvie, D.B. Buckley, F. Kazmi, M. Czerwinski, O. Parkinson, Biotransformation of Xenobiotics, in: C. D. Klaassen and J. B. Watkins (Eds.), Essentials of Toxicology, McGraw-Hill Companies, USA, **2015**.

[10] H. Raza, A. John, Differential cytotoxicity of acetaminophen in mouse macrophage J774.2 and human hepatoma HepG2 cells: Protection by diallyl sulfide, PLOS ONE, 10 (**2016**) e0145965.

[11] Y. Masubuchi, T. Horie, Toxicological significance of mechanism-based inactivation of cytochrome P450 enzymes by drugs, Critical Reviews in Toxicology, 37 (**2007**) 389-412.

[12] V.V. Shumyantseva, T. Bulko, E. Shich, A. Makhova, A. Kuzikov, A. Archakov, Cytochrome P450 enzymes and electrochemistry: Crosstalk with electrodes as redox partners and electron sources, in: E. G. Hrycay and S. M. Bandiera (Eds.), Monooxygenase, Peroxidase and Peroxygenase Properties and Mechanisms of Cytochrome P450, **2015**, pp. 229-246.

[13] U.M. Zanger, M. Schwab, Cytochrome P450 enzymes in drug metabolism: regulation of gene expression, enzyme activities, and impact of genetic variation, Pharmacol Ther, 138 (**2013**) 103-141.

[14] F.P. Guengerich, Mechanisms of cytochrome P450 substrate oxidation: MiniReview, Journal of Biochemical and Molecular Toxicology, 21 (**2007**) 163-168.

[15] A.W. Munro, K.J. McLean, J.L. Grant, T.M. Makris, Structure and function of the cytochrome P450 peroxygenase enzymes, Biochemical Society Transactions, 46 (**2018**) 183–196.

[16] F.P. Guengerich, Common and uncommon cytochrome P450 reactions related to metabolism and chemical toxicity, Chem Res Toxicol, 14 (**2001**) 611-650.

[17] M. Sono, M.P. Roach, E.D. Coulter, J.H. Dawson, Heme-Containing Oxygenases, Chem Rev, 96 (**1996**) 2841-2888.

[18] L. Dellafiora, P. Mena, D. Del Rio, P. Cozzini, Modeling the effect of phase II conjugations on topoisomerase I poisoning: pilot study with luteolin and quercetin, J Agric Food Chem, 62 (**2014**) 5881-5886.

[19] P.J. van Bladeren, Glutathione conjugation as a bioactivation reaction, Chemico-Biological Interactions, 129 (**2000**) 61-76.

[20] G.L. Weber, R.C. Steenwyk, S.D. Nelson, P.G. Pearson, Identification of N-acetylcysteine conjugates of 1,2-dibromo-3-chloropropane: Evidence for cytochrome P450 and glutathione mediated bioactivation pathways, Chemical Research in Toxicology, 8 (**1995**) 560-573.

[21] T.J. Monks, M.W. Anders, W. Dekant, J.L. Stevens, S.S. Lau, P.J. van Bladeren, Glutathione conjugate mediated toxicities, Toxicol Appl Pharmacol, 106 (**1990**) 1-19.

[22] J.T. Hancock, R. Desikan, S.J. Neill, Role of reactive oxygen species in cell signalling pathways, Biochemical Society Transactions, 29 (**2001**) 345-349.

[23] K. Apel, H. Hirt, Reactive oxygen species: Metabolism, oxidative stress, and signal transduction, Annual Review of Plant Biology, 55 (**2004**) 373-399.

[24] U. von Gunten, Oxidation processes in water treatment: Are we on track?, Environ Sci Technol, 52 (**2018**) 5062-5075.

[25] L. Zhu, B. Santiago-Schubel, H. Xiao, H. Hollert, S. Kueppers, Electrochemical oxidation of fluoroquinolone antibiotics: Mechanism, residual antibacterial activity and toxicity change, Water Res, 102 (**2016**) 52-62.

[26] X. Xu, J. Chen, S. Wang, J. Ge, R. Qu, M. Feng, V.K. Sharma, Z. Wang, Degradation kinetics and transformation products of chlorophene by aqueous permanganate, Water Res, 138 (**2018**) 293-300.

[27] A. Tekle-Rottering, C. von Sonntag, E. Reisz, C.V. Eyser, H.V. Lutze, J. Turk, S. Naumov, W. Schmidt, T.C. Schmidt, Ozonation of anilines: Kinetics, stoichiometry, product identification and elucidation of pathways, Water Res, 98 (**2016**) 147-159.

[28] A. Tawk, M. Deborde, J. Labanowski, H. Gallard, Chlorination of the beta-triketone herbicides tembotrione and sulcotrione: Kinetic and mechanistic study, transformation products identification and toxicity, Water Res, 76 (**2015**) 132-142.

[29] O. Rozas, C. Vidal, C. Baeza, W.F. Jardim, A. Rossner, H.D. Mansilla, Organic micropollutants (OMPs) in natural waters: Oxidation by UV/H2O2 treatment and toxicity assessment, Water Res, 98 (**2016**) 109-118.

[30] A. Konig, C. Weidauer, B. Seiwert, T. Reemtsma, T. Unger, M. Jekel, Reductive transformation of carbamazepine by abiotic and biotic processes, Water Res, 101 (**2016**) 272-280.

[31] H.C. Lan, Z.F. Jiao, X. Zhao, W.J. He, A.M. Wang, H.J. Liu, R.P. Liu, J.H. Qu, Removal of glyphosate from water by electrochemically assisted MnO2 oxidation process, Separation and Purification Technology, 117 (**2013**) 30-34.

[32] J. Taborsky, M. Svidrnoch, O. Kurka, L. Borovcova, P. Bednar, P. Bartak, J. Skopalova, Electrochemical oxidation of zopiclone, Monatshefte Fur Chemie, 147 (**2016**) 53-60.

[33] K. Gandhi, S. Lari, D. Tripathi, G. Kanade, Advanced oxidation processes for the treatment of chlorpyrifos, dimethoate and phorate in aqueous solution, Journal of Water Reuse and Desalination, 6 (**2016**) 195-203.

[34] A.M. Parker, Y. Lester, E.K. Spangler, U. von Gunten, K.G. Linden, UV/H2O2 advanced oxidation for abatement of organophosphorous pesticides and the effects on various toxicity screening assays, Chemosphere, 182 (**2017**) 477-482.

[35] C.A. Martinez-Huitle, S. Ferro, Electrochemical oxidation of organic pollutants for the wastewater treatment: direct and indirect processes, Chem Soc Rev, 35 (**2006**) 1324-1340.

[36] R. Andreozzi, V. Caprio, A. Insola, R. Marotta, Advanced oxidation processes (AOP) for water purification and recovery, Catalysis Today, 53 (**1999**) 51-59.

[37] M.M. Najafpour, A.N. Moghaddam, S.I. Allakhverdiev, Govindjee, Biological water oxidation: lessons from nature, Biochim Biophys Acta, 1817 (**2012**) 1110-1121.

[38] U. Hubner, U. von Gunten, M. Jekel, Evaluation of the persistence of transformation products from ozonation of trace organic compounds - a critical review, Water Res, 68 (**2015**) 150-170.

[39] L. Wang, D.Y. Kong, Y.F. Ji, J.H. Lu, X.M. Yin, Q.S. Zhou, Formation of halogenated disinfection byproducts during the degradation of chlorophenols by peroxymonosulfate oxidation in the presence of bromide, Chemical Engineering Journal, 343 (**2018**) 235-243.

[40] European Food Safety Authority Panel on Contaminants in the Food Chain (EFSA CONTAM Panel), 2015 Scientific opinion on acrylamide in food, EFSA Journal, 13 (**2015**) 4104-4425.

[41] E.M. Fiss, K.L. Rule, P.J. Vikesland, Formation of chloroform and other chlorinated byproducts by chlorination of triclosan-containing antibacterial products, Environmental Science & Technology, 41 (**2007**) 2387-2394.

[42] U.V. Gunten, E. Salhi, C.K. Schmidt, W.A. Arnold, Kinetics and mechanisms of N-nitrosodimethylamine formation upon ozonation of N,N-dimethylsulfamide-containing waters: Bromide catalysis, Environmental Science & Technology, 44 (**2010**) 5762-5768.

[43] J. Unsworth, History of pesticide use. International Union of Pure and Applied Chemistry (IUPAC). https://agrochemicals.iupac.org/index.php?option=com_sobi2&sobi2Task=sobi2Details&catid=3&sobi2Id=31, (accessed 06 November 2018).

[44] D. Atwood, C. Paisley-Jones, Pesticides industry sales and usage 2008 - 2012 market estimates Environmental Protection Agency (EPA), Office of Chemical Safety and Pollution Prevention, Washington, DC , USA.

[45] A. De, R. Bose, A. Kumar, S. Mozumdar, Worldwide Pesticide Use, in: (Eds.), Targeted delivery of pesticides using biodegradable polymeric nanoparticles, Springer India, New Delhi, **2014**, pp. 5-6.

[46] The Rapid Alert System for Food and Feed (RASFF), 2016 annual report. available on https://ec.europa.eu/food/sites/food/files/safety/docs/rasff_annual_report_2016.pdf, **2017**, doi:10.2875/022237.

[47] The Rapid Alert System for Food and Feed (RASFF), 2017 annual report. available on file:///C:/Users/TESSEMA/Desktop/rasff_annual_report_2017.pdf, **2018**, doi:10.2875/767865.

[48] The Rapid Alert System for Food and Feed (RASFF). https://ec.europa.eu/food/safety/rasff/for_consumers_en, (accessed 01 October 2018).

[49] European Food Safety Authority (EFSA), The 2016 European Union report on pesticide residues in food, EFSA Journal, 16 (**2018**) e05348.

[50] European Commission Codex Alimentarius International Food Standards. http://www.fao.org/fao-who-codexalimentarius/thematic-areas/pesticides/en/#c452840, (accessed 10 October 2018).

[51] P. Xu, L. Huang, Stereoselective bioaccumulation, transformation, and toxicity of triadimefon in Scenedesmus obliquus, Chirality, 29 (**2017**) 61-69.

[52] The Stockholm Convention on Persistent Organic Pollutants (POPs), EU Commission, Stockholm, Sweden. available on http://chm.pops.int/TheConvention/Overview/tabid/3351/Default.aspx (accessed 5 August 2018).

[53] S.A. Mackintosh, N.G. Dodder, N.J. Shaul, L.I. Aluwihare, K.A. Maruya, S.J. Chivers, K. Danil, D.W. Weller, E. Hoh, Newly identified DDT-related compounds accumulating in southern california bottlenose dolphins, Environ Sci Technol, 50 (**2016**) 12129-12137.

[54] J. Zhan, Y. Liang, D. Liu, C. Liu, H. Liu, P. Wang, Z. Zhou, Organochlorine pesticide acetofenate and its hydrolytic metabolite in rabbits: Enantioselective metabolism and cytotoxicity, Pesticide Biochemistry and Physiology, 145 (**2018**) 76-83.

[55] P. Westlund, S. Isazadeh, A. Therrien, V. Yargeau, Endocrine activities of pesticides during ozonation of waters, Bull Environ Contam Toxicol, 100 (**2018**) 112-119.

[56] N. Michel, M. Freese, M. Brinkmann, J.D. Pohlmann, H. Hollert, U. Kammann, M. Haarich, N. Theobald, W. Gerwinski, W. Rotard, R. Hanel, Fipronil and two of its transformation products in water and European eel from the river Elbe, Sci Total Environ, 568 (**2016**) 171-179.

[57] G. Peng, Q. He, Y. Lu, D. Mmereki, Z. Zhong, Determination of organophosphorus pesticides and their major degradation product residues in food samples by HPLC-UV, Environ Sci Pollut Res Int, 23 (**2016**) 19409-19416.

[58] Z. Zhang, Z. Gao, Y. Wang, Y. Yuan, J. Dong, T. Yue, Transformation products elucidation of forchlorfenuron in postharvest kiwifruit by time-of-flight mass spectrometry, PLoS One, 12 (**2017**) e0184021.

[59] A. Bauer, J. Luetjohann, F.S. Hanschen, M. Schreiner, J. Kuballa, E. Jantzen, S. Rohn, Identification and characterization of pesticide metabolites in Brassica species by liquid chromatography travelling wave ion mobility quadrupole time-of-flight mass spectrometry (UPLC-TWIMS-QTOF-MS), Food Chem, 244 (**2018**) 292-303.

[60] N.I. Rousis, R. Bade, L. Bijlsma, E. Zuccato, J.V. Sancho, F. Hernandez, S. Castiglioni, Monitoring a large number of pesticides and transformation products in water samples from Spain and Italy, Environ Res, 156 (**2017**) 31-38.

[61] J.D. Fine, C.A. Mullin, Metabolism of N-methyl-2-pyrrolidone in honey bee adults and larvae: Exploring age related differences in toxic effects, Environ Sci Technol, 51 (**2017**) 11412-11422.

[62] N. Negreira, J. Regueiro, S. Valdersnes, M.H.G. Berntssen, R. Ornsrud, Comprehensive characterization of ethoxyquin transformation products in fish feed by traveling-wave ion mobility spectrometry coupled to quadrupole time-of-flight mass spectrometry, Anal Chim Acta, 965 (**2017**) 72-82.

[63] J.F. Garcia-Reyes, A. Molina-Diaz, A.R. Fernandez-Alba, Identification of pesticide transformation products in food by liquid chromatography/time-of-flight mass

spectrometry via "fragmentation-degradation" relationships, Anal Chem, 79 (**2007**) 307-321.

[64] B. Du, J.M. Lofton, K.T. Peter, A.D. Gipe, C.A. James, J.K. McIntyre, N.L. Scholz, J.E. Baker, E.P. Kolodziej, Development of suspect and non-target screening methods for detection of organic contaminants in highway runoff and fish tissue with high-resolution time-of-flight mass spectrometry, Environ Sci Process Impacts, 19 (**2017**) 1185-1196.

[65] Y. Pico, D. Barcelo, Transformation products of emerging contaminants in the environment and high-resolution mass spectrometry: a new horizon, Anal Bioanal Chem, 407 (**2015**) 6257-6273.

[66] Pesticide Action Network (PAN). https://pan-germany.org/download/ngo-factsheet-eu-should-ban-brain-harming-chlorpyrifos/, (accessed 03 October 2018).

[67] Oregon State University, National Pesticides Information Center (NPIC). http://www.npic.orst.edu/NPRO/, (accessed 28.08.2018).

[68] European Union (EU) Pesticides Database. http://ec.europa.eu/food/plant/pesticides/eu-pesticides-database/public/?event=pesticide.residue.CurrentMRL&language=EN&pestResidueId=56, (accessed 3 January 2018).

[69] European Commission, Directorate-General for Health and Food Safety, Commission Regulation (EU) 2018/687 of 4 May 2018 amending Annexes II and III to Regulation (EC) No 396/2005 of the European Parliament and of the Council as regards maximum residue levels for acibenzolar-S-methyl, benzovindiflupyr, bifenthrin, bixafen, chlorantraniliprole, deltamethrin, flonicamid, fluazifop-P, isofetamid, metrafenone, pendimethalin and teflubenzuron in or on certain products (Text with EEA relevance), Official Journal of the European Union, L 121, 61 (**2018**) 63.

[70] T. Eleršek, M. Filipič, Organophosphorus pesticides - mechanisms of their toxicity, in: (Eds.), Pesticides - The Impacts of Pesticide Exposure, InTech Europe, Slovenia, **2011**, pp. 243-260.

[71] M. Supreeth, N.S. Raju, Biotransformation of chlorpyrifos and endosulfan by bacteria and fungi, Appl Microbiol Biotechnol, 101 (**2017**) 5961-5971.

[72] K. Choi, H. Joo, R.L. Rose, E. Hodgson, Metabolism of chlorpyrifos and chlorpyrifos oxon by human hepatocytes, J Biochem Mol Toxicol, 20 (**2006**) 279-291.

[73] W. Bicker, M. Lammerhofer, W. Lindner, Determination of chlorpyrifos metabolites in human urine by reversed-phase/weak anion exchange liquid chromatography-electrospray ionisation-tandem mass spectrometry, J Chromatogr B Analyt Technol Biomed Life Sci, 822 (**2005**) 160-169.

[74] J. Tang, Y. Cao, R.L. Rose, A.A. Brimfield, D. Dai, J.A. Goldstein, E. Hodgson, Metabolism of chlorpyrifos by human cytochrome P450 isoforms and human, mouse, and rat liver microsomes, Drug Metabolism and Disposition, 29 (**2001**) 1201-1204.

[75] J.V. Sancho, O.J. Pozo, F. Hernandez, Direct determination of chlorpyrifos and its main metabolite 3,5, 6-trichloro-2-pyridinol in human serum and urine by coupled-column liquid chromatography/electrospray-tandem mass spectrometry, Rapid Commun Mass Spectrom, 14 (**2000**) 1485-1490.

[76] R. Zabar, M. Sarakha, A.T. Lebedev, O.V. Polyakova, P. Trebse, Photochemical fate and photocatalysis of 3,5,6-trichloro-2-pyridinol, degradation product of chlorpyrifos, Chemosphere, 144 (**2016**) 615-620.

[77] N. Rafique, S.R. Tariq, K. Ahad, T. Taj, Cu(2+) and Fe(2+) mediated photodegradation studies of soil-incorporated chlorpyrifos, Environ Sci Pollut Res Int, 23 (**2016**) 4473-4480.

[78] M.S. Bootharaju, T. Pradeep, Understanding the degradation pathway of the pesticide, chlorpyrifos by noble metal nanoparticles, Langmuir, 28 (**2012**) 2671-2679.

[79] E.L. Croom, A.D. Wallace, E. Hodgson, Human variation in CYP-specific chlorpyrifos metabolism, Toxicology, 276 (**2010**) 184-191.

[80] D.L. Eaton, R.B. Daroff, H. Autrup, J. Bridges, P. Buffler, L.G. Costa, J. Coyle, G. McKhann, W.C. Mobley, L. Nadel, D. Neubert, R. Schulte-Hermann, P.S. Spencer, Review of the toxicology of chlorpyrifos with an emphasis on human exposure and neurodevelopment, Crit Rev Toxicol, 38 Suppl 2 (**2008**) 1-125.

[81] J. Femia, M. Mariani, C. Zalazar, I. Tiscornia, Photodegradation of chlorpyrifos in water by UV/H2O2 treatment: toxicity evaluation, Water Sci Technol, 68 (**2013**) 2279-2286.

[82] A. Fadaei, M. Kargar, Photocatalytic degradation of chlorpyrifos in water using titanium dioxide and zinc oxide, Fresenius Environmental Bulletin, 22 (**2013**) 2442-2447.

[83] A.G. de Oliveira, J.P. Ribeiro, J.T. de Oliveira, D. De Keukeleire, M.S. Duarte, R.F. do Nascimento, Degradation of the pesticide chlorpyrifos in aqueous solutions with UV/H_2O_2: Optimization and effect of interfering anions, Journal of Advanced Oxidation Technologies, 17 (**2014**) 133-138.

[84] J. Femia, M. Mariani, A. Cassano, C. Zalazar, I. Tiscornia, Decontamination of commercial chlorpyrifos in water using the UV/H2O2 process, in: M. I. Litter, R. J. Candal and J. M. Meichtry (Eds.), Advanced Oxidation Technologies - Sustainable Solutions for Environmental Treatments, **2014**, pp. 149-161.

[85] J. Wu, D.A. Laird, Abiotic transformation of chlorpyrifos to chlorpyrifos oxon in chlorinated water, Environ Toxicol Chem, 22 (**2003**) 261-264.

[86] Y. Samet, L. Agengui, R. Abdelhedi, Electrochemical degradation of chlorpyrifos pesticide in aqueous solutions by anodic oxidation at boron-doped diamond electrodes, Chemical Engineering Journal, 161 (**2010**) 167-172.

[87] H. Sierotzki, G. Scalliet, A review of current knowledge of resistance aspects for the next-generation succinate dehydrogenase inhibitor fungicides, Phytopathology, 103 (**2013**) 880-887.

[88] European Food Safety Authority (EFSA), Conclusion on the peer review of the pesticide risk assessment of the active substance fluopyram, EFSA Journal, 11 (**2013**) 3052 - 3128.

[89] Australian Pesticides and Veterinary Medicines Authority (APVMA), Public release summary on the evaluation of the new active fluopyram in the product luna privilege fungicide. https://apvma.gov.au/sites/.../publication/14166-prs-fluopyram.pdf, (accessed 25 Jul 2017).

[90] P. Wei, Y. Liu, W. Li, Y. Qian, Y. Nie, D. Kim, M. Wang, Metabolic and dynamic profiling for risk assessment of fluopyram, a typical phenylamide fungicide widely applied in vegetable ecosystem, Sci Rep, 6 (**2016**) 33898 - 33909.

[91] B. Dong, J. Hu, Photodegradation of the novel fungicide fluopyram in aqueous solution: kinetics, transformation products, and toxicity evolvement, Environ Sci Pollut Res Int, 23 (**2016**) 19096-19106.

[92] E.F.A. Brandon, C.D. Raap, I. Meijerman, J.H. Beijnen, J.H.M. Schellens, An update on in vitro test methods in human hepatic drug biotransformation research: pros and cons, Toxicology and Applied Pharmacology, 189 (**2003**) 233-246.

[93] C. Wiese, E. Grosse Maestrup, F. Galla, D. Schepmann, A. Hiller, S. Fischer, F.A. Ludwig, W. Deuther-Conrad, C.K. Donat, P. Brust, L. Buter, U. Karst, B. Wunsch, Comparison of in silico, electrochemical, in vitro and in vivo metabolism of a homologous series of (radio)fluorinated sigma1 receptor ligands designed for positron emission tomography, ChemMedChem, 11 (**2016**) 2445-2458.

[94] H. Kimura, Y. Sakai, T. Fujii, Organ/body-on-a-chip based on microfluidic technology for drug discovery, Drug Metab Pharmacokinet, 33 (**2018**) 43-48.

[95] L. Lin, J.M. Lin, Development of cell metabolite analysis on microfluidic platform, J Pharm Anal, 5 (**2015**) 337-347.

[96] P.M. van Midwoud, E. Verpoorte, G.M. Groothuis, Microfluidic devices for in vitro studies on liver drug metabolism and toxicity, Integr Biol (Camb), 3 (**2011**) 509-521.

[97] D.K. Badyal, C. Desai, Animal use in pharmacology education and research: The changing scenario, Indian Journal of Pharmacology, 46 (**2014**) 257-265.

[98] D. Zhang, G. Luo, X. Ding, C. Lu, Preclinical experimental models of drug metabolism and disposition in drug discovery and development, Acta Pharmaceutica Sinica B, 2 (**2012**) 549-561.

[99] U. Jurva, L. Weidolf, Electrochemical generation of drug metabolites with applications in drug discovery and development, Trac-Trends in Analytical Chemistry, 70 (**2015**) 92-99.

[100] M.J.G. Elizabeth, A.H. Martin, The evolution of cytochrome P450 enzymes as biocatalysts in drug discovery and development, Current Topics in Medicinal Chemistry, 13 (**2013**) 2254-2280.

[101] S. Kern, K. Fenner, H.P. Singer, R.P. Schwarzenbach, J. Hollender, Identification of transformation products of organic contaminants in natural waters by computer-aided

prediction and high-resolution mass spectrometry, Environ Sci Technol, 43 (**2009**) 7039-7046.

[102] C. Liao, U.J. Kim, K. Kannan, A review of environmental occurrence, fate, exposure, and toxicity of benzothiazoles, Environ Sci Technol, 52 (**2018**) 5007-5026.

[103] A. Tomasevic, D. Mijin, A. Marinkovic, M. Radisic, N. Prlainovic, R. Durovic-Pejcev, S. Gasic, The photocatalytic degradation of carbofuran and Furadan 35-ST: the influence of inert ingredients, Environ Sci Pollut Res Int, 24 (**2017**) 13808-13822.

[104] B. Sevilla-Moran, L. Calvo, C. Lopez-Goti, J.L. Alonso-Prados, P. Sandin-Espana, Photodegradation behaviour of sethoxydim and its comercial formulation Poast((R)) under environmentally-relevant conditions in aqueous media. Study of photoproducts and their toxicity, Chemosphere, 168 (**2017**) 501-507.

[105] C. Berberidou, V. Kitsiou, E. Kazala, D.A. Lambropoulou, A. Kouras, C.I. Kosma, T.A. Albanis, I. Poulios, Study of the decomposition and detoxification of the herbicide bentazon by heterogeneous photocatalysis: Kinetics, intermediates and transformation pathways, Applied Catalysis B-Environmental, 200 (**2017**) 150-163.

[106] Y. Yu, D.A. Reckhow, Formation and occurrence of N-chloro-2,2-dichloroacetamide, a previously overlooked nitrogenous disinfection byproduct in chlorinated drinking waters, Environ Sci Technol, 51 (**2017**) 1488-1497.

[107] S. Hussain, J.R. Steter, S. Gul, A.J. Motheo, Photo-assisted electrochemical degradation of sulfamethoxazole using a Ti/Ru0.3Ti0.7O2 anode: Mechanistic and kinetic features of the process, Journal of Environmental Management, 201 (**2017**) 153-162.

[108] Z. Tasic, V.K. Gupta, M.M.Antonijevic, The mechanism and kinetics of degradation of phenolics in wastewaters using electrochemical oxidation, International Journal of Electrochemical Science, 9 (**2014**) 3473 - 3490.

[109] D.H. Evans, One-electron and two-electron transfers in electrochemistry and homogeneous solution reactions, Chemical Reviews, 108 (**2008**) 2113-2144.

[110] S. Bruckenstein, R. Raogadde, Use of a porous electrode for in-situ mass spectrometric determination of volatile electrode reaction products, Journal of the American Chemical Society, 93 (**1971**) 793-794.

[111] G. Hambitzer, J. Heitbaum, Electrochemical thermospray mass spectrometry, Analytical Chemistry, 58 (**1986**) 1067-1070.

[112] T.A. Getek, W.A. Korfmacher, T.A. McRae, J.A. Hinson, Utility of solution electrochemistry mass spectrometry for investigating the formation and detection of biologically important conjugates of acetaminophen, Journal of Chromatography, 474 (**1989**) 245.

[113] K.J. Volk, R.A. Yost, A. Brajter-Toth, On-line electrochemistry/thermospray/tandem mass spectrometry as a new approach to the study of redox reactions: the oxidation of uric acid, Analytical Chemistry, 61 (**1989**) 1709-1717.

[114] G.J. Van Berkel, S.A. McLuckey, G.L. Glish, Electrochemical origin of radical cations observed in electrospray ionization mass spectra, Analytical Chemistry, 64 (**1992**) 1586-1593.

[115] T. Zhang, A. Brajter-Toth, On-line investigation of the generation of nonaqueous intermediate radical cations by electrochemistry/mass spectrometry, Anal Chem, 72 (**2000**) 2533-2540.

[116] M.C.S. Regino, A. BrajterToth, An electrochemical cell for on-line electrochemistry mass spectrometry, Analytical Chemistry, 69 (**1997**) 5067-5072.

[117] W. Lu, X. Xu, R.B. Cole, On-line linear sweep voltammetry-electrospray mass spectrometry, Anal Chem, 69 (**1997**) 2478-2484.

[118] U. Jurva, H.V. Wikstrom, L. Weidolf, A.P. Bruins, Comparison between electrochemistry/mass spectrometry and cytochrome P450 catalyzed oxidation reactions, Rapid Commun Mass Spectrom, 17 (**2003**) 800-810.

[119] H. Simon, G. Hoffmann, F. Hubner, H.U. Humpf, U. Karst, Electrochemical simulation of metabolic reactions of the secondary fungal metabolites alternariol and alternariol methyl ether, Anal Bioanal Chem, 408 (**2016**) 2471-2483.

[120] H. Faber, D. Melles, C. Brauckmann, C.A. Wehe, K. Wentker, U. Karst, Simulation of the oxidative metabolism of diclofenac by electrochemistry/(liquid chromatography/)mass spectrometry, Anal Bioanal Chem, 403 (**2012**) 345-354.

[121] S.M. van Leeuwen, B. Blankert, J.M. Kauffmann, U. Karst, Prediction of clozapine metabolism by on-line electrochemistry/liquid chromatography/mass spectrometry, Anal Bioanal Chem, 382 (**2005**) 742-750.

[122] S.M. van Leeuwen, H. Hayen, U. Karst, Liquid chromatography-electrochemistry-mass spectrometry of polycyclic aromatic hydrocarbons, Anal Bioanal Chem, 378 (**2004**) 917-925.

[123] U. Karst, Electrochemistry/mass spectrometry (EC/MS)--a new tool to study drug metabolism and reaction mechanisms, Angew Chem Int Ed Engl, 43 (**2004**) 2476-2478.

[124] H. Hayen, U. Karst, Analysis of phenothiazine and its derivatives using LC/Electrochemistry/MS and LC/Electrochemistry/Fluorescence, Analytical Chemistry, (**2003**) 4833-4840.

[125] G. Diehl, U. Karst, On-line electrochemistry--MS and related techniques, Anal Bioanal Chem, 373 (**2002**) 390-398.

[126] L. Buter, L.M. Frensemeier, M. Vogel, U. Karst, Dual reductive/oxidative electrochemistry/liquid chromatography/mass spectrometry: Towards peptide and protein modification, separation and identification, J Chromatogr A, 1479 (**2017**) 153-160.

[127] C.N. Cramer, K.F. Haselmann, J.V. Olsen, P.K. Nielsen, Disulfide linkage characterization of disulfide bond-containing proteins and peptides by reducing electrochemistry and mass spectrometry, Analytical Chemistry, 88 (**2016**) 1585-1592.

[128] L. Switzar, S. Nicolardi, J.W. Rutten, S.A.J.L. Oberstein, A. Aartsma-Rus, Y.E.M. van der Burgt, In-depth characterization of protein disulfide bonds by online liquid chromatography-electrochemistry-mass spectrometry, Journal of the American Society for Mass Spectrometry, 27 (**2016**) 50-58.

[129] T. Wigger, A. Seidel, U. Karst, Electrochemistry coupled to (LC-)MS for the simulation of oxidative biotransformation reactions of PAHs, Chemosphere, 176 (**2017**) 202-211.

[130] J. Keller, H. Haase, M. Koch, Electrochemical simulation of biotransformation reactions of citrinin and dihydroergocristine compared to UV irradiation and Fenton-like reaction, Anal Bioanal Chem, 409 (**2017**) 4037-4045.

[131] H.T. Madsen, E.G. Sogaard, J. Muff, Study of degradation intermediates formed during electrochemical oxidation of pesticide residue 2,6-dichlorobenzamide (BAM) at boron doped diamond (BDD) and platinum-iridium anodes, Chemosphere, 109 (**2014**) 84-91.

[132] S. Mohle, M. Zirbes, E. Rodrigo, T. Gieshoff, A. Wiebe, S.R. Waldvogel, Modern electrochemical aspects for the synthesis of value-added organic products, Angew Chem Int Ed Engl, 57 (**2018**) 6018-6041.

[133] W. Lohmann, U. Karst, Electrochemistry meets enzymes: instrumental on-line simulation of oxidative and conjugative metabolism reactions of toremifene, Anal Bioanal Chem, 394 (**2009**) 1341-1348.

[134] U. Bussy, P. Giraudeau, V. Silvestre, T. Jaunet-Lahary, V. Ferchaud-Roucher, M. Krempf, S. Akoka, I. Tea, M. Boujtita, In situ NMR spectroelectrochemistry for the structure elucidation of unstable intermediate metabolites, Anal Bioanal Chem, 405 (**2013**) 5817-5824.

[135] L. Buter, M. Vogel, U. Karst, Adduct formation of electrochemically generated reactive intermediates with biomolecules, Trac-Trends in Analytical Chemistry, 70 (**2015**) 74-91.

[136] J.F. de-la-Mora, G.J. Van-Berkel, C.G. Enke, R.B. Cole, M. Martinez-Sanchez, J.B. Fenn, Special feature: Discussion electrochemical processes in electrospray ionization mass spectrometry, JOURNAL OF MASS SPECTROMETRY, 35 (**2000**) 939–952.

[137] H. Girault, B. Liu, L. Qiao, H. Bi, M. Prudent, N. Lion, M. Abonnenc, Electrochemical reactions and ionization processes, Eur J Mass Spectrom (Chichester), 16 (**2010**) 341-349.

[138] C. Roussel, L. Dayon, N. Lion, T.C. Rohner, J. Josserand, J.S. Rossier, H. Jensen, H.H. Girault, Generation of mass tags by the inherent electrochemistry of electrospray for protein mass spectrometry, J Am Soc Mass Spectrom, 15 (**2004**) 1767-1779.

[139] L. Dayon, C. Roussel, H.H. Girault, On-line electrochemical tagging of free cysteines in peptides during nanospray ionisation mass spectrometry: An overview, Chimia, 58 (**2004**) 204-207.

[140] J.S. Lu, X. Hua, Y.T. Long, Recent advances in real-time and in situ analysis of an electrode-electrolyte interface by mass spectrometry, Analyst, 142 (**2017**) 691-699.

[141] Z.Y. Wang, Y.Y. Zhang, B.W. Liu, K. Wu, S. Thevuthasan, D.R. Baer, Z.H. Zhu, X.Y. Yu, F.Y. Wang, In situ mass spectrometric monitoring of the dynamic electrochemical process at the electrode-electrolyte interface: A SIMS approach, Analytical Chemistry, 89 (**2017**) 960-965.

[142] A.P. Bruins, An overview of electrochemistry combined with mass spectrometry, Trac-Trends in Analytical Chemistry, 70 (**2015**) 14-19.

[143] F. Di Girolamo, I. Lante, M. Muraca, L. Putignani, The role of mass spectrometry in the "Omics" era, Curr Org Chem, 17 (**2013**) 2891-2905.

[144] H. Faber, M. Vogel, U. Karst, Electrochemistry/mass spectrometry as a tool in metabolism studies-a review, Anal Chim Acta, 834 (**2014**) 9-21.

[145] A. Baumann, T. Pfeifer, D. Melles, U. Karst, Investigation of the biotransformation of melarsoprol by electrochemistry coupled to complementary LC/ESI-MS and LC/ICP-MS analysis, Anal Bioanal Chem, 405 (**2013**) 5249-5258.

[146] Antec Scientific. https://antecscientific.com/, (accessed 01 October 2018).

[147] T.F. Mekonnen, U. Panne, M. Koch, New photodegradation products of the fungicide fluopyram: Structural elucidation and mechanism identification, Molecules, 23 (**2018**) 2940-2952.

[148] T. Pluskal, S. Castillo, A. Villar-Briones, M. Orešič, MZmine 2: Modular framework for processing, visualizing, and analyzing mass spectrometry-based molecular profile data, BMC Bioinformatics, 11 (**2010**) 395-395.

[149] M.C. Chambers, B. Maclean, R. Burke, D. Amodei, D.L. Ruderman, S. Neumann, L. Gatto, B. Fischer, B. Pratt, J. Egertson, K. Hoff, D. Kessner, N. Tasman, N. Shulman, B. Frewen, T.A. Baker, M.-Y. Brusniak, C. Paulse, D. Creasy, L. Flashner, K. Kani, C. Moulding, S.L. Seymour, L.M. Nuwaysir, B. Lefebvre, F. Kuhlmann, J. Roark, P. Rainer, S. Detlev, T. Hemenway, A. Huhmer, J. Langridge, B. Connolly, T. Chadick, K. Holly, J. Eckels, E.W. Deutsch, R.L. Moritz, J.E. Katz, D.B. Agus, M. MacCoss, D.L. Tabb, P. Mallick, A cross-platform toolkit for mass spectrometry and proteomics, Nature Biotechnology, 30 (**2012**) 918-920.

[150] T.F. Mekonnen, L. Byrne, U. Panne, M. Koch, Investigation of chlorpyrifos and its transformation products in fruits and spices by combining electrochemistry and liquid chromatography coupled to tandem mass spectrometry, Food Analytical Methods, 11 (**2018**) 2657-2665.

[151] J. Roeser, N.F. Alting, H.P. Permentier, A.P. Bruins, R. Bischoff, Boron-doped diamond electrodes for the electrochemical oxidation and cleavage of peptides, Anal Chem, 85 (**2013**) 6626-6632.

[152] T.F. Mekonnen, U. Panne, M. Koch, Electrochemistry coupled online to liquid chromatography-mass spectrometry for fast simulation of biotransformation reactions of the insecticide chlorpyrifos, Anal Bioanal Chem, 409 (**2017**) 3359-3368.

[153] S. Jahn, U. Karst, Electrochemistry coupled to (liquid chromatography/) mass spectrometry--current state and future perspectives, J Chromatogr A, 1259 (**2012**) 16-49.

[154] T.F. Mekonnen, U. Panne, M. Koch, Prediction of biotransformation products of the fungicide fluopyram by electrochemistry coupled online to liquid chromatography-mass spectrometry and comparison with in vitro microsomal assays, Anal Bioanal Chem, 410 (**2018**) 2607-2617.

[155] O. Hammerich, Oxidation of organic hydrocarbons, in: O. Hammerich and B. Speiser (Eds.), Organic electrochemistry: Revised and expanded, CRC Press, New York, **2016**, pp. 891-911.

[156] S. Jahn, A. Baumann, J. Roscher, K. Hense, R. Zazzeroni, U. Karst, Investigation of the biotransformation pathway of verapamil using electrochemistry/liquid chromatography/mass spectrometry - a comparative study with liver cell microsomes, J Chromatogr A, 1218 (**2011**) 9210-9220.

[157] T. Johansson, L. Weidolf, U. Jurva, Mimicry of phase I drug metabolism--novel methods for metabolite characterization and synthesis, Rapid Commun Mass Spectrom, 21 (**2007**) 2323-2331.

[158] A.R. Mani, S. Ippolito, J.C. Moreno, T.J. Visser, K.P. Moore, The metabolism and dechlorination of chlorotyrosine in vivo, J Biol Chem, 282 (**2007**) 29114-29121.

[159] D. Giustarini, P. Fanti, E. Matteucci, R. Rossi, Micro-method for the determination of glutathione in human blood, J Chromatogr B Analyt Technol Biomed Life Sci, 964 (**2014**) 191-194.

[160] R.M. Nthumbi, J.C. Ngila, Electrospun and functionalized PVDF/PAN nanocatalyst-loaded composite for dechlorination and photodegradation of pesticides in contaminated water, Environ Sci Pollut Res Int, 23 (**2016**) 20214-20231.

[161] S. Verma, R.B. Nasir Baig, M.N. Nadagouda, R.S. Varma, Aerobic oxidation of alcohols in visible light on Pd-grafted Ti cluster, Tetrahedron, 73 (**2017**) 5577-5580.

[162] D.J. Reynolds, O.T. Wong, R. Simlot, J.-J. Chang, I.H. Hall, Acute toxic and teratogenic effects of cyclic imides in rodents, Archiv der Pharmazie, 327 (**1994**) 237-245.

[163] H.D. Burrows, M. Canle L, J.A. Santaballa, S. Steenken, Reaction pathways and mechanisms of photodegradation of pesticides, Journal of Photochemistry and Photobiology B: Biology, 67 (**2002**) 71-108.

[164] R. Li, L. He, T. Zhou, X. Ji, M. Qian, Y. Zhou, Q. Wang, Simultaneous determination of chlorpyrifos and 3,5,6-trichloro-2-pyridinol in duck muscle by modified QuEChERS coupled to gas chromatography tandem mass spectrometry (GC-MS/MS), Anal Bioanal Chem, 406 (**2014**) 2899-2907.

[165] H. Oberacher, F. Pitterl, J.P. Chervet in *"Omics" Applications of electrochemistry coupled to mass spectrometry - a review*, *Vol. 28* LCGC Europe, **2015**, pp. 138-150.

[166] European Commission, Guidance document on analytical quality control and validation procedures for pesticide residues analysis in food and feed, SANTE/11813/2017. available on. https://ec.europa.eu/food/sites/food/files/plant/docs/pesticides_mrl_guidelines_wrkdoc_2017-11813.pdf, (accessed 10 March 2018).

[167] K. Singh, S.U. Khan, M.H. Akhtar, S. Kacew, N.D.G. White, Nature and bioavailability of nonextractable (bound) residues in stored wheat treated with chlorpyrifos-methyl, Journal of Agricultural and Food Chemistry, 41 (**1993**) 2421-2425.

APPENDIX I-Supplementary Figures

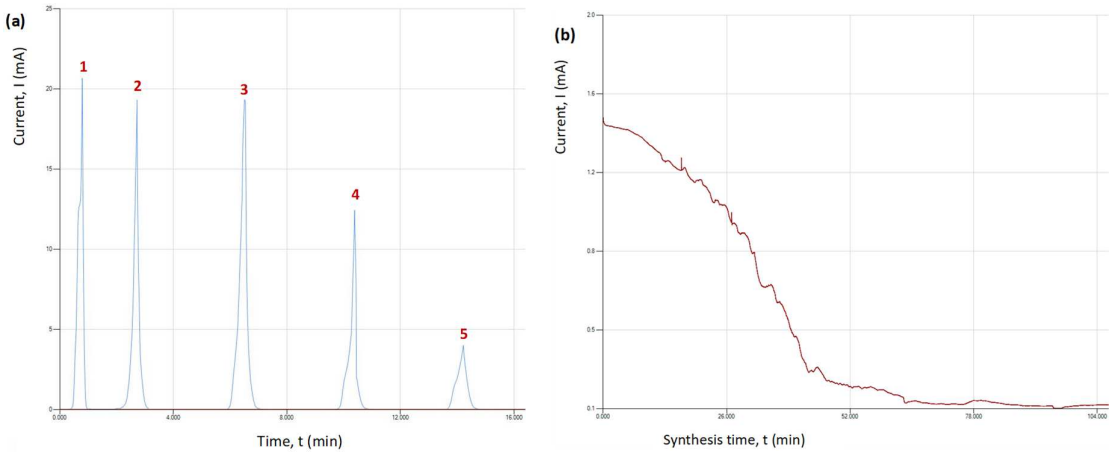

Fig. A1 Current *vs* time of CPF recorded for five continuous full scans within 1,800 – 2,300 mV with 10 mV/s (a) and DC potential at 2,000 mV (b) using BDD as WE

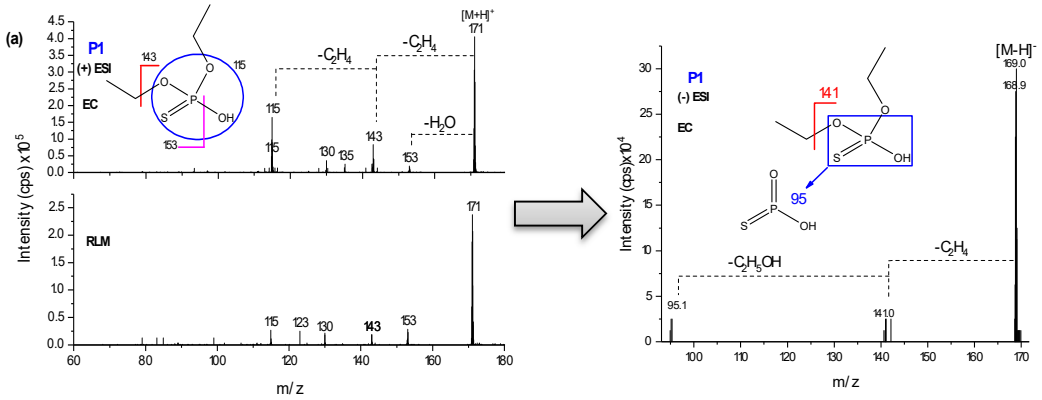

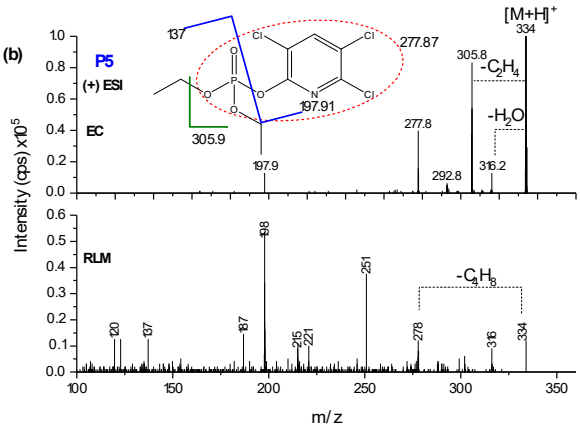

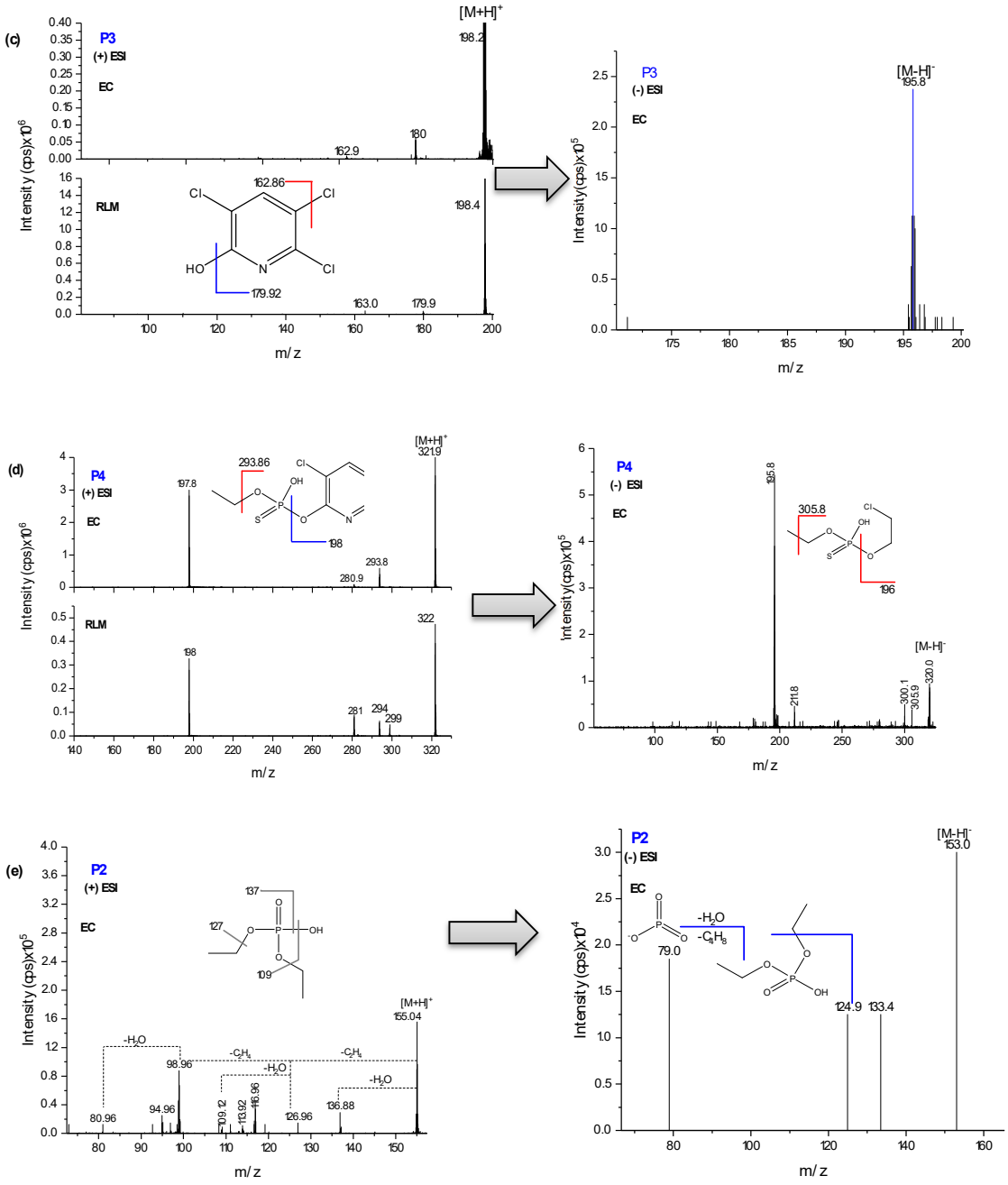

Fig. A2 Product ion spectra of P1: DETP (a), P5: oxon (b), P3: TCP (c), P4: Des-CPF (d), and P2: DEP (e) on both (+) (left side) and (-) ESI-MS/MS (right side) from EC/MS *vs* RLM metabolites

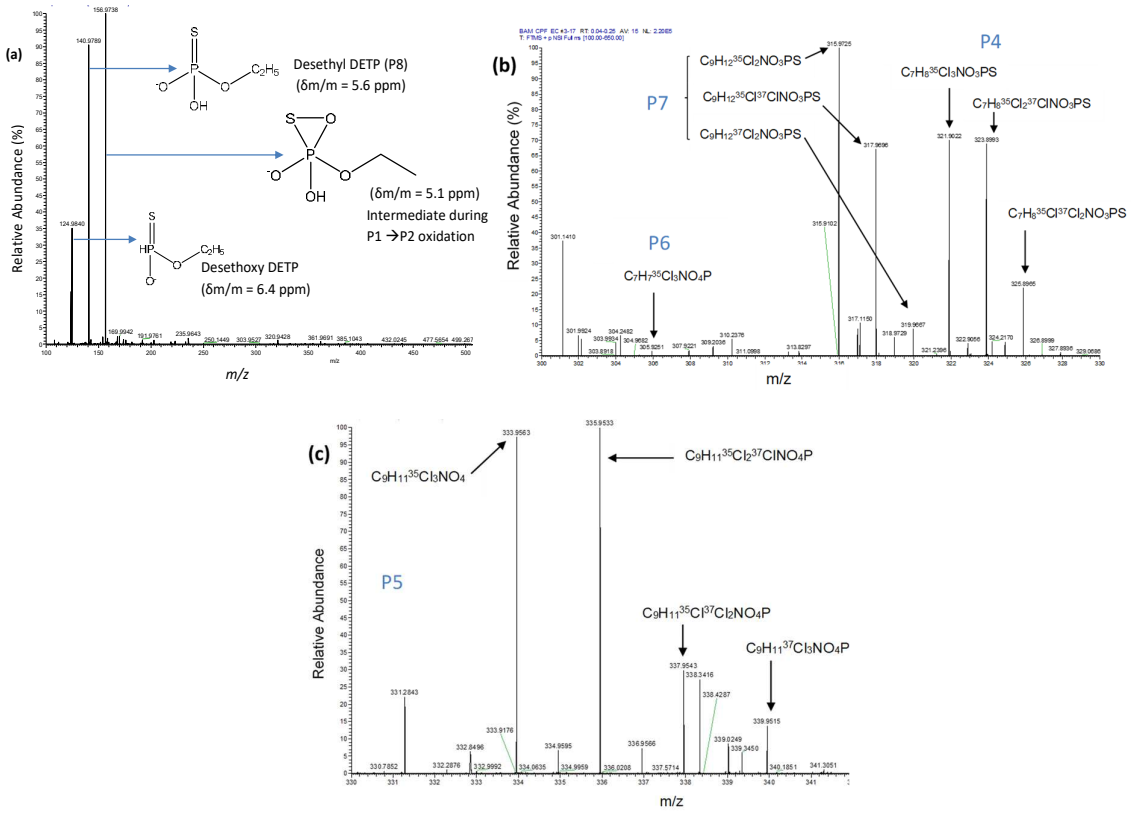

Fig. A3 FT-ICR-HRMS spectra of selected CPF oxidative products from EC/MS effluents; P8: desethyl DETP on (-) ESI (a), P4, P6, and P7 (b), and P5 (c) on (+) ESI

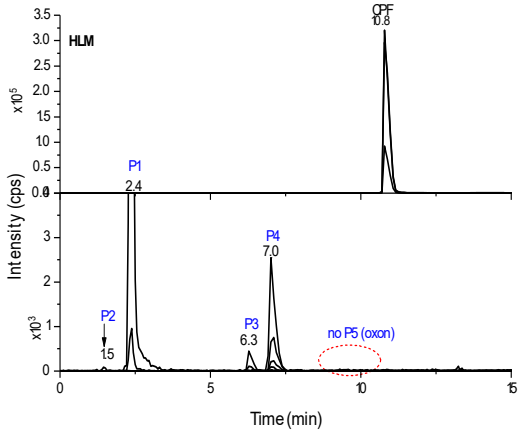

Fig. A4 EIC of CPF metabolites after incubation with HLM

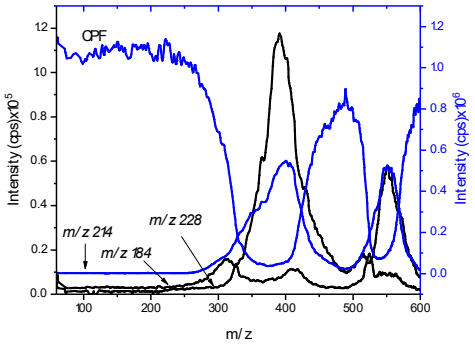

Fig. A5 Mass voltammograms of CPF metabolism intermediates (*m/z* 184: I1, 214: I2, and 228: I3)

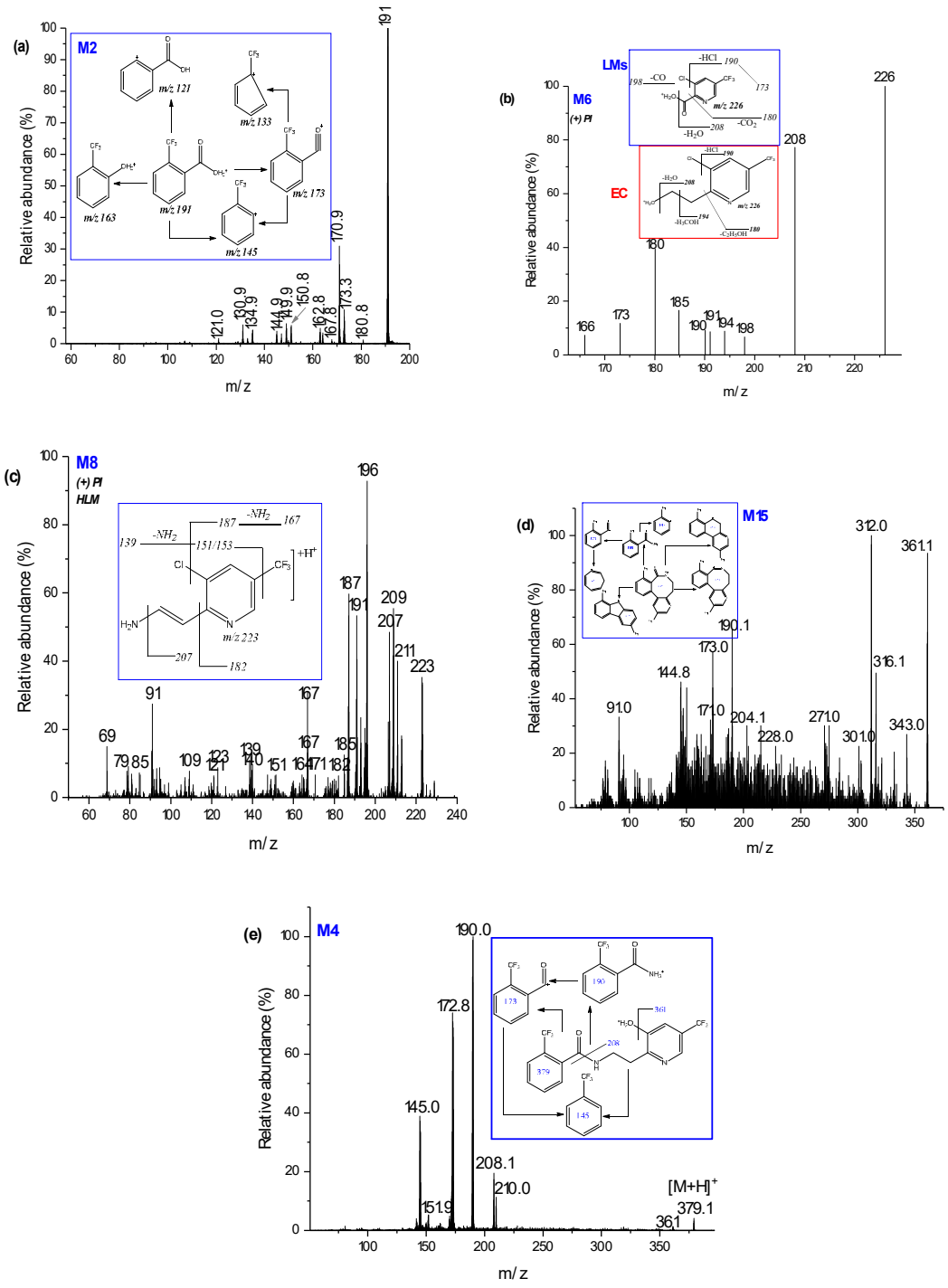

Fig. A6 (+) ESI-MS/MS spectra of selected EC and HLM products of FLP recorded by QTRAP: M2 (a), M6 (b), M8 (c), M15 (d), and M4 (e)

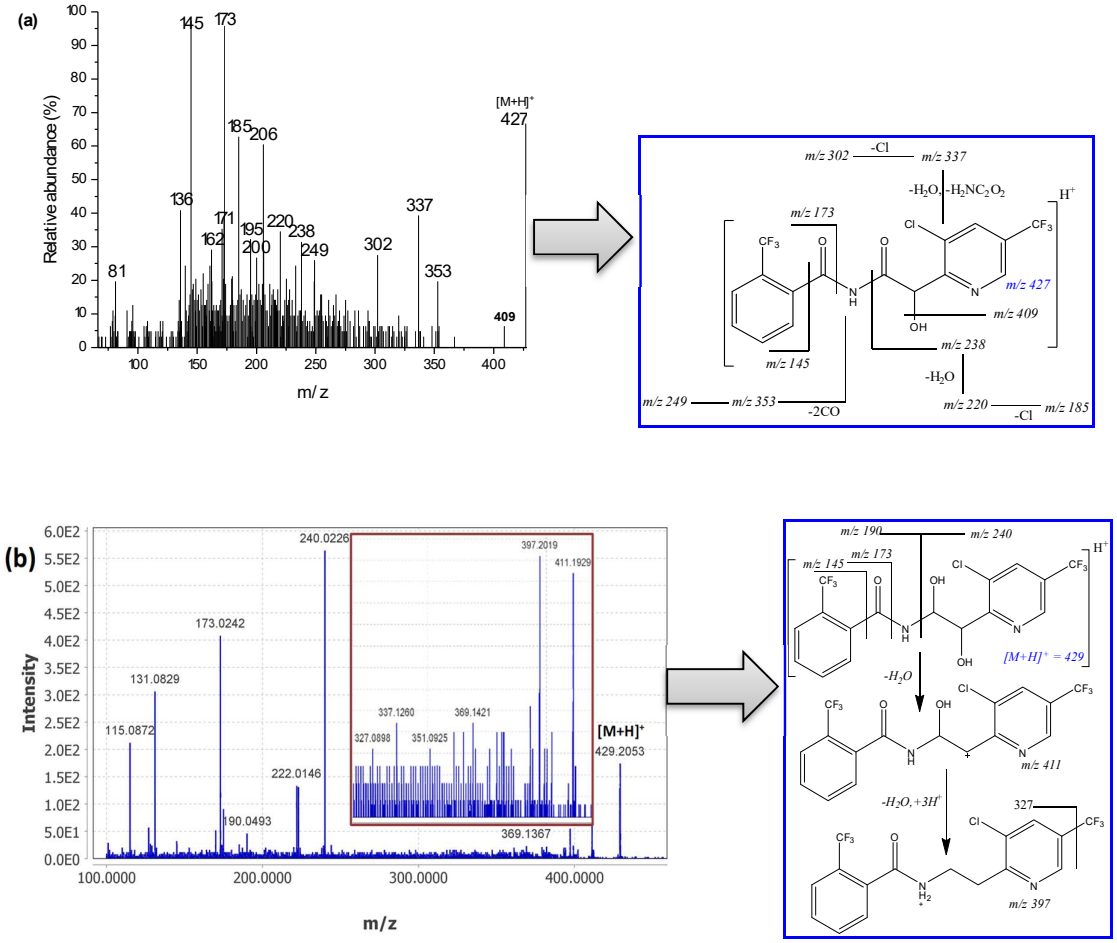

Fig. A7 (+) ESI-MS/MS spectra of P15: hydroxylimide (a) and P17: dihydroxyl FLP (b) PPs of FLP and their corresponding proposed fragmentation pattern measured by TripleTOF

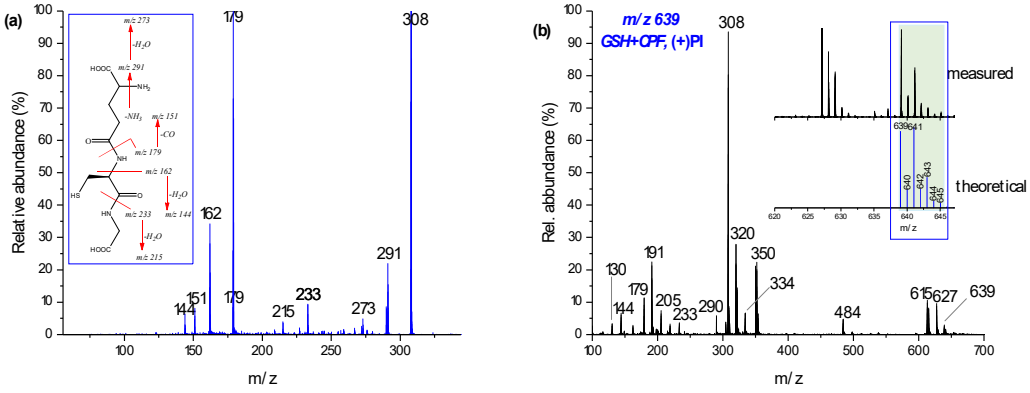

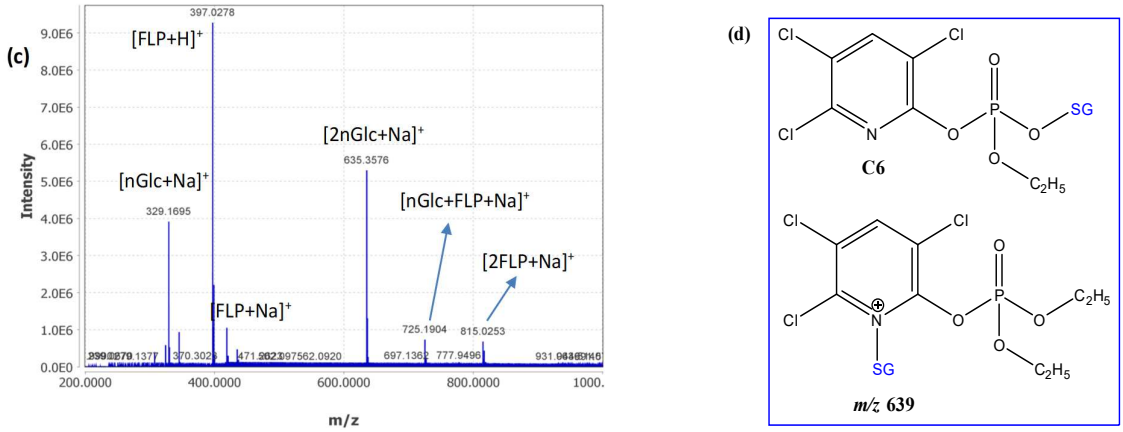

Fig. A8 (+) ESI-MS/MS spectra of standard GSH (a) and *m/z* 639 from CPF and GSH (b) measured on QTRAP; and n-Glc mixture with FLP oxidative products scanned by TripleTOF within *m/z* 200 – 1,000 Da (c) and proposed structures of C6 and *m/z* 639 conjugate (d)

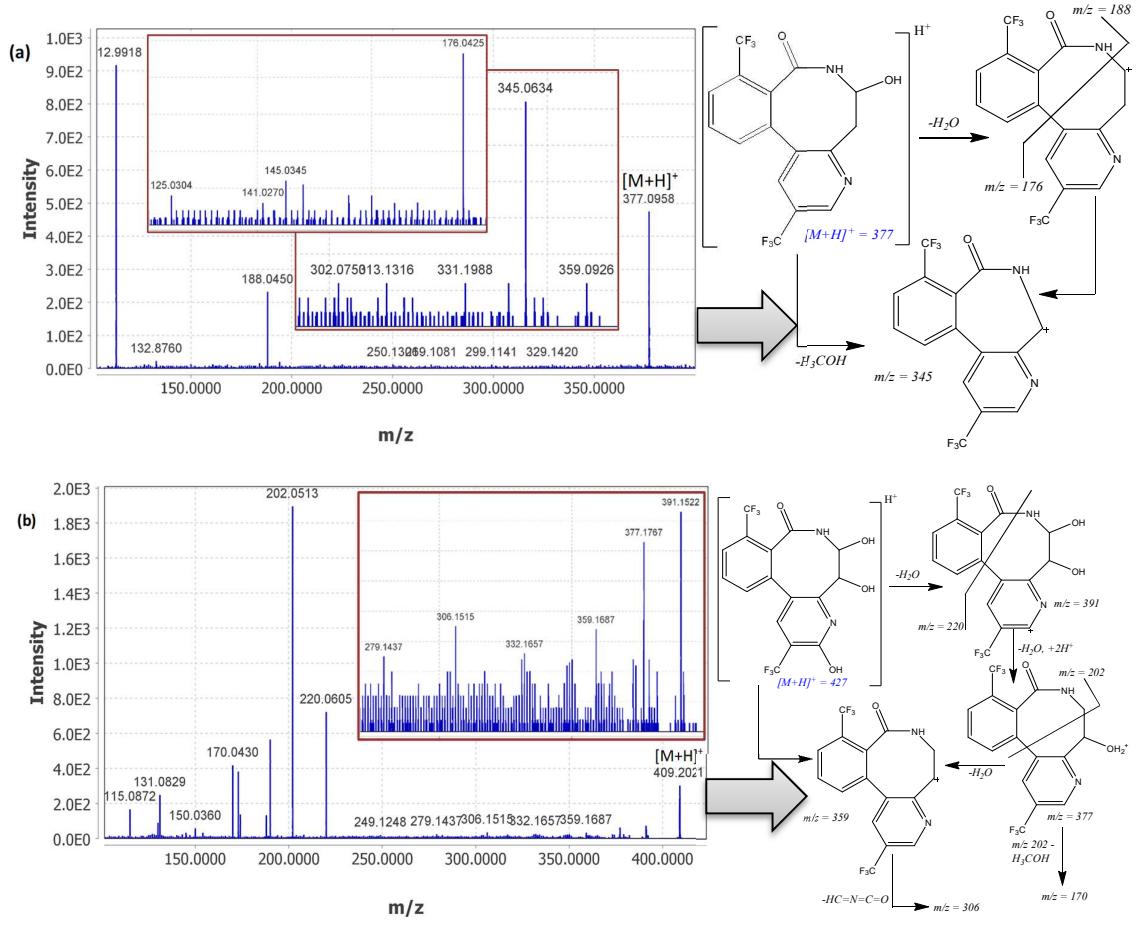

Fig. A9 (+) ESI-MS/MS spectra of P19: mono- (a) and P14: trihydroxyl (b) lactam FLP photodegradation products and their corresponding suggested fragmentations measured by TripleTOF

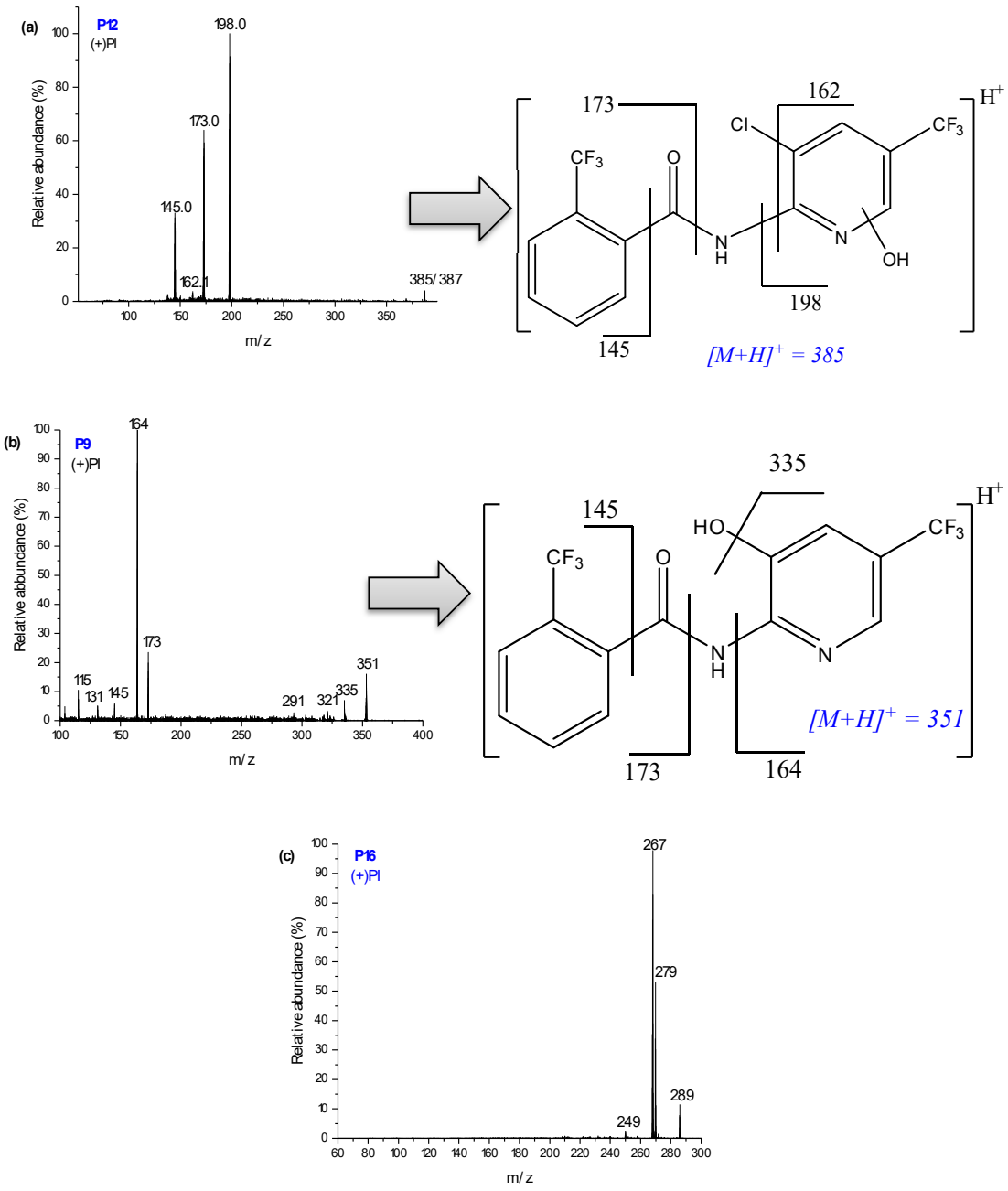

Fig. A10 (+) ESI-MS/MS spectra of P12 (a), P9 (b), and P16 (c) formed by rearrangement and their proposed fragmentation mechanisms measured by QTRAP

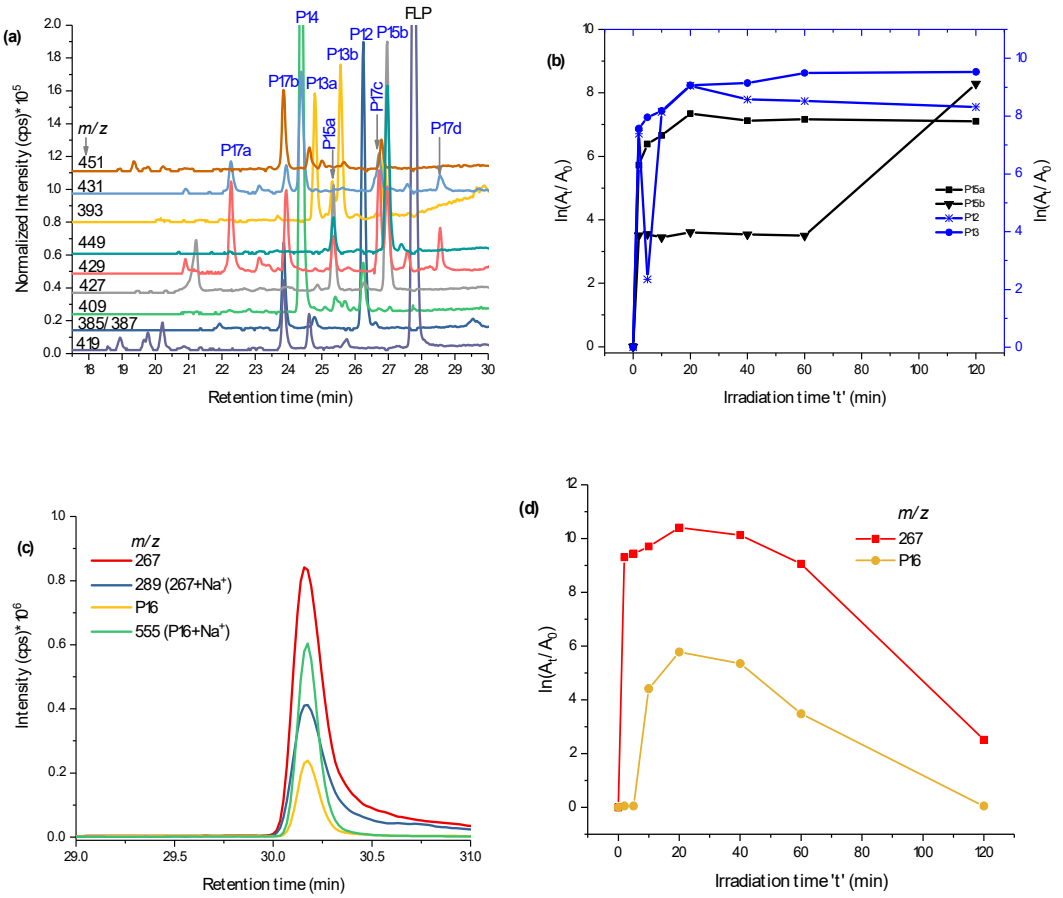

Fig. A11 EIC of selected PPs with their $+Na^+$ and $+K^+$-adducts (a), kinetics of P12, P13, and P15 PPs formation (b), EIC of P16 and m/z 267 with their respective $+Na^+$-adduct (c), and kinetics of P16 and m/z 267 PPs (d) measured by LC-MS/MS on (+) ESI

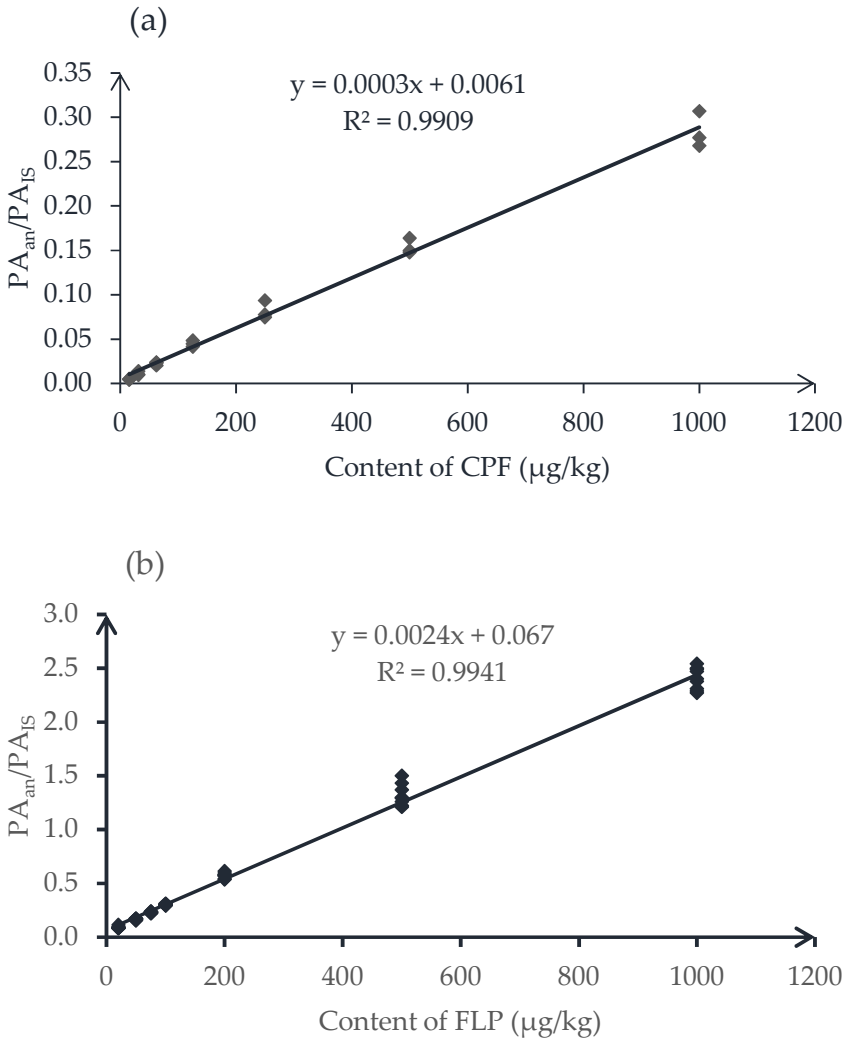

Fig. A12 Matrix matched calibration curve of CPF (*m*/*z* 350→198) in hot chili-paper (a) and FLP (397→208) in grapes (b) extracted by QuEChERS and measured by LC-MS/MS on (+) MRM mode

APPENDIX II-Manuscripts copyright

This agreement between Tessema F. Mekonnen and the licence content publisher (Springer Nature) consists of your license details and the terms and conditions provided by Springer Nature and Copyright Clearance centre.

License Number 4442490864684 (Oct 05, 2018): T.F. Mekonnen, U. Panne, M. Koch, Electrochemistry coupled online to liquid chromatography-mass spectrometry for fast simulation of biotransformation reactions of the insecticide chlorpyrifos, Anal Bioanal Chem 409(13), 2017.

License Number 4347550440858 (May 14, 2018): T.F. Mekonnen, U. Panne, M. Koch, Prediction of biotransformation products of the fungicide fluopyram by electrochemistry coupled online to liquid chromatography-mass spectrometry and comparison with *in vitro* microsomal assays, Anal Bioanal Chem 410 (10), 2018.

License Number 4442490416941 (Oct 05, 2018): T.F. Mekonnen, L. Byrne, U. Panne, M. Koch, Investigation of Chlorpyrifos and Its Transformation Products in Fruits and Spices by Combining Electrochemistry and Liquid Chromatography Coupled to Tandem Mass Spectrometry, Food Analytical Methods, 11(10), 2018.

Purpose and content of use

Type of use	Thesis/Dissertation
Requestor type	Academic/university or research institute
Format	Print and electronic
Portion	Full article/chapter
Will you be translating?	No
Title of dissertation	Investigating Biotic and Abiotic Transformation Processes of Selected Pesticides Using Electrochemistry Coupled to Mass Spectrometry
Institution/University	Humboldt-Universität zu Berlin
Expected presentation date	Feb 2019
Order reference number	3000358967
Requestor and address	Tessema Fenta Mekonnen Kopenicker Landstr. 124, 12437 Berlin

Terms and Conditions

Springer Nature Customer Service Centre GmbH (the Licensor) hereby grants you a non-exclusive, world-wide licence to reproduce the material and for the purpose and requirements specified in the attached copy of your order form, and for no other use, subject to the conditions below:

1. The Licensor warrants that it has, to the best of its knowledge, the rights to license reuse of this material. However, you should ensure that the material you are requesting is original to the Licensor and does not carry the copyright of another entity (as credited in the published version). If the credit line on any part of the material you have requested indicates that it was reprinted or adapted with permission from another source, then you should also seek permission from that source to reuse the material.
2. Where **print only** permission has been granted for a fee, separate permission must be obtained for any additional electronic re-use.
3. Permission granted **free of charge** for material in print is also usually granted for any electronic version of that work, provided that the material is incidental to your work as a whole and that the electronic version is essentially equivalent to, or substitutes for, the print version.
4. A licence for 'post on a website' is valid for 12 months from the licence date. This licence does not cover use of full text articles on websites.
5. Where '**reuse in a dissertation/thesis**' has been selected the following terms apply: Print rights of the final author's accepted manuscript (for clarity, NOT the published version) for up to 100 copies, electronic rights for use only on a personal website or institutional repository as defined by the Sherpa guideline (www.sherpa.ac.uk/romeo/).
6. Permission granted for books and journals is granted for the lifetime of the first edition and does not apply to second and subsequent editions (except where the first edition permission was granted free of charge or for signatories to the STM Permissions Guidelines http://www.stm-assoc.org/copyright-legal-affairs/permissions/permissions-guidelines/), and does not apply for editions in other languages unless additional translation rights have been granted separately in the licence.
7. Rights for additional components such as custom editions and derivatives require additional permission and may be subject to an additional fee. Please apply to Journalpermissions@springernature.com/ bookpermissions@springernature.com for these rights.
8. The Licensor's permission must be acknowledged next to the licensed material in print. In electronic form, this acknowledgement must be visible at the same time as the figures/tables/illustrations or abstract, and must be hyperlinked to the journal/book's homepage. Our required acknowledgement format is in the Appendix below.
9. Use of the material for incidental promotional use, minor editing privileges (this does not include cropping, adapting, omitting material or any other changes that affect the meaning, intention or moral rights of the author) and copies for the disabled are permitted under this licence.
10. Minor adaptations of single figures (changes of format, colour and style) do not require the Licensor's approval. However, the adaptation should be credited as shown in Appendix.

The terms and conditions of the Creative Commons Attribution (CC BY) license (http://creativecommons.org/licenses/by/4.0/) has been applied for the following articles

T.F. Mekonnen, U. Panne, M. Koch, New photodegradation products of the fungicide fluopyram: Structural elucidation and mechanism identification, Molecules, 23 (2018) 2940-2952